0 0 0 5 3 0 1 5 7 8
BERKELEY LAB
MAY 3 1979
LIBRARY AND
DOCUMENTS SECTION
RECEIVED
LAWRENCE
BERKELEY LABORATORY
MAY 30 1979
LIBRARY AND
DOCUMENTS SECTION

UC-11
LBL-8696c.1

ATMOSPHERIC AEROSOL RESEARCH

ANNUAL REPORT 1977-78

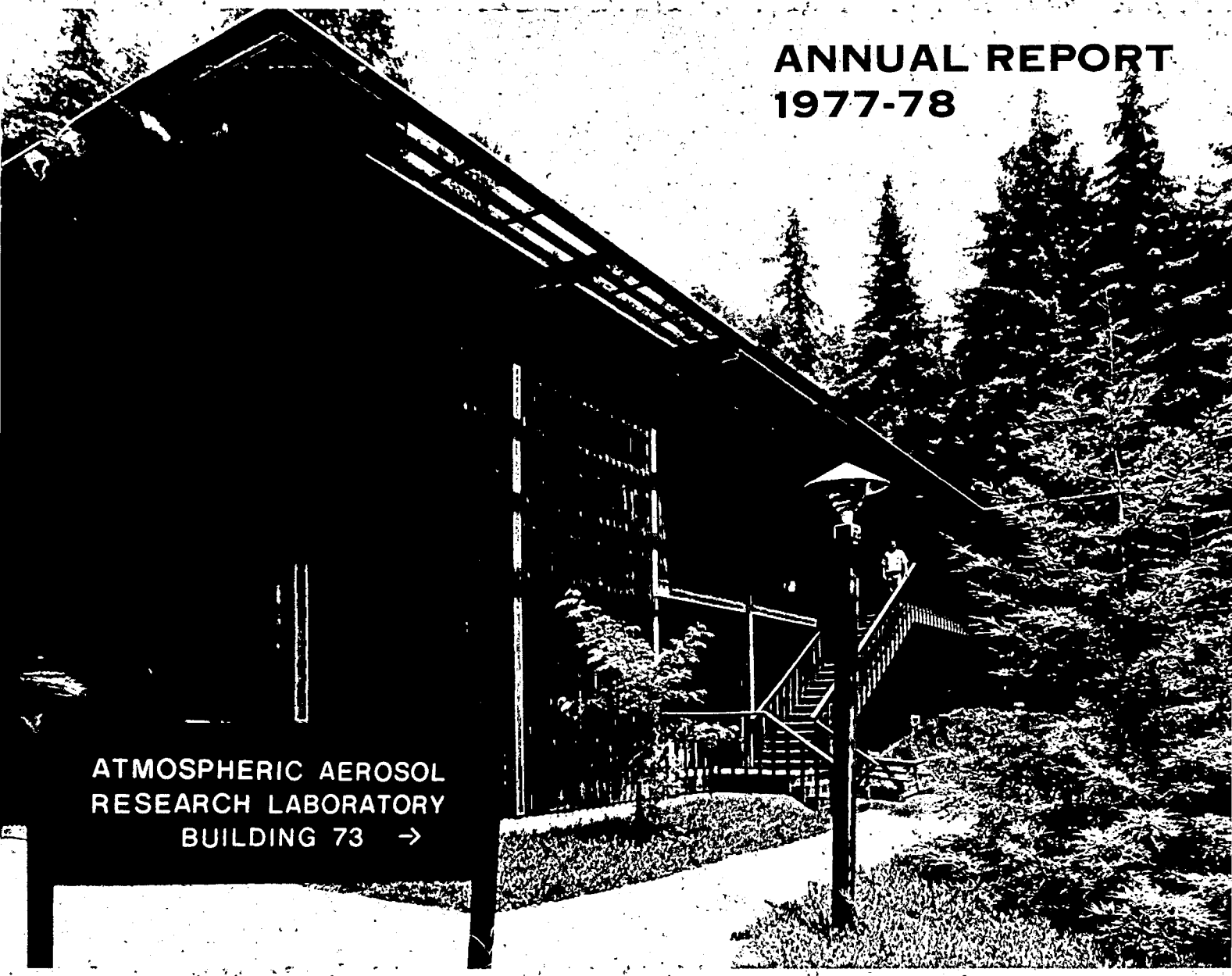

ENERGY & ENVIRONMENT DIVISION
LAWRENCE BERKELEY LABORATORY
UNIVERSITY OF CALIFORNIA, BERKELEY

For Reference
Not to be taken from this room

PREPARED FOR THE DEPARTMENT OF ENERGY
UNDER CONTRACT W-7405-ENG-48

LBL-8696c

LEGAL NOTICE

This report was prepared as an account of work sponsored by the United States Government. Neither the United States nor the United States Department of Energy, nor any of their employees, nor any of their contractors, subcontractors, or their employees, makes any warranty, express or implied, or assumes any legal liability or responsibility for the accuracy, completeness or usefulness of any information, apparatus, product or process disclosed, or represents that its use would not infringe privately owned rights.

Printed in the United States of America
Available from
National Technical Information Service
U.S. Department of Commerce
5285 Port Royal Road
Springfield, VA 22161
Price Code: A08

DISCLAIMER

This document was prepared as an account of work sponsored by the United States Government. While this document is believed to contain correct information, neither the United States Government nor any agency thereof, nor the Regents of the University of California, nor any of their employees, makes any warranty, express or implied, or assumes any legal responsibility for the accuracy, completeness, or usefulness of any information, apparatus, product, or process disclosed, or represents that its use would not infringe privately owned rights. Reference herein to any specific commercial product, process, or service by its trade name, trademark, manufacturer, or otherwise, does not necessarily constitute or imply its endorsement, recommendation, or favoring by the United States Government or any agency thereof, or the Regents of the University of California. The views and opinions of authors expressed herein do not necessarily state or reflect those of the United States Government or any agency thereof or the Regents of the University of California.

0 0 0 0 5 3 0 1 3 7 9

LBL-8696
UC-11

UNIVERSITY OF CALIFORNIA
LAWRENCE BERKELEY LABORATORY
ENERGY AND ENVIRONMENT DIVISION
ATMOSPHERIC AEROSOL RESEARCH

ANNUAL REPORT
1977-1978

PARTICIPANTS: T. Novakov, Principal Investigator
S.-G. Chang, Co-principal Investigator
H. Rosen, Co-principal Investigator
W.H. Benner
R. Brodzinsky
M. Clemenson
S. Cohen
R.L. Dod
R.D. Giauque
L.A. Gundel
A.D.A. Hansen
R. Kellner*
S.S. Markowitz
G.E. Mason
S.B. Oblath
A. Sawaya
R.C. Schmidt
R. Toossi
L. Wroth

Editor: H. Rosen

*On leave from the Technical University of Vienna

TABLE OF CONTENTS

Acknowledgments iii

Analytical Methods Development 1

Optico-Thermal Analysis of the Carbonaceous Fraction of Aerosol Particles 2
R.L. Dod, H. Rosen, and T. Novakov

Solvent-Extraction-Aided Morphology Study (SEAMS) 11
W.H. Benner and T. Novakov

Contributions to the Problem of Quantitative Infrared Spectroscopic Analysis of Sulfates and Nitrates in Airborne Particles: A Modified Sampling System 20
R. Kellner and T. Novakov

Determination of Nitrogen in Atmospheric Aerosols by Proton Activation Analysis 28
M. Clemenson, T. Novakov, and S.S. Markowitz

A Size-Segregating Aerosol Sampler 33
A.D.A. Hansen, R.C. Schmidt, and T. Novakov

Physical and Chemical Characterization: Physical 41

Optical Characterization of Ambient and Source Particulates 42
A.D.A. Hansen, H. Rosen, R.L. Dod, W.H. Benner, and T. Novakov

Optical Attenuation: A Measurement of the Absorbing Properties of Aerosol Particles 54
H. Rosen and T. Novakov

Identification of the Optically Absorbing Component in Urban Aerosols 58
H. Rosen, A.D.A. Hansen, L. Gundel, and T. Novakov

Physical and Chemical Characterization: Chemical 67

Characterization of Source and Ambient Particulate Samples by Solvent Extraction 68
L.A. Gundel, G.E. Mason, and T. Novakov

Characterization of Particulate Amines 79
L.A. Gundel, S.-G. Chang, M. Clemenson, S.S. Markowitz, and T. Novakov

Atmospheric Chemistry: Laboratory Studies 87

SO_2 Oxidation by Water Droplets Containing Combustion Nuclei 88
W.H. Benner, H. Rosen, and T. Novakov

Kinetics and Mechanism of the Reactions of NO_x with SO_2 in Aqueous Solutions 100
S.B. Oblath, S.S. Markowitz, T. Novakov, and S.-G. Chang

Kinetics and Mechanism for the Catalytic Oxidation of SO_2 on Carbon in Aqueous Suspensions 110
R. Brodzinsky, S.-G. Chang, S.S. Markowitz, and T. Novakov

Atmospheric Chemistry: Modelling 125

A Carbon and Lead Emission Inventory for the Greater San Francisco Bay Area 126
A.D.A. Hansen, W.H. Benner, and T. Novakov

Relative Importance of Various Sulfate Production Mechanisms in Aqueous Droplets 132
R. Toossi, T. Novakov, and S.-G. Chang

Sulfur Dioxide Oxidation in a Dispersing Plume 138
R. Toossi, S.-G. Chang, P.J. Pagni, and T. Novakov

Lifetime of Liquid Water Drops in Ambient Air: Consideration of the Effects of Surfactants and Chemical Reactions 149
R. Toossi, S.-G. Chang, and T. Novakov

ACKNOWLEDGMENTS

The research described in this report is supported by the National Science Foundation (NSF) and the U.S. Department of Energy (DOE). We would like to express our appreciation and thanks to our NSF program manager, Dr. R.A. Carrigan, and our DOE program managers, Dr. F.P. Hudson, and Dr. D. Ballantine, for their continuing support.

We gratefully acknowledge and thank the following:

Dr. A.M. Sessler, Director of Lawrence Berkeley Laboratory (LBL), for his continued strong support of our program.

Dr. P.T. Cunningham, Dr. R. Kumar, and Dr. S. Johnson of Argonne National Laboratory; the Bay Area Air Quality Management District; and the South Coast Air Quality Management District for their cooperation in our sampling program.

Dr. T.L. Hayes and Mr. C.E. Lai from Donner Laboratory at LBL for providing the scanning electron microscope analysis.

Prof. H.L. Strauss of the University of California, Berkeley, for his permission to use the Nicolet 7199 FTIR system, and his coworkers D. McPhail and J. Offenbach for their help in recording the spectra.

Dr. B.W. Loo of LBL for advice on aerosol sampling and for elemental analyses of particulate samples using the X-ray fluorescence technique.

Mr. E.R. Mayo, Highway Superintendent, California State Department of Transportation, Caldecott Tunnel, and his staff for helping us to conduct the experiments in the Caldecott Tunnel.

Mr. K.M. Hagerty for his assistance in sampling in the parking garage of the Associated Students of the University of California.

The personnel at the U.S. Naval Weapons Station at Concord, California, and the U.S. Coast Guard Light Station at Point Bonita, California, for their cooperation in our field sampling program.

Dr. C. Spicer, Battelle Columbus Laboratories, Columbus, Ohio, for performing analyses of particulate samples.

We would also like to acknowledge fruitful discussions with Dr. R.A. Carrigan, Prof. G.E. Gordon, Prof. R.J. Charlson, Prof. L. Brewer, Dr. P. Middleton, and Prof. H.S. Johnston.

0 0 0 0 5 3 0 1 3 8 2

ANALYTICAL METHODS DEVELOPMENT

Optico-Thermal Analysis of the Carbonaceous Fraction of Aerosol Particles

R.L. Dod, H. Rosen, and T. Novakov

Analysis of the carbonaceous fraction of atmospheric particulate material is complicated by the diversity of forms in which it exists. Total carbon can be determined readily by combustion, but chemical information is generally obtained only by tedious separation and analysis by such techniques as solvent extraction, GC, or GC-MS.

Malissa has reported a method of analysis[1] for the carbonaceous component of atmospheric aerosol particulate material by evolved gas analysis during a temperature-programmed combustion in oxygen. We have extended this analysis by constructing an apparatus which simultaneously measures the optical transmission of the particulate matter collected on a filter. Since the optical absorptivity of this material has been shown to be due to a graphitic component,[2] this combination of analytical techniques may provide a direct determination of the light-absorbing fraction of the sample. This technique is also applicable to analysis of other carbonaceous materials, such as coals and oil shales, in which there appears to be a correlation between optical absorptivity and the fraction of these fuels that is aromatic in chemical nature (Fig. 1).

The apparatus constructed for these analyses is shown schematically in Fig. 2. The combustion tube is supplied with $\sim$ 1 ℓ/min of oxygen which has been scrubbed of carbon-containing species. A flow of 177 ml/min is maintained through the combustion tube and the CO_2 analyzer by a pump operating through a critical orifice. The excess oxygen passes out of the system through a hole in the upstream end of the combustion tube. After passing and/or reacting with the sample, the gas stream is passed through a furnace section filled with CuO maintained at 900°C to assure conversion of all carbon species to CO_2. The CO_2-laden oxygen is then passed through a MSA LIRA 202S infrared CO_2 analyzer with a range of 0-50 ppm CO_2 in oxygen. The sample, on a prefired quartz fiber filter, is positioned perpendicular to the furnace axis, allowing incident light from a 0.5-mW He-Ne laser to be intercepted. The forward scattered light is collected by a quartz light pipe and conducted to a photomultiplier detector system. The combustion furnace temperature is increased in a linear ramp from near room temperature to 600-800°C at a rate of 10 C°/min. The signals from both the CO_2 analyzer and the photomultiplier are fed to a stripchart recorder to produce a composite thermogram.

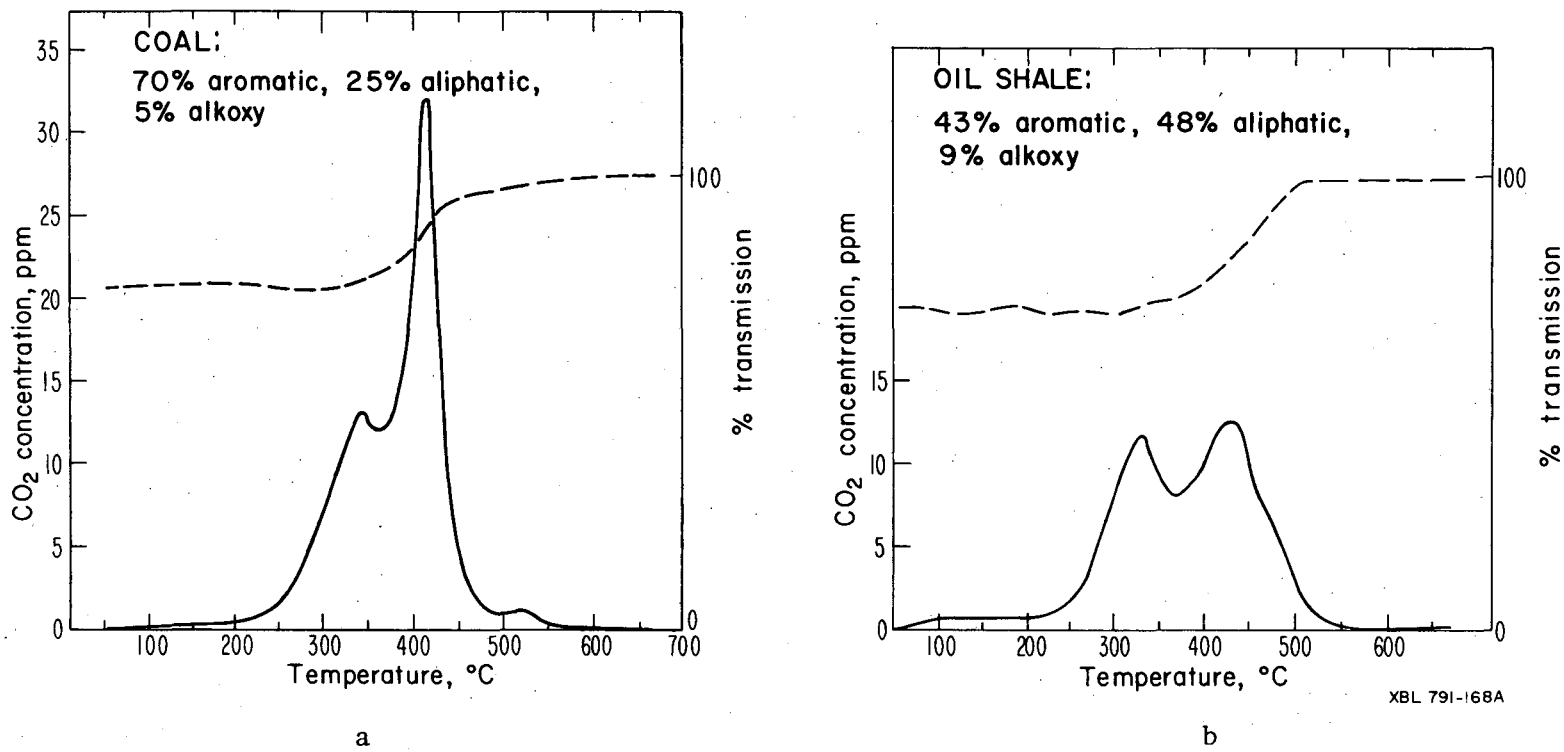

Figure 1. Combustion thermograms of solid fossil fuels. Organic functional type determined by NMR spectroscopy. Dashed line is optical transmission.

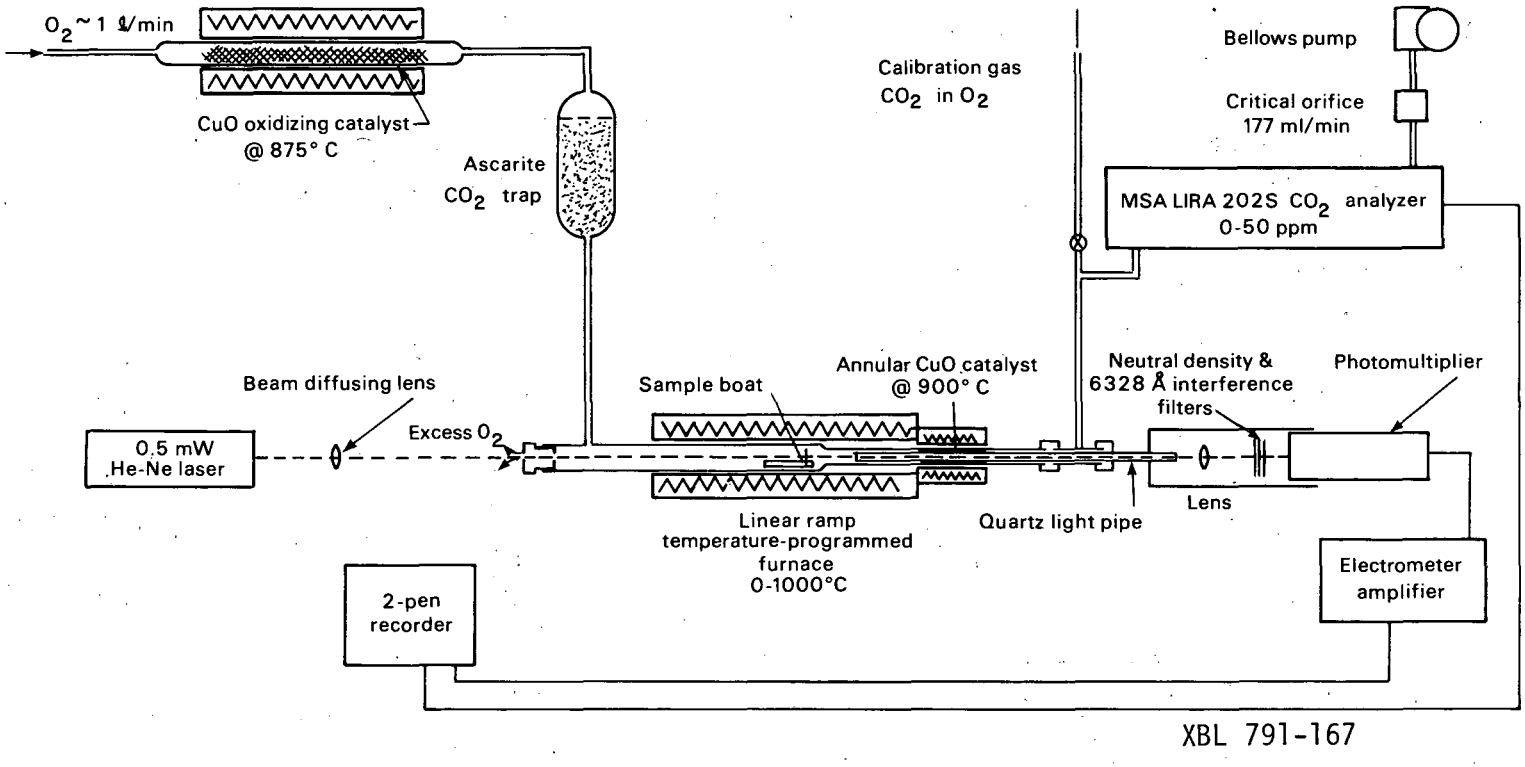

Figure 2. Schematic diagram of the programmed combustion apparatus.

Analysis of weighed samples of carbon and pure organic compounds, as well as portions of filter samples analyzed by another combustion technique,[3] shows the method to be quantitative for carbon within about 10%. Reproducibility is somewhat better, with duplicate samples from a single filter agreeing within 3-5% and being identical in qualitative nature.

Thermograms of ambient and source samples generally show three characteristic features: (1) a low-temperature CO_2 peak corresponding to volatilization and incomplete combustion of material which is not optically absorbing, (2) a CO_2 peak at 300-350°C corresponding to combustion (and pyrolysis) of material which also is not optically absorbing, and (3) a high-temperature CO_2 peak which includes the optically absorbing component of the sample. The three peaks are not usually well separated but show varying degrees of overlap, which might be expected of a complex mixture of organic and elemental carbon species.

Source samples show a wider diversity in their thermograms, probably as a result of uniform combustion conditions with different fuels. Some samples show the carbonaceous particulate material to be composed almost entirely of light-absorbing material, probably graphitic in character (Figs. 3b, 4a); others show a dominant volatile fraction (Fig. 4b); and some are closer to an ambient aerosol in nature (Fig. 3a). In addition, a single source may show a different character at different times. It would be reasonable for ambient particulate carbon to be a composite of the various types of source constituents.

Ambient samples collected in widely separated locations show a substantial degree of similarity with variations in the relative amounts of the three characteristic carbon types (Fig. 5). We observed some variation in combustion temperature for the high-temperature (absorbing) component, as well as variation in the structure of the CO_2 peak from the low-temperature (volatile) fraction. Experiments with graphite ground to varying particle sizes show that the temperature at which the absorbing component burns can be a function of particle size, with smaller particles burning at a lower temperature. Other effects, such as surface functional groups and varying porosity, undoubtedly affect the combustion temperature also.

The 300-350°C peak in the thermogram is subject to much less variation in shape and position, although combustion of this material may be accompanied in some samples by a substantial amount of pyrolysis, which can be seen from the increase in the optical absorption of the sample (e.g., Fig. 5c). We have labeled this fraction the polymeric fraction since this behavior could be observed with

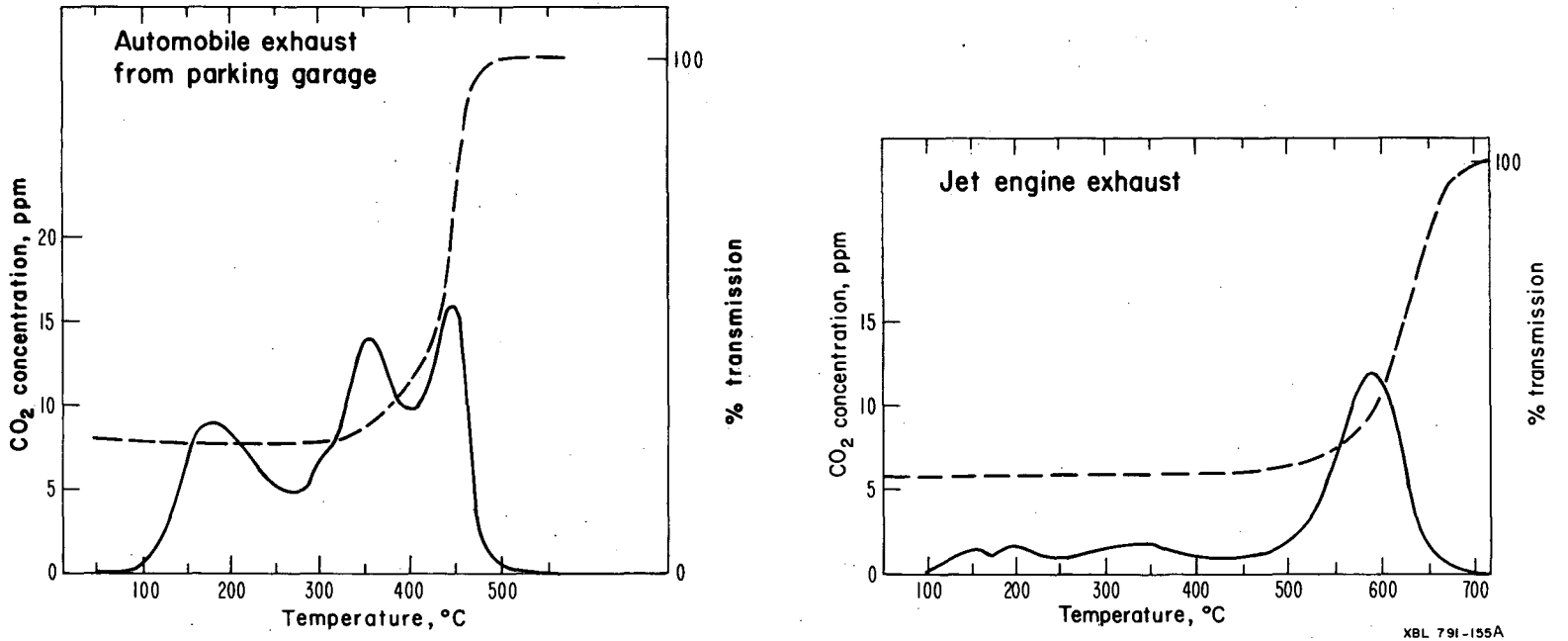

a b

Figure 3. Example of combustion thermograms of particulate material emitted from mobile sources. Dashed line is optical transmission.

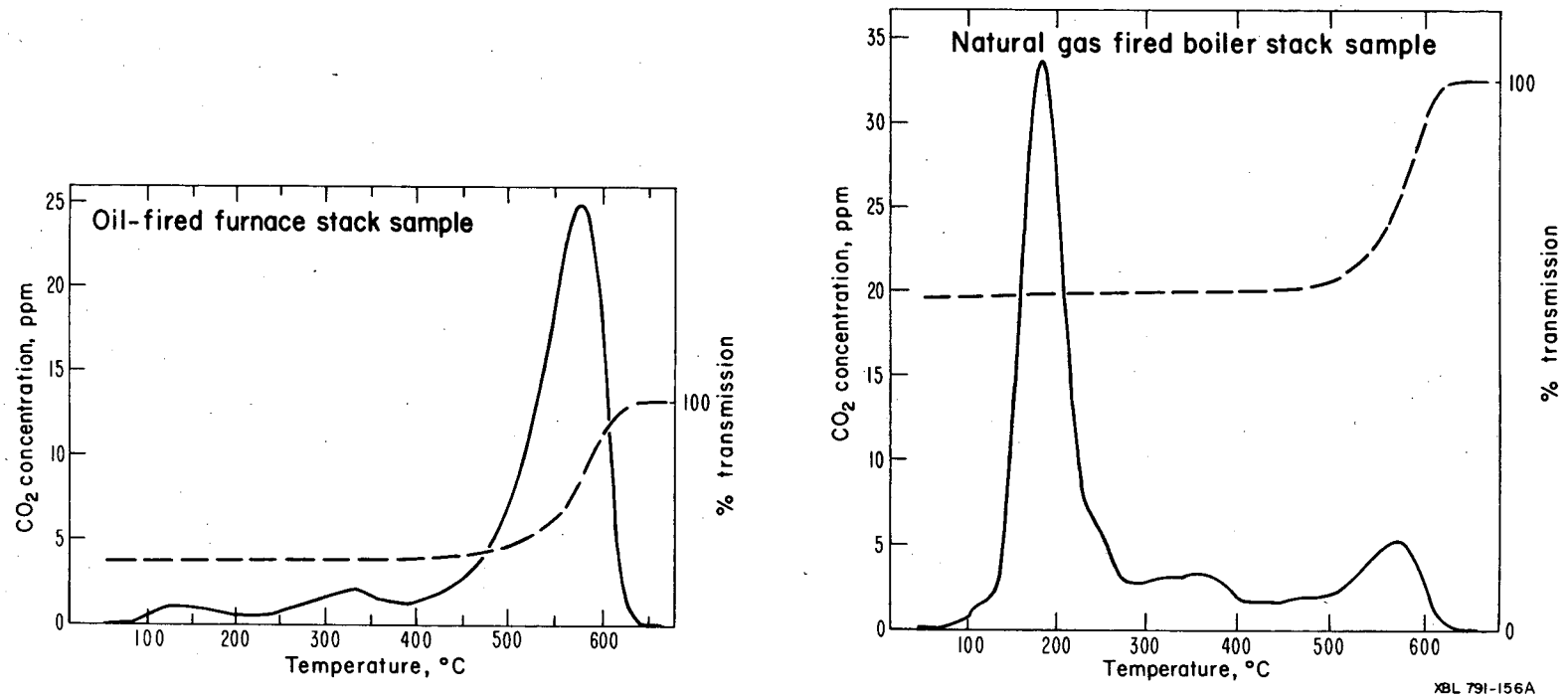

a b

Figure 4. Example of combustion thermograms of particulate material emitted from stationary sources. Dashed line is optical transmission.

0 0 0 0 3 0 1 3 8 5

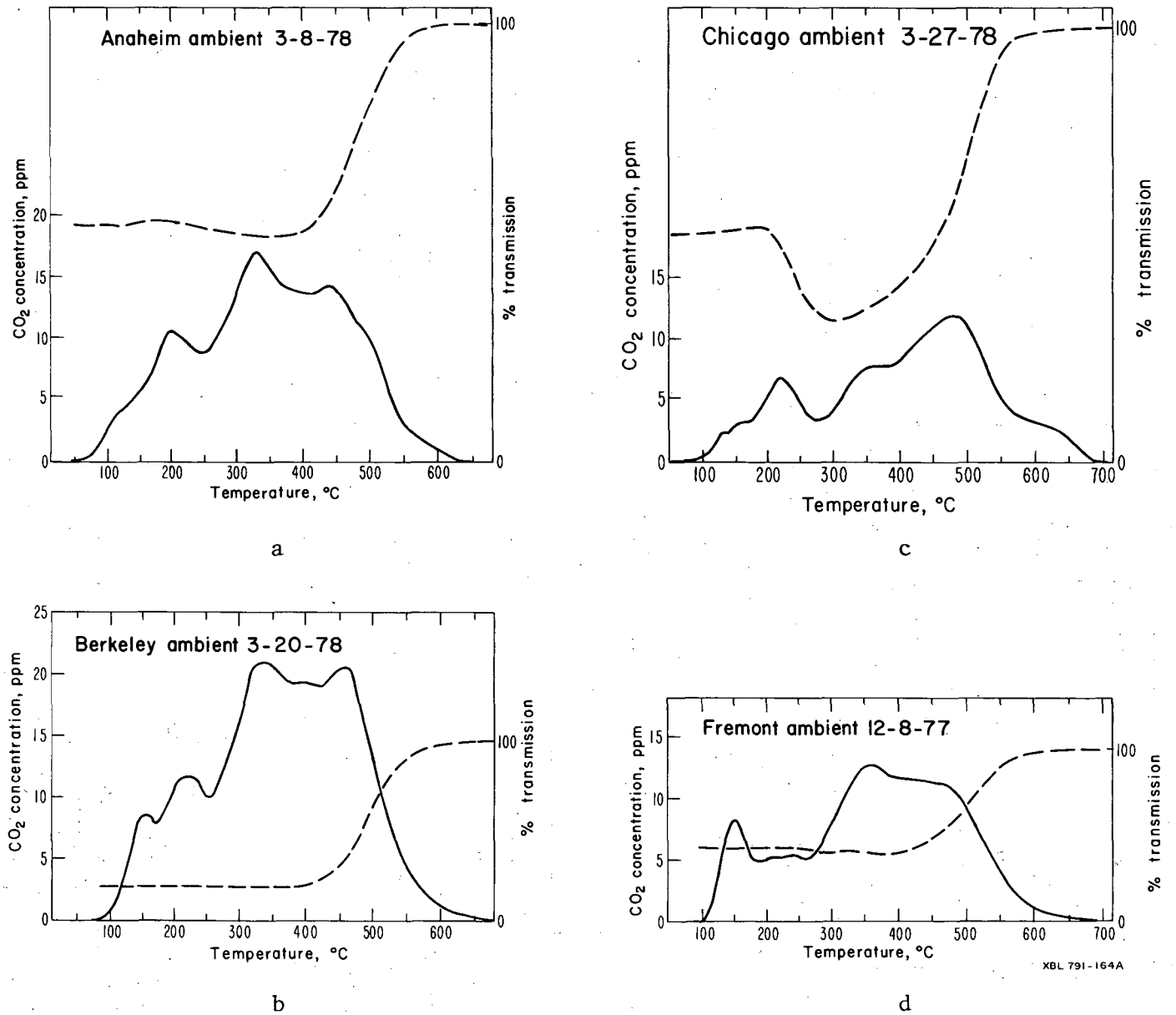

Figure 5. Typical combustion thermograms of ambient particulate material from different geographical regions. Dashed line is optical transmission.

a polymer such as polystyrene, although we have not characterized the material in any other way.

The low-temperature material is variable in amount and in structure in the CO_2 thermogram. In this region one would expect to find small organic molecular materials volatilizing and burning. This material is removed by solvent extraction with benzene and methanol-chloroform.

The predominant compounds identified in secondary organic aerosol are the C_4-C_6 organic di-acids.[4,5] These materials have relatively low melting points and generally decompose at temperatures below $\sim$ 300°C. The thermograms of these acids all show sharp decomposition or volatilization at temperatures below 250°C (e.g., Fig. 6). Similar sharp low-temperature combustion was seen for a variety of aliphatic and aromatic compounds ranging to C_{19} (methyl stearate). Based on these observations, the low-temperature CO_2 peak probably represents a complex mixture of both primary and secondary organic compounds. If these compounds are found to volatilize and/or combust only in this temperature region, it should be possible to place a general upper limit on their relative amount in ambient carbonaceous aerosol. In general, no more than 20-30% of total carbon falls in the low-temperature CO_2 peak. Since this would include both primary and secondary organics, the relative mass of photochemically produced secondary aerosol is clearly much less than has been assumed.

Further development of this technique is currently under way with attempts to identify at least portions of the volatile and polymeric fractions. We also hope to quantitate the absorbing material, a measurement of substantial importance because the graphitic material in soot has been shown to be catalytically active in SO_2 oxidation[6] and has a potential for catalytic activity in other atmospheric reactions.

References

1. H. Malissa, H. Puxbaum, and E. Pell, "Zur simultanen relativkondukto-metrischen Kohlenstoff- und Schwefelbestimmung in Stäuben," Z. Anal. Chem. 282, 109 (1976).
2. H. Rosen, A.D.A. Hansen, L. Gundel, and T. Novakov, "Identification of the optically absorbing component in urban aerosols," Appl. Opt. 17, 3859 (1978).
3. P.K. Mueller, R.W. Mosley, and L.B. Pierce, "Carbonate and non-carbonate carbon in atmospheric particles," in Proceedings, Second International Clean Air Congress (1970).

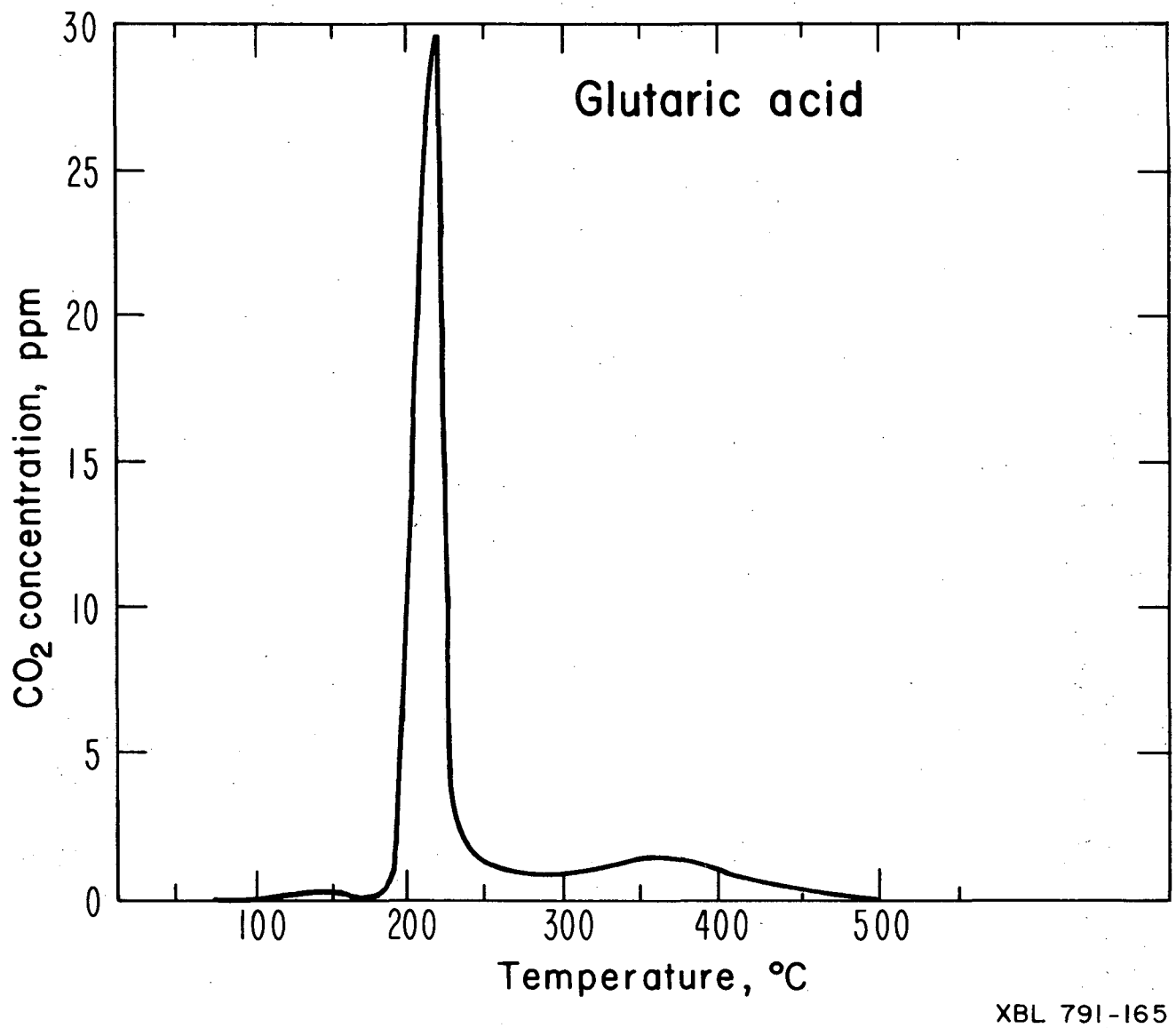

Figure 6. Carbon combustion thermogram of glutaric acid (optical attenuation not measured).

4. D. Schuetzle, D. Cronn, A.L. Crittenden, and R.J. Charlson, "Molecular composition of secondary aerosol and its possible origin," Environ. Sci. and Technol. 9, 838 (1975).

5. D. Grosjean, K. Van Cauwenberghe, J.P. Schmid, P.E. Kelley, and J.N. Pitts, Jr., "Identification of C_3-C_{10} aliphatic dicarboxylic acids in airborne particulate matter," Environ. Sci. and Technol. 12, 313 (1978).

6. S.-G. Chang, R. Brodzinsky, R. Toossi, S.S. Markowitz, and T. Novakov, "Catalytic oxidation of SO_2 on carbon in aqueous suspensions," Proceedings, Conference on Carbonaceous Particles in the Atmosphere, Lawrence Berkeley Laboratory, Berkeley California (in press).

Solvent-Extraction-Aided Morphology Study (SEAMS)

W.H. Benner and T. Novakov

Electron microscopy (EM) is one of the many techniques used to characterize ambient particulate matter. Russell[1] used EM in combination with X-ray spectroscopy and reported that ambient particles were often predominantly carbonaceous and that if nonmineral sulfur were present in the sample, the sulfur would be associated with the carbonaceous particles. Chung et al.[2] sequentially exposed soot particles to SO_2 and H_2O, to vacuum, and to NH_3 in a small chamber in an electron microscope. They observed that the particles became coated with a vacuum-stable reaction product and concluded that soot particles can serve as sites for SO_2 oxidation. This conclusion supports the SO_2 oxidation mechanism of Chang et al.[3] Husar[4] noted that liquid ambient aerosols can contain electron-dense nuclei. We have extended the use of EM to study the changes in morphology of ambient particulate matter that can be induced by solvent extraction and heat treatment. The preliminary observations indicate the presence of a liquid-like material in submicron aerosol particles. This material can be removed by suitable solvent extraction or by heat treatment procedures to expose a core of agglomerates morphologically similar to carbon black.

Experimental

Ambient and source-enriched air samples were collected on a multiple-jet four-stage impactor.[5] Samples from the first stage (Dp = 0.14-0.4 μm) and second stage (Dp = 0.4-1.6 μm) were examined by scanning electron microscopy (SEM) before and after treatment. Particulate samples from an urban atmosphere, an underground parking garage, a freeway tunnel, and a natural gas boiler (300,000 Btu/hr) were impacted onto copper or aluminum foils.

Spots of impacted particles were cut from the metal foil impaction surfaces, and several spots were extracted separately in methanol or benzene. A few samples were subjected to heat treatment. Extraction was performed by suspending the particle-laden piece of foil in 100 ml of warm solvent for 2 hr. The heat-treated samples were heated from room temperature to 350°C in an oven temperature programmed to heat at 10 C°/min. Several impaction spots were also analyzed by a thermal analysis technique which recorded the amount of CO_2 evolved versus temperature as the sample was heated in pure oxygen.[6]

Results

Figures 1-5 show SEM pictures of four types of impacted particles. The impaction spots were typically black and consisted of particles formed from agglomerates of smaller particles. Some samples also contained a liquid-like material. This material had apparently been more fluid earlier, as evidenced by cracks in the bulk of the deposit, thought to have formed as a result of drying or exposure to vacuum (Fig. 1). For the samples examined, only second-stage ambient samples were totally inundated by this material. Ambient particles collected on the first stage possessed a coating of the material but were never completely immersed in the liquid-like deposit (Fig. 2). Particles other than ambient contained various amounts of this liquid-like deposit and the following samples (all second stage) are ranked according to the amount of liquid-like material (Figs. 1-5):

ambient > boiler > parking garage > freeway tunnel .

Solvent extraction of the impactor spots removed a major portion of the liquid-like material and exposed individual particles morphologically similar to carbon black (Figs. 1, 3-5). Visual comparison of methanol- and benzene-extracted samples showed that methanol removed more of the material than benzene did (Fig. 3). Thermal treatment of an impaction spot indicated that heat could cause morphological changes similar to the changes that occurred when a sample was extracted in methanol (Fig. 3). In addition to causing morphological changes, heating to 350°C removed 70% of the carbon from ambient second-stage particles. Undoubtedly heating also caused some of the sublayer particles to oxidize, so it is not possible to know from this analysis what fraction of the pyrolyzed carbon came from the liquid-like deposit. It is known from other studies in our laboratory that only a small fraction of graphitic carbon (source of the black color)[7] is removed when soot particles are heated to 350°C.

Discussion

The composition of the liquid-like material associated with many of the samples is unknown. Solubility of the material in methanol and benzene suggested the material was partly hydrocarbonaceous. X-ray fluorescence (XRF) analysis of boiler particles indicated that the composition of the material was dominated by elements of $Z < 14$, which suggests C, H, N, and O as possible components. However, composition of the ambient material was more soluble in methanol and benzene than the boiler sample was. The evolution of carbon from a heated ambient

NATURAL GAS FIRED BOILER PARTICLES
ON 1st STAGE OF AN IMPACTOR
(Dp = 0.14 - 0.4 μm)

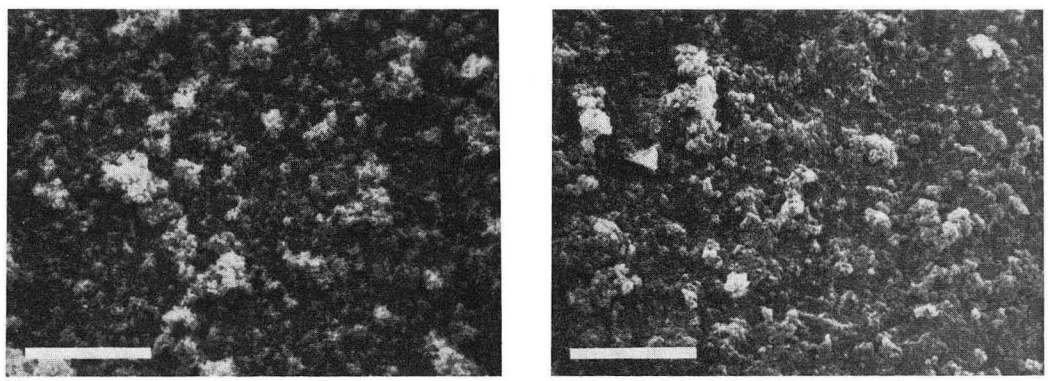

(a) Untreated (b) Methanol extracted

NATURAL GAS FIRED BOILER PARTICLES
ON 2nd STAGE OF AN IMPACTOR
(Dp = 0.4 - 1.6 μm)

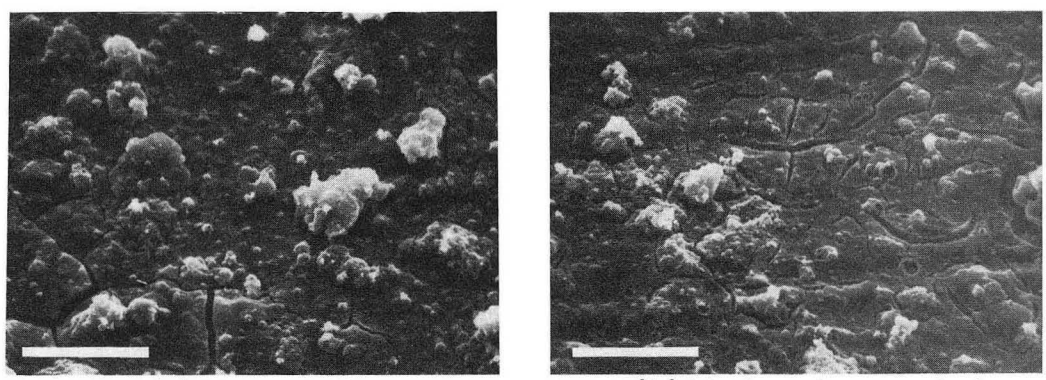

(a) Untreated (b) Methanol extracted

XBB 7812-15912

Figure 1. Comparison between untreated and methanol-extracted natural gas fired boiler particles. The white bar represents 10 μm.

AMBIENT PARTICLES ON 1st AND 2nd STAGE OF AN IMPACTOR

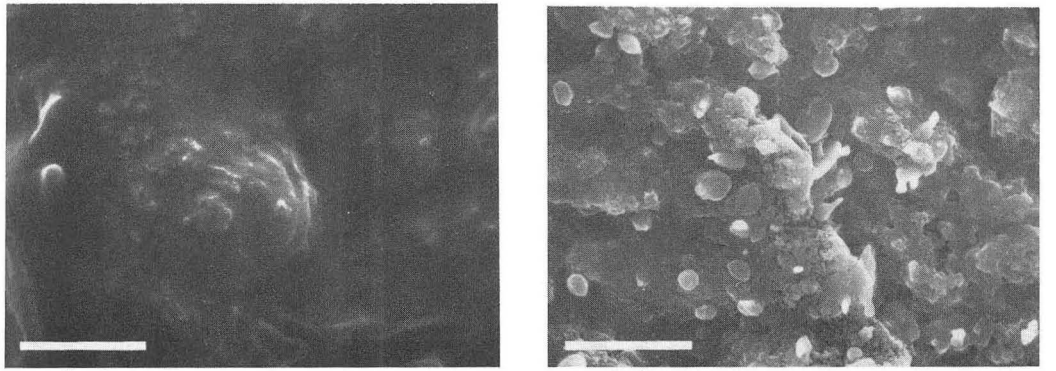

(a) Untreated, 2nd stage
(Dp = 0.4 - 1.6 μm)

(b) Untreated, 1st stage
(Dp = 0.14 - 0.4 μm)

XBB 7812-15914

Figure 2. Particles collected from the ambient air in Berkeley, California, on a moderately hazy day. The white bar represents 10 μm.

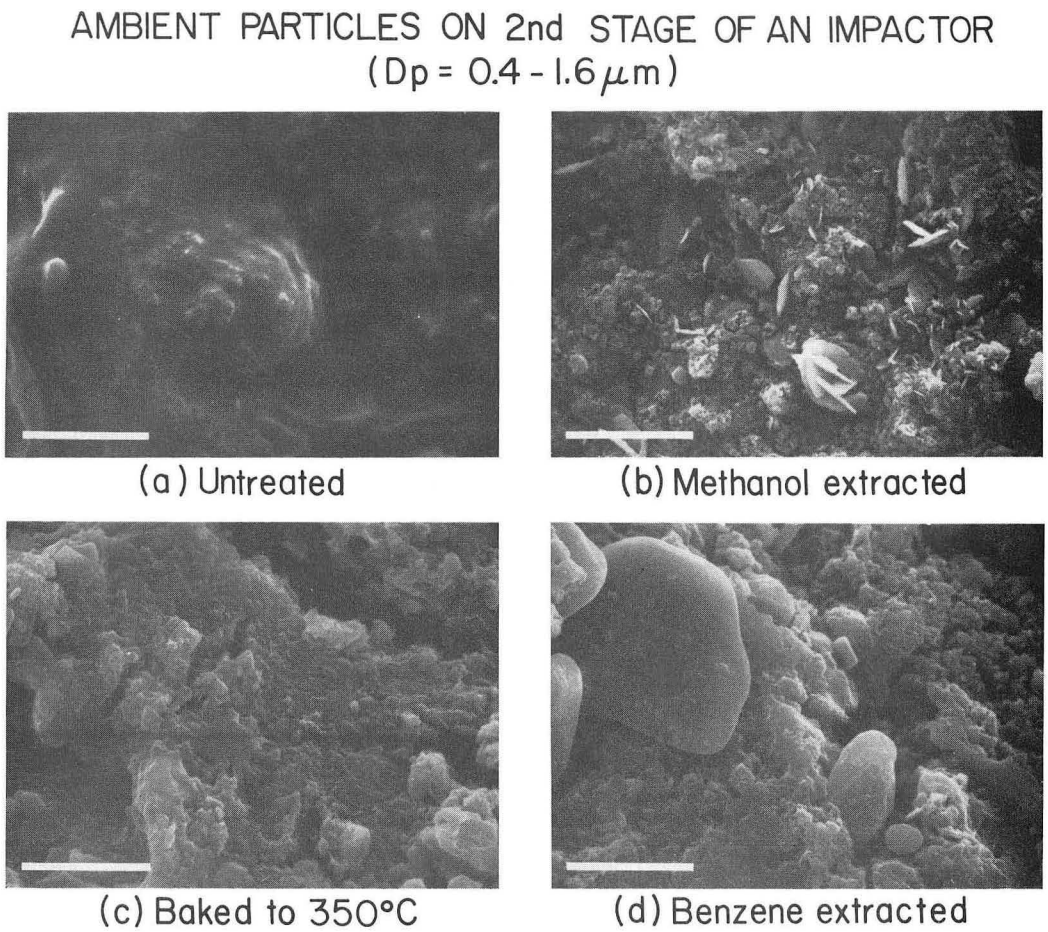

XBB 7812-15910

Figure 3. Morphological changes that occur when particles are exposed to various treatments. The particles were collected from the ambient air in Berkeley, California, on a moderately hazy day. The white bar represents 10 μm.

FREEWAY TUNNEL PARTICLES ON 2nd STAGE OF AN IMPACTOR
(Dp= 0.4 - 1.6 μm)

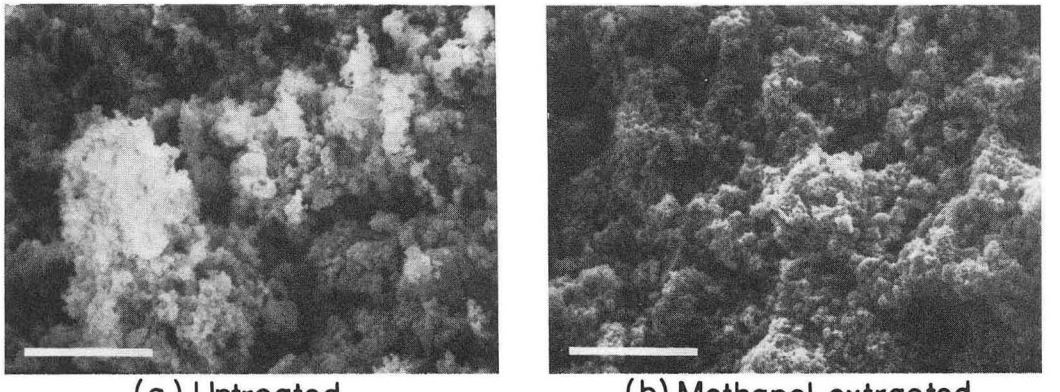

(a) Untreated (b) Methanol extracted

XBB 7812-15913

Figure 4. Comparison between untreated and methanol-extracted freeway tunnel particles. The white bar represents 10 μm.

PARKING GARAGE PARTICLES ON 1st STAGE OF AN IMPACTOR
(Dp = 0.14 - 0.4 μm)

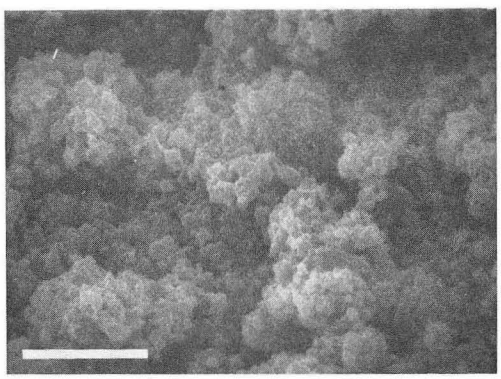

(a) Untreated

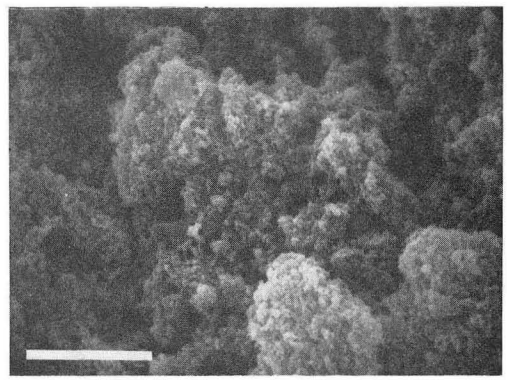

(b) Methanol extracted

PARKING GARAGE PARTICLES ON 2nd STAGE OF AN IMPACTOR
(Dp = 0.4 - 1.6 μm)

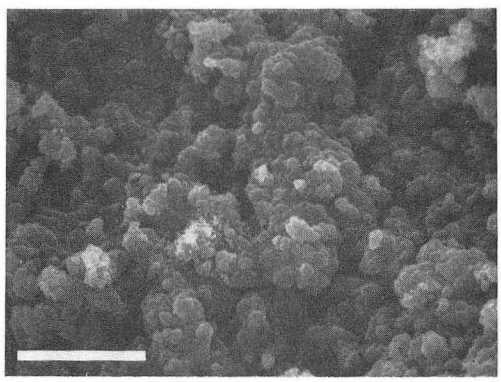

(a) Untreated

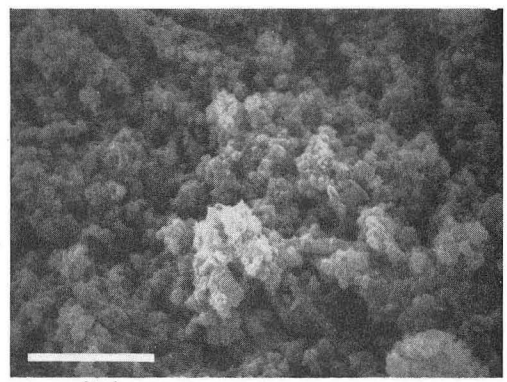

(b) Methanol extracted

XBB 7812-15911

Figure 5. Comparison between untreated and methanol-extracted parking garage particles. The white bar represents 10 μm.

sample, the morphological changes, and the knowledge that the evolved carbon probably did not come from the graphitic carbon suggest that this liquid-like material in the ambient sample was, in part, carbonaceous. Since the ambient sample was not analyzed by XRF, the presence of sulfur or nitrogen in the ambient sample cannot be ruled out. Ammonium sulfate, ammonium bisulfate, and ammonium nitrate melt or decompose below 280°C; and pyrolysis of these compounds could possibly have been related to morphological changes in the ambient sample.

Ambient particles collected on filters sometimes look like liquid droplets, but a thick layer of a liquid-like deposit has not been observed in filter samples to our knowledge. One possible mechanism for the formation of this deposit involves the presence of liquid water, which is known to condense onto airborne particles, even at relative humidities less than 100%. When these wet particles are closely packed together, as in the impaction spot, the water could have coalesced into a layer of material covering the nuclei of the original particles. Evaporation of this layer, which presumably would contain nonvolatile dissolved substances, would then leave a vacuum-stable deposit. These observations could also have been due to a sampling artifact since water could have condensed onto the particles when the particle-laden air expanded adiabatically as it exited the impactor jet.

Conclusions

Solvent extraction and heating of impacted samples of ambient and source particulate matter were found to cause dramatic morphological changes in the sample. Variable amounts of liquid-like material were found to be associated with ambient and source samples. The composition and origin of the material is not known, and characterization of this material will be pursued in future experimentation.

References

1. P.A. Russell, "Carbonaceous particulates in the atmosphere: Illumination by electron microscopy," Conference on Carbonaceous Particles in the Atmosphere, Proceedings, Lawrence Berkeley Laboratory, Berkeley, Ca. (in press).
2. T.T. Chung, J. Dash, and R.J. O'Brien, "Preliminary observations of SO_2-soot interaction by controlled atmosphere transmission electron microscopy," Conference on Carbonaceous Particles in the Atmosphere, Proceedings, Lawrence Berkeley Laboratory, Berkeley, California (in press).
3. S.-G. Chang, R. Brodzinsky, R. Toossi, S.S. Markowitz, and T. Novakov, "Catalytic oxidation of SO_2 on carbon in aqueous suspensions," Conference on Carbonaceous Particles in the Atmosphere, Proceedings, Lawrence Berkeley Laboratory, Berkeley, California (in press).

4. R.B. Husar, W.H. White, and D.L. Blumenthal, "Direct evidence of heterogeneous aerosol formation in Los Angeles smog," Environ. Sci. Technol. 10, 490 (1976).

5. H. Malissa, "Some analytical approaches to the chemical characterization of carbonaceous particulates," Conference on Carbonaceous Particles in the Atmosphere, Proceedings, Lawrence Berkeley Laboratory, Berkeley, California (in press).

6. R.L. Dod, H. Rosen, and T. Novakov, "Optico-thermal analysis of the carbonaceous fraction of aerosol particles," this report.

7. H. Rosen, A.D.A. Hansen, L. Gundel, and T. Novakov, "Identification of the optically absorbing component in urban aerosols," Appl. Optics 17, 3859 (1978).

Contributions to the Problem of Quantitative Infrared Spectroscopic Analysis of Sulfates and Nitrates in Airborne Particles: A Modified Sampling System

R. Kellner* and T. Novakov

Sulfates and nitrates are major components of the respirable fraction of airborne particles.[1] Previous studies by ESCA[2] on impactor and filter samples and by wet chemical techniques[3] indicate that airborne particles do not often contain $(NH_4)_2SO_4$ and NH_4NO_3 in their well-defined stoichiometry. It is therefore important to quantitatively determine the various molecular forms of the sulfate and nitrate species. We believe that infrared (IR) spectroscopy is extremely well suited for this characterization because of its high structural selectivity, high sensitivity, and potential applicability to quantitative analysis.[4]

Several attempts to use IR spectroscopy for a qualitative speciation have been published earlier[5-9]; but, except for the work of Cunningham et al. with a Lundgren impactor,[9] no reliable quantitative IR-spectroscopic speciation for 1- to 10-μg samples (compatible with a size-selective sampling method) has yet been reported. The major problems preventing quantitative speciation are unreliable standard materials; the IR opacity of the materials used for the collection of airborne particles, which makes a transfer step of the particles necessary; and difficulties of sample preparation, such as particle-size and matrix effects. Our work shows that these problems can be overcome and that a quantitative IR-spectroscopic analysis of infrared active molecules or ions, especially sulfates, in microgram amounts of airborne particles is possible under the following conditions:

1. Composition of the sampling system — ring jet impactor (design by A. Berner[10]) with particle-size segregation: stage 1, 0.14-0.4 μm; stage 2, 0.4-1.6 μm; stage 3, 1.6-6.4 μm; stage 4, 6.4-25 μm aerodynamic diameter.

2. Direct deposition of the aerosols on the pelleting material (no scraping).

3. Application of a vibrating mill to ensure homogenization of the samples and to eliminate particle-size effects.

4. Use of wet chemical techniques to standardize the IR method.

*On leave from the Institute of Analytical Chemistry and Microchemistry, Technical University, Vienna, Austria.

Sampling System

The sampling system is a crucial point in this method of analysis. Berner's impactor was first used in chemical aerosol characterization by H. Malissa[11,12] because of the many advantages it offers in sharp particle size separation, low wall losses (< 5%), and compatibility with several methods used in integrated dust analysis. In this method, the airborne particles are deposited on thin Cu or Al foils to allow a gravimetric mass determination. This sampling technique is not a priori IR compatible because the sample must be scraped from the foil and transferred to the pelleting material, which means a loss of sample material. In several cases samples even stuck to Mylar and could not be removed quantitatively. Therefore, the sampling system had to be modified to make it IR compatible while maintaining the advantages of the original design.

As shown in Fig. 1, two 3-mm KBr pellets in 13-mm sample holders were mounted on stages 1, 2, and 3 so that the pellet surface is located in the plane of the Cu surface. This technique allows direct depositions on the KBr pellet, as well as simultaneous collection on the Cu substrate for gravimetric and further chemical analysis.[13,14] Other foil materials, such as Al or Mylar, have also been used. Since we were interested in the respirable part of the aerosols, stage 4 particles were not collected in this modified way.

Sample Preparation

The two loaded KBr pellets on each stage were first weighed (W_1), then transferred to the capsule of a vibrating mill and ground for 3 minutes. In an earlier study,[15] it was found that this grinding step is sufficient to prevent particle-size and matrix effects on IR absorbance measurements as described in the literature. Duyckaerts[16] describes a dramatic effect of particle size on IR absorbance in the > 1-μm particle diameter range. Grinding was also performed on stage 1 samples to disperse probable agglomerates of single particles or amorphous masses in ambient and source samples,[17] and to provide a necessary dilution step to overcome the matrix effect by the soot content of the particles.[15] The homogenized samples were pressed into pellet form and weighed again (W_2). The ratio W_2/W_1 and the weight per spot (determined by the total weight and the number of spots on the Cu foil) permitted the calculation of the sample weight in the KBr pellet.

Standardization

$(NH_4)_2SO_4$ is generally considered to be the most abundant form of S(VI) compound in respirable airborne particles, although sampling artifacts

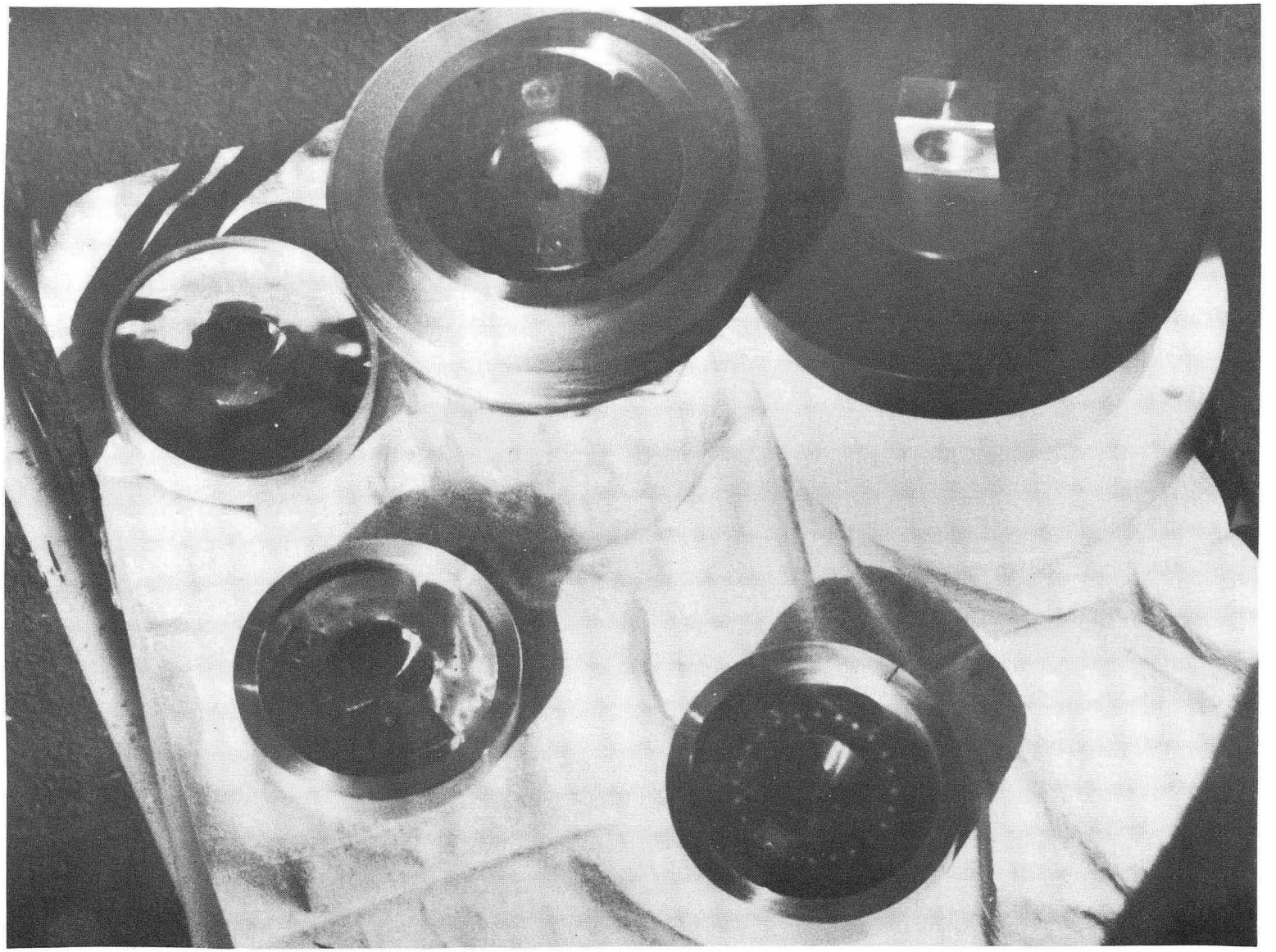

CBB 791-1072

Figure 1. Berner's ring jet impactor equipped with Cu foils and KBr pellets on stages 1, 2, and 3.

(neutralization) may enhance the $(NH_4)_2SO_4$ concentration even during sampling by impaction (Fig. 2). A working curve (Fig. 3) for the IR-spectroscopic determination of $(NH_4)_2SO_4$ was established by weighing different amounts of that substance, preparing KBr pellets according to the procedure described above, and measuring the respective absorbance values by FTIR spectroscopy (Nicolet 7199 FTIR-TGS detector; velocity of moving mirror, 0.227 cm/sec; resolution, 2 cm^{-1}; NDP, 8192; NTP, 16384; Happ-Genzel apodization; no smoothing). The actual amount of $SO_4^{=}$ in the aliquots of the samples analyzed was determined gravimetrically. An IR-spectroscopic nitrate determination of samples collected in Vienna on Cu foils has been developed[15] and should be easily adaptable to modified sampling.

Results

Figure 4 shows the IR spectra of samples with an obvious content of $(NH_4)_2SO_4$; and Table 1 shows the results of the quantitative evaluation of the $(NH_4)_2SO_4$ content of various samples, assuming that the sharp line located at 1110 cm^{-1} is due exclusively to this species. In general, the IR spectra of the aerosols collected in this work show more complexity in the sulfate region than do the IR spectra of $(NH_4)_2SO_4$. This is considered to be evidence of different degrees of acidity.[9] Based on the modified sampling technique described here, which allows a quantitative transfer of aerosol samples down to 1 μg from the collection surface to the final sample pellet, further model analyses will be carried out to elucidate the contribution to the atmospheric particulate burden of sulfate species other than $(NH_4)_2SO_4$.

Table 1. $(NH_4)_2SO_4$ determination on various aerosol samples.

Sample Site	Date	Stage	Particulate Loading (μg/m³)	Weight μg/m³ $(NH_4)_2SO_4$	Weight %$(NH_4)_2SO_4$
Lawrence Berkeley Laboratory	9/25/78	1	22.5	2.6	11.7
		2	24.8	1.6	6.3
		3	20.3	0.9	4.4
Fremont	11/02/78	1	19.2	2.1	10.7
		2	39.9	2.5	6.3
		3	9.9	(peak overlapping)	
Los Angeles	11/10/78	1	8.7	1.3	14.4
		2	12.5	4.0	32.1
		3	14.6	2.2	14.7
Tunnel	10/03/78	1	68	6.2	9.1

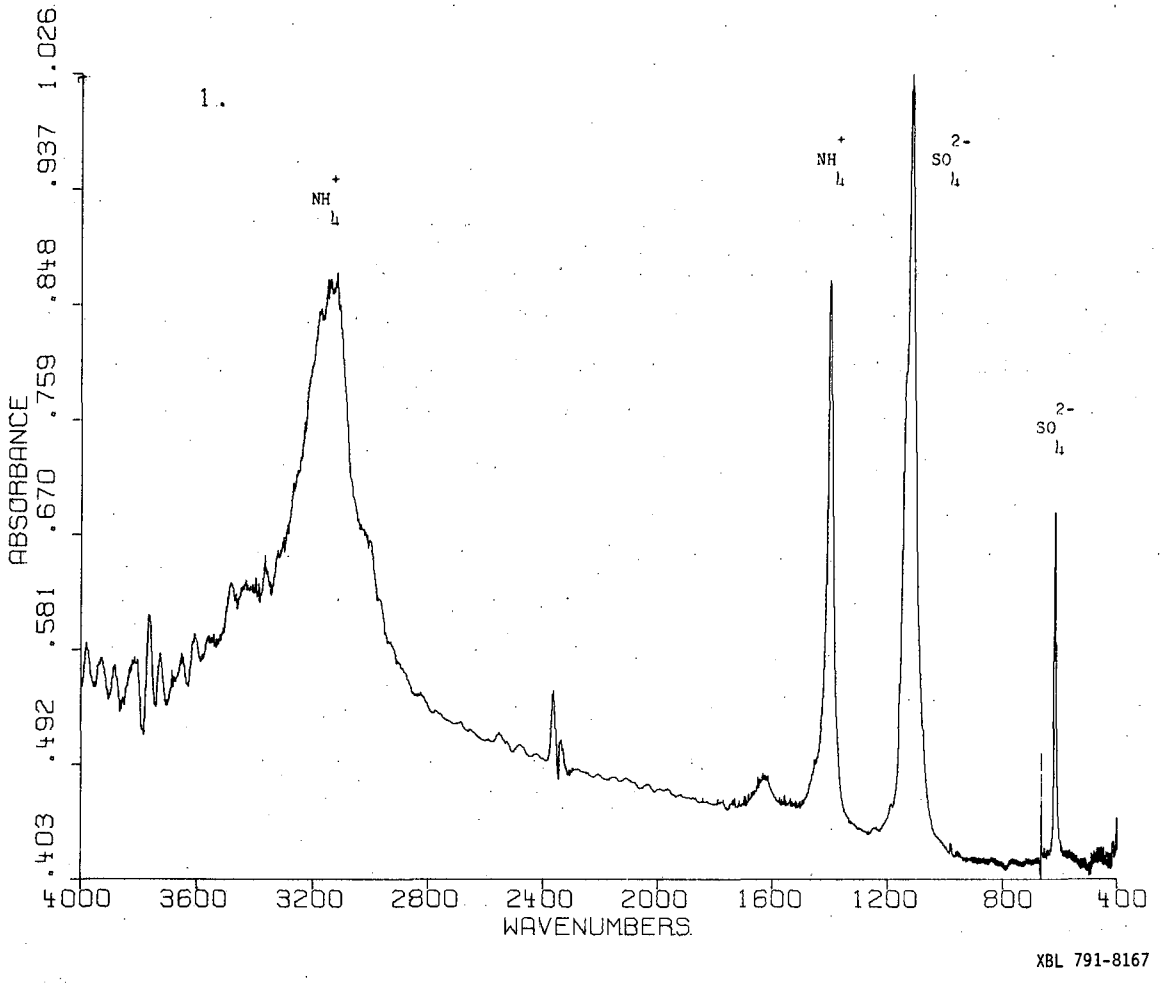

Figure 2. IR spectrum of 4.75-μg $(NH_4)_2SO_4$ in KBr.

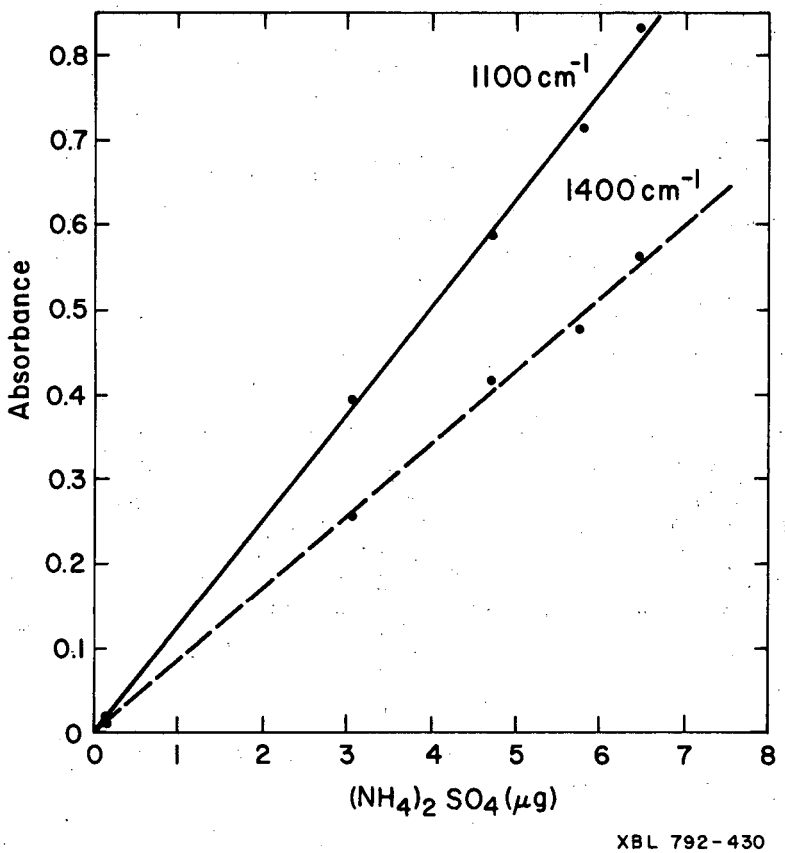

Figure 3. Working curve for an IR spectroscopic $(NH_4)_2SO_4$ determination.

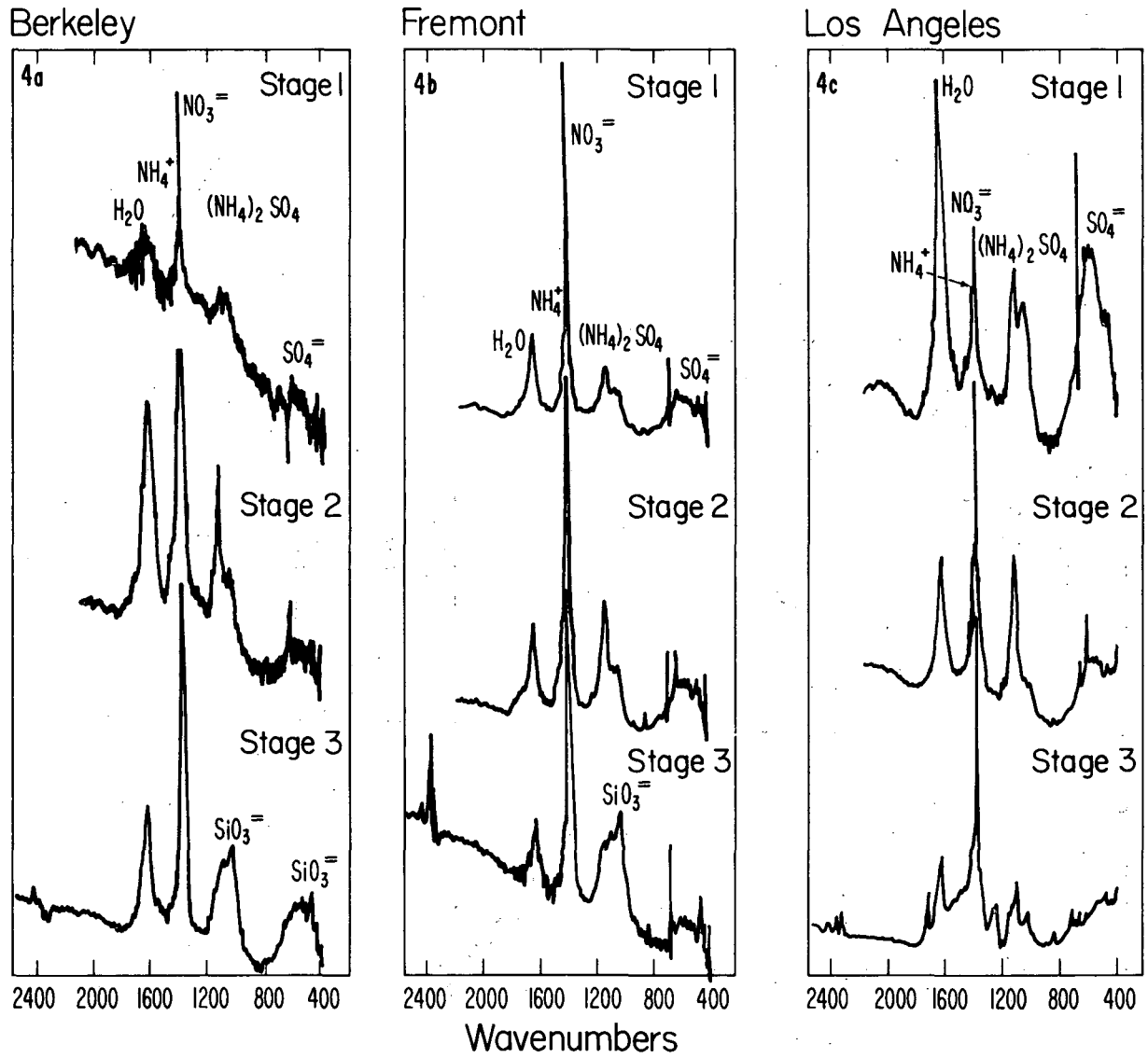

XBL 792-431

Figure 4. IR spectra of ambient samples collected on stages 1, 2, and 3 of Berner's impactor.

a. 9/25/78, 10:15am-4:15pm; air volume 26.6 m^3, heavily loaded air (100 μg part./m^3 on stages 1-4).

b. 11/2/78, 10:20am-2:25pm; air volume 18 m^3 (97 μg part./m^3 on stages 1-4).

c. 11/10/78, 2pm-5pm; air volume 13.2 m^2, relatively light loading (55 μg part./m^3 on stages 1-4).

References

1. National Air Sampling Network, 1964-1965, U.S. Dept. of Health, Education, and Welfare (Cincinnati, 1966).

2. T. Novakov, P.K. Mueller, A.E. Alcocer, and J.W. Otvos, "Chemical composition of Pasadena aerosol by particle size and time of day. III. Chemical states of N and S by photoelectron spectroscopy," in Aerosols and Atmospheric Chemistry, G.M. Hidy, ed. (New York, Academic, 1972).

3. C. Brosset, "Air-borne particles: Black and white episodes," Ambio 5, 157 (1976).

4. R. Kellner, "Infrared spectroscopy, extraction and chromatography," in Analysis of Airborne Particles by Physical Methods, H. Malissa, ed. (Miami Beach, CRC Press, 1978).

5. A.J. Blanco and G.B. Hoidale, "Microspectrophotometric technique for obtaining the infrared spectrum of microgram quantities of atmospheric dust," Atmos. Environ. 2, 327 (1968).

6. A.J. Blanco and R.G. McIntyre, "An infrared spectroscopic view of atmospheric particulates over El Paso, Texas," Atmos. Environ. 6, 557 (1972).

7. A. Mangia, "Determination of α quartz in atmospheric dust: A comparison between IR spectroscopy and X-ray diffraction techniques," Anal. Chem. 47, 927 (1975).

8. P.T. Cunningham, S.A. Johnson, and R.T. Yang, "Variations in chemistry of airborne particulate material with particle size and time," Environ. Sci. Technol. 8, 131 (1974).

9. P.T. Cunningham and S.A. Johnson, "Spectroscopic observation of acid sulfate in atmospheric particulate samples," Science 191, 77 (1976).

10. A. Berner, "Ein fuenfstufiger Kaskadenimpaktor zur Messung der Massen-Groessen-Verteilung von Aerosolen," preprint Chem. Eng. Tech. (in press).

11. H. Malissa, "Integrated dust analysis by physical methods," Angew. Chemie. Int. Ed. Engl. 15, 141 (1976).

12. H. Malissa, "Some analytical approaches to the chemical characterization of carbonaceous particulates," Proceedings, Conference on Carbonaceous Particles in the Atmosphere, Lawrence Berkeley Laboratory, Berkeley, California (in press).

13. M. Grasserbauer, H. Puxbaum, and O. Weiss, "Analysis of the respirable fraction of airborne particles collected by impactors," Z. anal. Chem. 291, 354 (1978).

14. H. Malissa, H. Puxbaum, and E. Pell, "Zur simultanen relativkonduktrometrischen Kohlenstoff- and Schwefelbestimmung in Stauben," Z. anal. Chem. 282, 109 (1976).

15. H. Malissa, R. Kellner, H. Puxbaum, and Ch. Thalhammer, "Integrated dust analysis, infrared techniques," paper presented at the 7th Ann. Symposium on the Analytical Chemistry of Pollutants, Lake Lanier Island, Georgia, April 1977.

16. G. Duyckaerts, "The infrared analysis of solid substances," Analyst 84, 201 (1959).

17. W.H. Benner and T. Novakov, "Solvent-extraction-aided morphology study (SEAMS)," this report.

Determination of Nitrogen in Atmospheric Aerosols by Proton Activation Analysis*

M. Clemenson, T. Novakov, and S.S. Markowitz

The X-ray fluorescence method, an important tool in the determination of heavy-element concentrations, is of little use for low-Z elements because of large X-ray absorptive effects and low fluorescence yields. Neutron activation analysis is also limited by low reaction cross sections and the unsuitability of the induced radioactivity for counting. Combustion analysis is a useful tool for the analysis of most of the important low-Z elements; however, it is not a very sensitive technique. It is also destructive of the sample and thus does not allow other analyses to be performed on the same sample. These difficulties have led us to develop a new method of determination of one of the low-Z elements, nitrogen, utilizing protons of sufficient energy to induce the $^{14}N(p,\alpha)^{11}C$ nuclear reaction. The radioactive decay of the 20.4-min ^{11}C is followed via its 0.511-MeV annihilation radiation. The method offers a simple approach to the problem of nitrogen analysis in atmospheric aerosols and is applicable to the routine analysis of these particles for nitrogen.

Irradiations were performed at the Lawrence Berkeley Laboratory 88-inch cyclotron. The initial energy of the proton beam was 16.0 MeV. Aluminum foils were placed in front of the sample foils to degrade the beam from the initial energy to the desired energy for each irradiation. The range-energy tables of Williamson, Boujot, and Picard were used to calculate the required aluminum thickness.[1] The length of bombardment was 1 minute and the average beam intensity was 1 μA. The targets were irradiated at different energies by the stacked-foil technique. The total charge received from the Faraday cup was measured by an integrating electrometer.

Counting

The irradiated samples were analyzed by detecting the 0.511-MeV positron annihilation radiation of ^{11}C using a high resolution Ge(Li) detector coupled to a computer-controlled 4096-channel analyzer with a magnetic tape unit. The Ge(Li) detector used for this work was manufactured by Ortec, Inc., and has an active volume of 60 cm^3. The decay of the 0.511-MeV γ-ray photopeak of an activated melamine target is shown in Fig. 1. The decay is a single component with a 20.4-min half-life corresponding to the decay of ^{11}C in the target. The decay curves were analyzed using the CLSQ computer code.[2]

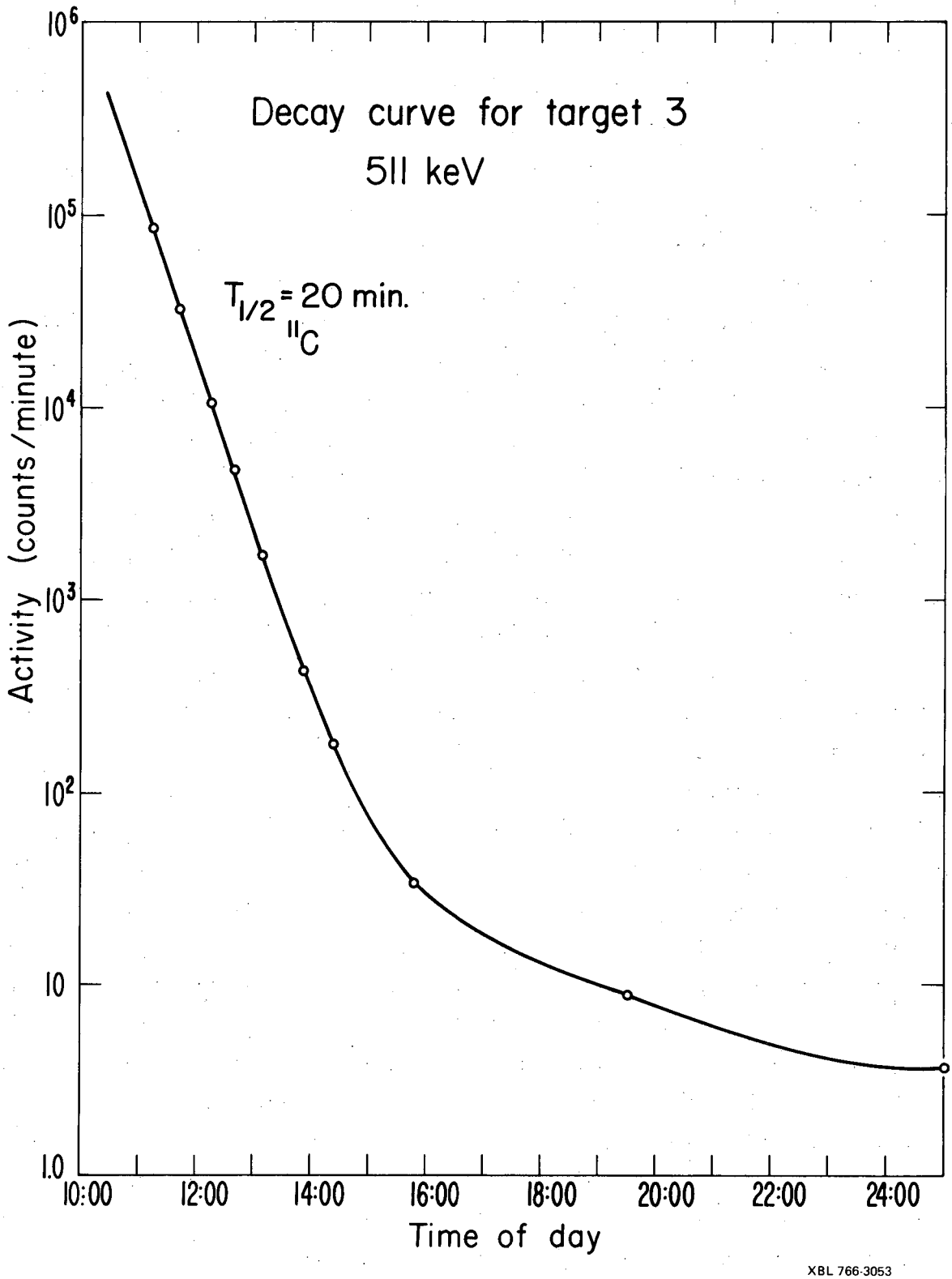

Figure 1. Decay curve of the 20-min ^{11}C annihilation radiation for a melamine target.

Aerosol Sample Analyses

Silver-membrane filters were used for the collection of the ambient aerosol. The aerosol loading was approximately 500 $\mu g/cm^2$ for a typical filter sample. Two filter samples were irradiated in a single stack at proton energies of 7.5 and 6.0 MeV. Following the "relative" method of activation analysis, we irradiated a melamine target, which was used as the nitrogen standard, in the same stack with the aerosol samples. The nitrogen standard was irradiated at a proton energy of 9.2 MeV. The decay of the 0.511-MeV annihilation peak was then followed for 3 or 4 hours. A typical decay curve for the integrated 0.511-MeV photopeak is shown in Fig. 2. There are four components present in the decay curve: (1) a 10.0-min component due to ^{13}N produced from the $^{16}O(p,\alpha)^{13}N$ and $^{13}C(p,n)^{13}N$ nuclear reactions, (2) a 20.4-min component from the $^{14}N(p,\alpha)^{11}C$ reaction, (3) a 109.8-min component due to ^{18}F produced by the $^{18}O(p,n)^{18}F$ reaction, and (4) a 6.5-hr component due to activation of the silver filter itself to produce ^{107}Cd by the $^{107}Ag(p,n)^{107}Cd$ nuclear reaction. By far the dominant component in this decay curve is the 20.4-min component, ^{11}C, which results from activation of the nitrogen in the aerosol. The amount of nitrogen present was calculated by comparing the A_0 value for the ^{11}C component in the aerosol to the A_0 value for the ^{11}C component in the nitrogen standard. Several blank filters were also analyzed for nitrogen and found to contain approximately 0.5 $\mu g/cm^2$; this is normally a very small known correction to the total nitrogen found.

Samples containing varying amounts of nitrogen were nondestructively analyzed using the proton activation method. The same samples were then analyzed for nitrogen using a destructive combustion method; the results of these analyses are summarized in Table 1. The samples can be divided into two groups. One group of samples was prepared in the laboratory by depositing either ammonium sulfate $(NH_4)_2SO_4$, or ammonium oxalate, $(NH_4)_2C_2O_4$, on a silver membrane filter. These samples correspond to the first nine listed in Table 1. The second group of eight samples is composed of ambient aerosols collected in the San Francisco Bay Area under widely varying atmospheric conditions.

The comparison of the nitrogen found by proton activation analysis and that found by the independent combustion method shows an average percent difference of 14% for the 17 samples analyzed. This difference is essentially the same whether one compares only the laboratory-prepared samples or the ambient samples. It should also be noted that the agreement between the two methods holds over a range which spans two orders of magnitude in nitrogen concentration.

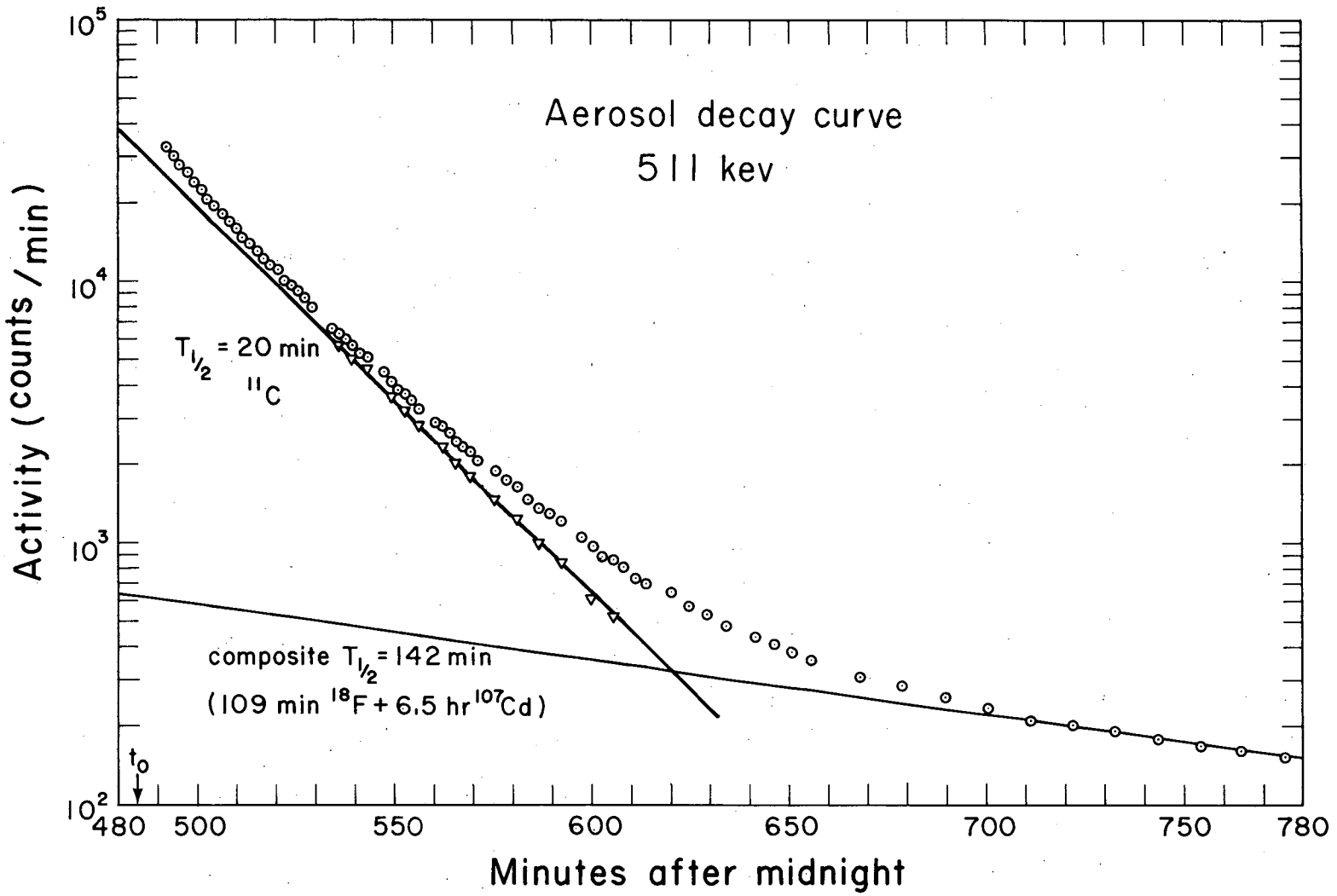

Figure 2. Decay of the 511-keV annihilation radiation intensity with time following proton irradiation of an atmospheric aerosol sample. Length of bombardment = 1 min, at a beam intensity of 1 μA.

0 0 0 0 5 3 0 1 3 6 8

Table 1. Comparison of methods for nitrogen determination in atmospheric aerosols.[a]

Sample	N found, μg/cm^2 Proton activation	Combustion
AS-1	129	144
AS-2	110	130
AS-3	326	368
AS-4	68	52
AO-1	162	147
AO-2	210	207
AO-3	261	279
AO-4	134	143
AO-5	136	133
AA-1	4.0	3.5
AA-2	8.0	6.5
AA-3	15	13
AA-4	76	99
AA-5	16	18
AA-6	59	59
AA-7	36	37
AA-8	46	54

[a]AS are the laboratory-prepared ammonium sulfate samples; AO, the laboratory-prepared ammonium oxalate samples; and AA, the ambient aerosol samples.

References

1. C.F. Williamson, J.P. Boujot, and J. Picard, Tables of Range and Stopping Power of Chemical Elements for Charged Particles of Energy, 0.05 to 500 MeV, Report CEA-R 3042, Centre d'Etudes Nucléaires de Saclay, France, (1966).

2. J.B. Cumming, "CLSQ, the Brookhaven decay curve analysis program," in Applications of Computers to Nuclear and Radiochemistry, G.D. O'Kelly, ed., Nuclear Science Series NAS-NS 3107 (National Academy of Science-National Research Council, 1963).

*Paper presented at the 176th National Meeting of the American Chemical Society, Miami Beach, Florida, Sept. 9-14, 1978, by SSM. Full paper, as LBL-8446, submitted to Analytical Chemistry, November 1978.

A Size-Segregating Aerosol Sampler

A.D.A. Hansen, R.C. Schmidt, and T. Novakov

Introduction

A routine daily ambient aerosol sampling program was established in mid-1977 with stations at Lawrence Berkeley Laboratory, Fremont (some 40 miles south of Berkeley), and Anaheim (in the Los Angeles area). To further investigate the nature and chemical composition of the aerosol, it was decided to deploy size-segregating samplers at sites widely separated in terms of both location and environment. As part of this program, 12 aerosol samplers were designed and constructed at LBL to the following requirements:

1. To collect two parallel samples on prefired quartz fiber and Millipore filters.
2. To require a minimum number of operations when changing filters.
3. To have the option of complete aerosol collection or size-segregated collection (exclusion of particles of diameter $\geq$ 1.5 μm).
4. To give an airflow rate of 1 to 2.5 m^3/cm^2-day through each filter, necessary to obtain suitable deposition for 24-hour samples of ambient air with carbon loadings in the range 5-30 $\mu g/cm^2$.
5. To be small, self contained, and lightweight.

The option of size segregation is achieved in this sampler by the use of a Nuclepore prefilter membrane to exclude large particles. The filtration properties of Nuclepore have been extensively studied[1,2]: at moderate face velocities, the mechanisms of impaction and interception remove from the air-stream most particles larger than a certain cut point, whose size depends on the prefilter pore size and the airstream's face velocity. The LBL sampler uses a Nuclepore prefilter of 8-μm pore size and face velocities in the range of 2 cm/sec to 5 cm/sec (see Table 1), resulting in the effective retention on the prefilter of particles of diameter greater than 1.5 μm (see Fig. 1). Optimum prefilter performance is achieved at these face velocities, many times smaller than the face velocities desired for adequate deposition on the sample-collecting filters. A size-analyzing sampler has been constructed by Cahill et al.[3] on the principles of sequential filtration, but uses a prefilter of the same size as the sample-collecting filter. By employing a prefilter of much larger diameter than the sample-collecting filters, we satisfy the face

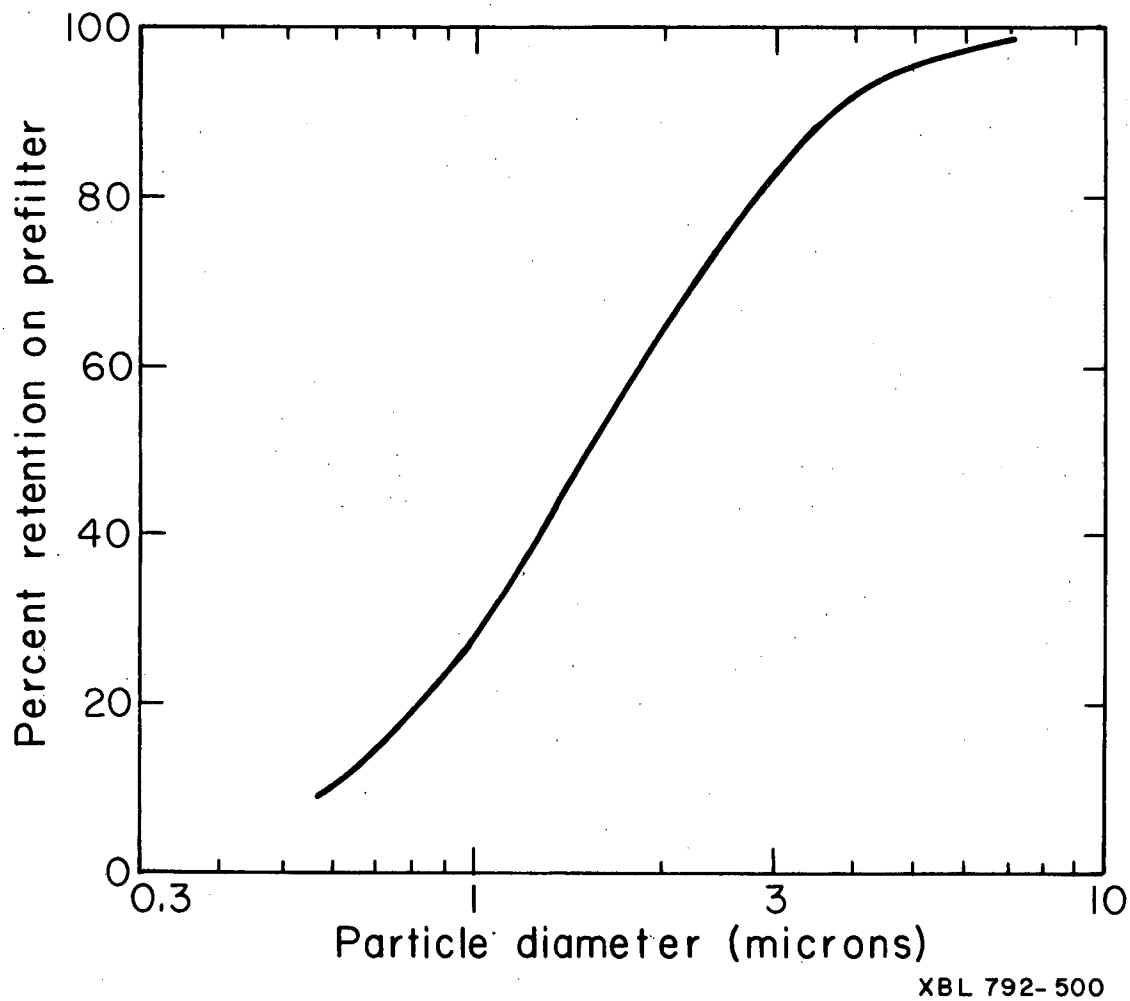

Figure 1. Filtration efficiency of 8-μm pore size Nuclepore prefilter as a function of particle size. Measurements were performed at prefilter face velocity of 4.0 cm/sec on monodisperse DOP particles produced by a vibrating-orifice aerosol generator.

velocity requirements as well as greatly increasing the lifetime of the prefilter against clogging.[4] In addition to incorporating these significant design improvements, the sampling head is constructed in such a way that with only one moving part, it locates the sample-collecting filters on their backing frits and clamps them by the pump suction acting on a pressure plate. While the pump is operating and the head top is in place, the filters cannot be accidentally dislodged or contaminated by touching. The filters may be either loose or mounted in 2"x2" slide frames, which allows for insertion and removal without tweezers or clean-handling procedures. All these features are attractive for unattended use with filter changing performed by unskilled personnel.

Table 1. Relationship of face velocity to flowrates.

Filter flowrate	1.0	1.5	2.0	2.5	m^3/cm^2-day
Filter face velocity	11.6	17.4	23.2	29.0	cm/sec
Prefilter face velocity	2.1	3.1	4.1	5.2	cm/sec

A photograph and diagrams of the sampler are shown in Figs. 2, 3, and 4. In the full-collection mode, the top prefilter membrane is omitted. The weather-shield, insect screens, and prefilter support frit prevent entry of rain, insects, etc.; but all suspended particulates are collected by the filters. For size-segregated collection, the prefilter is placed on top of the sample head, resulting in an effective cut-off for particles of diameter greater than 1.5 μm (see Fig. 1). This ensures collection of the majority of anthropogenic particulates, with the exclusion of windblown dust, pollen, etc. Under normal operating conditions in relatively dust-free locations, each prefilter can be used for one week without appreciable clogging.

Method of Operation (Fig. 3 and Table 2)

Air enters the sampler through the Nuclepore prefilter B, supported by its frit M. Face flow velocities through the prefilter range from approximately 2.1 cm/sec to 5.2 cm/sec for the flowrates used (see Table 1). Particles of diameter larger than about 1.5 μm are effectively retained by the prefilter (see Fig. 1). At the low flow rates involved, the pressure drop across the prefilter is normally extremely small, so the air in the upper chamber O is at essentially atmospheric pressure.

This prefiltered air then passes through the quartz and Millipore filters mounted on their frits P. The range of flowrates employed results in face

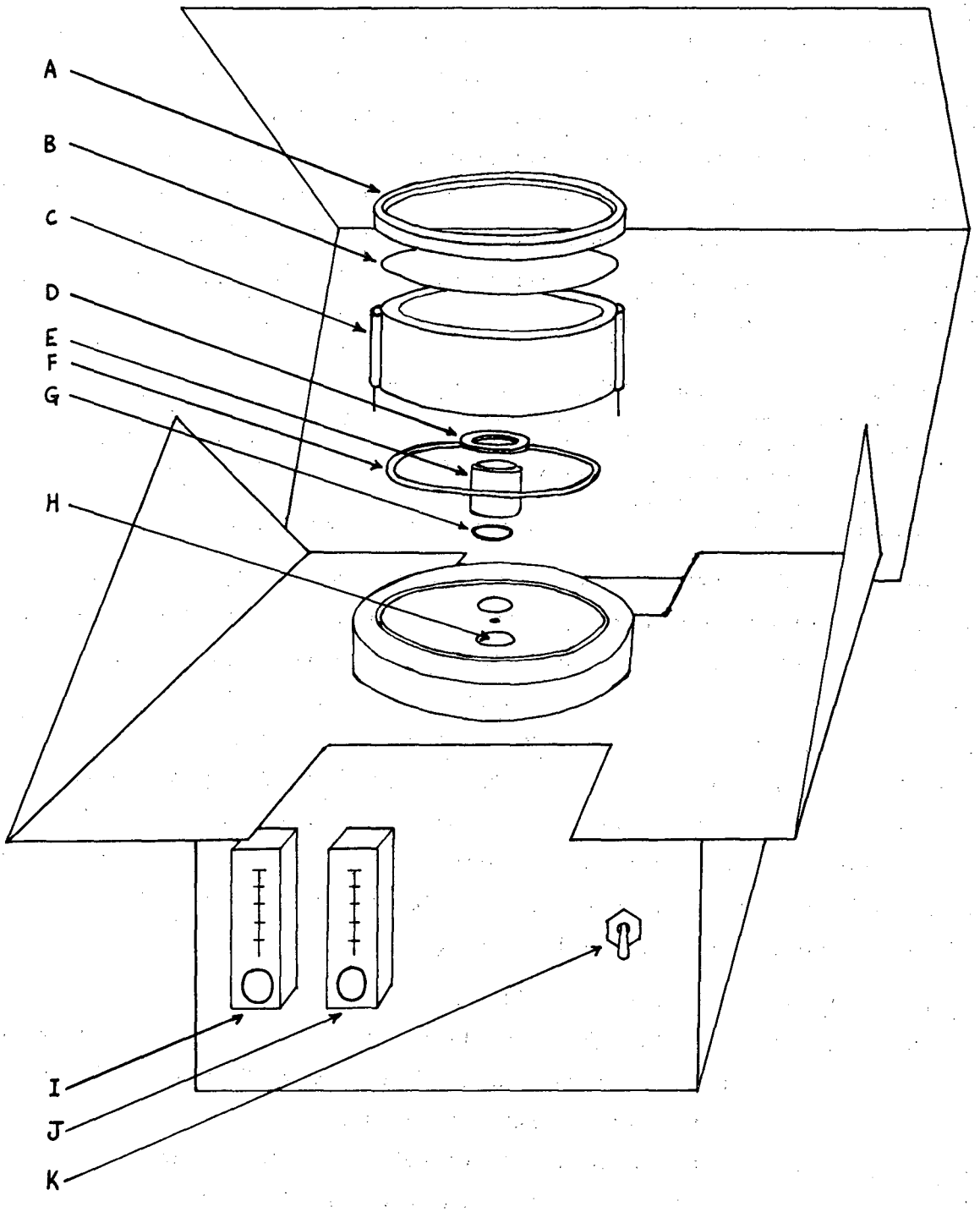

XBL 792-8300

Figure 2. Exploded diagram of the sampler.

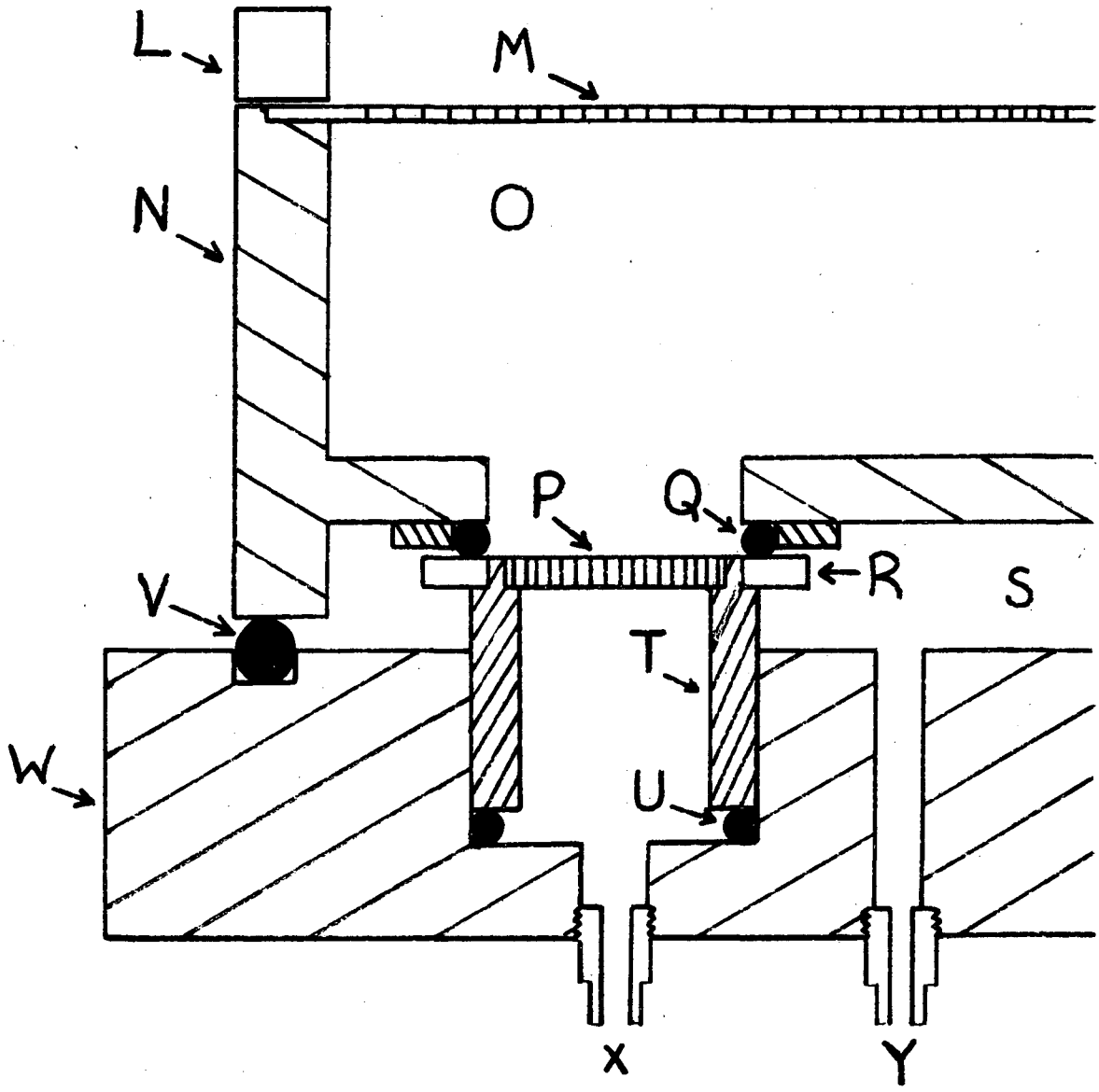

XBL 792-8301

Figure 3. Sectional drawing of one side of the sampler head (not to scale).

CBB 791-106

Figure 4. Size-segregating aerosol sampler.

velocities varying from 11.6 cm/sec to 28.9 cm/sec through these filters. Pump suction, applied via the rotameter and needle valve by connection X to the filter chamber T, results in a reduction of pressure downstream of the filter. Because of the reduced pressure within the flowmeters, flow calibration curves are supplied with each unit and must be used instead of the rotameter readings.

Table 2. Parts lists for Figures 2 and 3.

Figure 2:	Figure 3:
A - prefilter clamp ring	L - prefilter clamp ring
B - Nuclepore prefilter	M - prefilter support frit
C - upper chamber	N - upper chamber body
D - adapter ring (2)	O - upper chamber space
E - frit tube (2)	P - filter support frit
F - outer o-ring (2)	Q - filter clamp o-ring
G - frit tube lower o-ring (2)	R - adapter ring
H - frit tube hole in baseplate (2)	S - vacuum space
I - rotameter and needle valve for quartz filter station	T - frit tube
	U - frit tube lower o-ring
J - rotameter and needle valve for Millipore filter station	V - outer o-ring
	W - baseplate
K - main power switch	X - filter suction connection via rotameter and needle valve
	Y - clamping vacuum connection

Full pump vacuum is applied through port Y to space S, which is sealed by o-rings V, Q, and U. Since the pressure in the upper chamber O is essentially atmospheric, this causes the upper chamber body N to be firmly clamped to the baseplate W.

The filters are clamped and sealed on the frits P and adapter rings R by means of the o-ring Q. Sufficient compressibility is available from this o-ring and the lower o-ring U to accommodate filters of slightly varying thicknesses.

The pump used is an oil-less rotary carbon vane type, driven by an AC induction motor. Exhaust air from the pump itself is filtered before discharge into the atmosphere, so no recirculation contamination is anticipated. A fan draws air through the box louvres to cool the motor.

A tubular bulb mounted above the air intake warms the incoming air and the prefilter sufficiently to prevent dew condensation on the Nuclepore at night. Excessive condensation can effectively plug the Nuclepore, resulting in a destructively large vacuum in the upper chamber O. The upper chamber vacuum is monitored by a vacuum sensing switch in the main chassis, so that a pressure drop

of more than about 2 PSI in the upper chamber causes the motor to be turned off and to stay off until the main power switch is reset.

To date, eight units have been sent out. The returned samples appear to be of good quality, and routine analysis shows no evidence of contamination or sampler artifacts.

References

1. K.R. Spurny, J.P. Lodge, E.R. Frank, and D.C. Sheesley, "Aerosol filtration by means of Nuclepore filters," Environ. Sci. Technol. 3, 453 (1969).
2. O.T. Melo and C.R. Phillips, "Aerosol size spectra by means of Nuclepore filters," Environ. Sci. Technol. 9, 560 (1975).
3. T.A. Cahill et al., "Analysis of respirable fractions in atmospheric particulates via sequential filtration," J. Air Pollut. Contr. Ass. 27, 675 (1977).
4. K.R. Spurny, J. Harlova, J.P. Lodge, E.R. Ackerman, and D.C. Sheesley, "Aerosol filtration by means of Nuclepore filters: filter pore clogging," Environ. Sci. Tech. 8, 758 (1974).

PHYSICAL AND CHEMICAL CHARACTERIZATION: PHYSICAL

Optical Characterization of Ambient and Source Particulates

A.D.A. Hansen, H. Rosen, R.L. Dod, W.H. Benner, and T. Novakov

Introduction

Characterization of the ambient carbonaceous aerosol in terms of its primary and secondary components is essential if meaningful control strategies are to be devised. Primary carbonaceous particulate material is defined as that emitted directly from anthropogenic sources, usually combustion. It contains extractable organic matter and nonextractable material, including "graphitic" soot. Secondary carbonaceous particulate material is material originally emitted in a gaseous state that has been transformed into a particulate state by atmospheric processes. Examples of these processes are (1) the accretion by adsorption of vapors onto the surface of primary particles, and (2) gas-to-particle conversion reactions whose occurrence in the atmosphere has been postulated under highly photochemically active conditions. If primary particulate material is dominant in the ambient aerosol, then particulate air pollution abatement strategies should include particulate emission control. If secondary particulate material dominates, emphasis should be on the control of the gaseous precursors involved in these secondary reactions. Due to the complex nature of the ambient aerosol, it has been a difficult analytical problem to clearly distinguish the contributions from these two sources of particulate carbon.

The most striking feature of filter deposits collected in urban environments is their dark coloration, which we believe is due to the strongly absorbing primary "graphitic" soot component. We assume that secondary reactions cannot produce this material. The "graphitic" component of filter-collected particulates may be conveniently measured because of its large optical absorption and used as a tracer for primary carbonaceous particles. In this paper we report on the optical characterization of a statistically large number of ambient and source samples taken under a wide range of conditions.

Our central result is that primary material appears to compose a major fraction of the ambient carbonaceous aerosol studied in two California air basins under widely varying conditions. Furthermore, we have seen no evidence for the significant production of secondary carbonaceous particulate matter in correlation with the ozone concentration, a conventional indicator of photochemical activity.

Experimental Details

Sample Collection

Ambient aerosol samples have been collected daily since 1 June 1977 at Lawrence Berkeley Laboratory, Berkeley, California; since 15 July 1977 at the Bay Area Air Quality Management District monitoring station, Fremont, California; and since 19 August 1977 at the Southern California Air Quality Management District monitoring station, Anaheim, California. Samples were also taken from 23 March 1978 to 9 April 1978 at Argonne, Illinois. All these samples were taken in parallel on 47-mm diameter Millipore filter membranes (1.2-μm nominal pore size, type RATF) and prefired quartz fiber filters (Pallflex type 2500 QAO). The monitored flow rates varied between 1.0 and 2.6 m^3/cm^2-day (i.e., 0.24 to 0.62 CFM for the total exposed filter area of 9.6 cm^2), corresponding to face velocities of 11.6 to 30.1 cm/sec. The samples were not size segregated, but the filter holders faced vertically downward to avoid settling deposition of dust, etc. Three-day samples collected over each weekend are not included in the data presented. The samples spanned almost the entire range of weather and pollution conditions; to date, in excess of 900 filter pairs have been analyzed.

A number of representative sources have also been sampled. About 100 analyses have been made of the following particulate emissions: (1) exhaust collected in a freeway tunnel under conditions of moving traffic with few diesel trucks; (2) automobile exhaust collected in an underground parking garage under start-stop driving conditions with no diesel trucks; (3) exhaust from a small 2-stroke engine; (4) exhaust from a small 4-stroke diesel engine; and (5) stack samples from a natural-gas-fired domestic water heater.

Optical Attenuation Measurement

Both source and ambient aerosol samples have a large and uniform optical absorption throughout the visible spectral region; the dark coloration of the exposed filters is due to the "graphitic" soot component.[1,2] The attenuation measurements are made by a laser transmission method on samples collected on Millipore filter membranes. The quantity recorded is defined as

$$ATN = -100 \ln (I/I_0) \qquad (1)$$

where I_0 is the intensity of light transmitted through a blank Millipore filter, and I is that through the loaded filter.

Carbon Analysis

The carbon loading on the quartz fiber filters is determined by a total combustion/CO_2 evaluation method.[3] The filters are prefired overnight at 800°C to remove all combustible carbon before sample collection. Periodic analysis of blanks typically yields about 0.5 μg C/cm^2 compared with loadings after exposure in the range 20-100 μg C/cm^2.

Optical Attenuation Characterization

Theory

As shown in Refs. 1 and 2, the dark coloration of ambient and source samples can be ascribed to the "graphitic" component of the carbonaceous particulates. We assume that a quantitative relationship between the optical attenuation and the "graphitic" carbon component can be written as

$$[\mathrm{GRAPH}] = (1/K) \times \mathrm{ATN} \ . \tag{2}$$

In addition to "graphitic" soot, primary particulate material also contains organic material, which is not strongly optically attenuating. The total amount of carbon is

$$[\mathrm{C}] = [\mathrm{GRAPH}] + [\mathrm{ORG}] \ . \tag{3}$$

A fundamental characterization of a particulate sample is given by its attenuation per unit mass, i.e., its specific attenuation, σ, since this is a measure of the fraction of "graphitic" carbon to total carbon:

$$\sigma \equiv \mathrm{ATN}/\mathrm{C} = K \times [\mathrm{GRAPH}]/[\mathrm{C}] \tag{4}$$

Measurements of the specific attenuation of numbers of source samples give insights into the relative graphitic-to-total-carbon fraction of primary emissions and the source variabilities.

The ambient aerosol contains primary carbonaceous particulates (from a large number of individual sources) and secondary material (as defined in the introduction). The total optical attenuation and total particulate carbon mass are then given by a summation over all components, i.e.,

$$\mathrm{ATN}_T = \sum_i \mathrm{ATN}_i \tag{5}$$

$$\mathrm{C}_T = \sum_i \mathrm{C}_i$$

and the specific attenuation of the ambient sample is

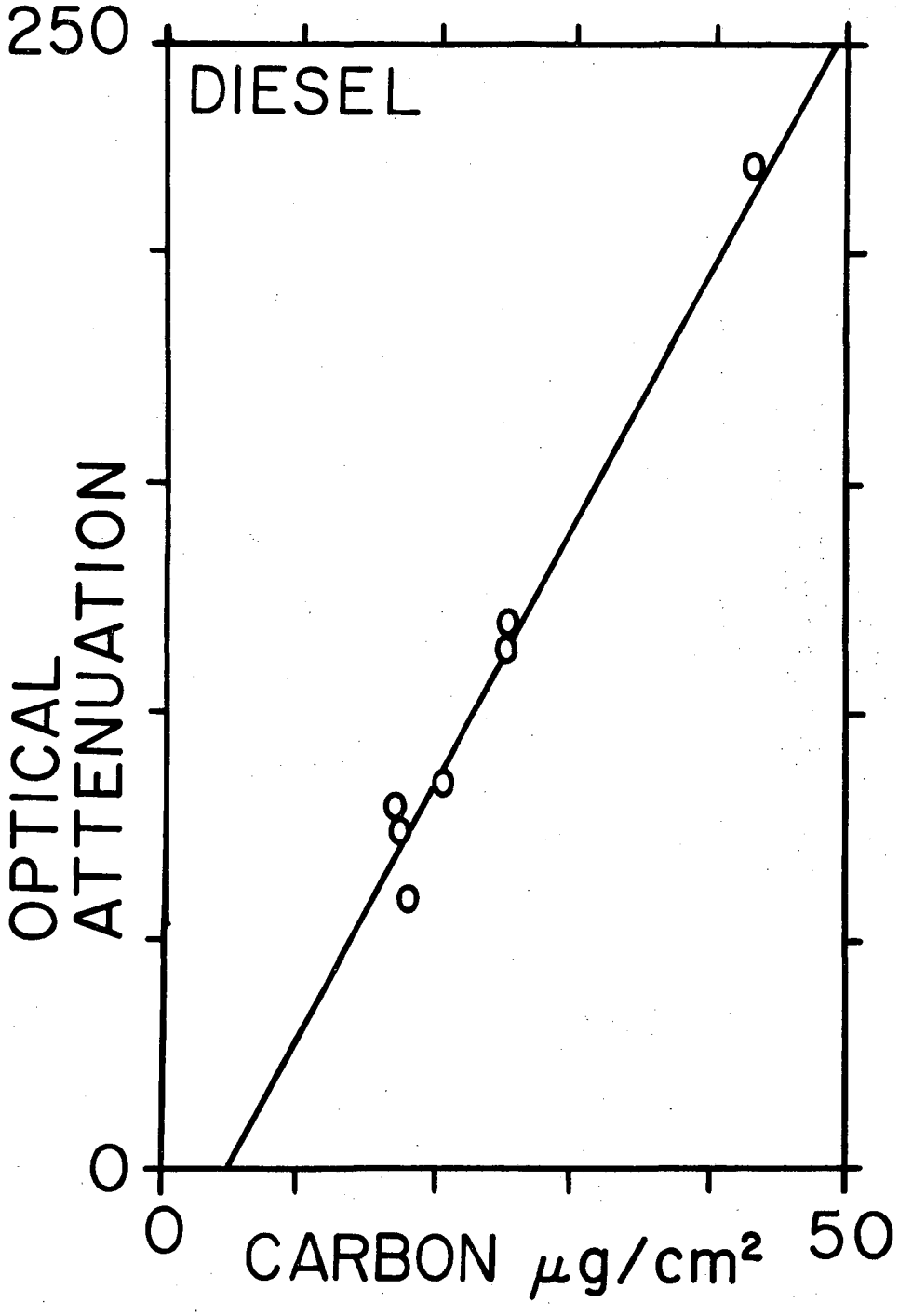

XBL 788-9881

Figure 1. Optical attenuation versus carbon loading for samples of diesel exhaust particulates from an engine running at constant speed under constant load. Least-squares fit line shown.

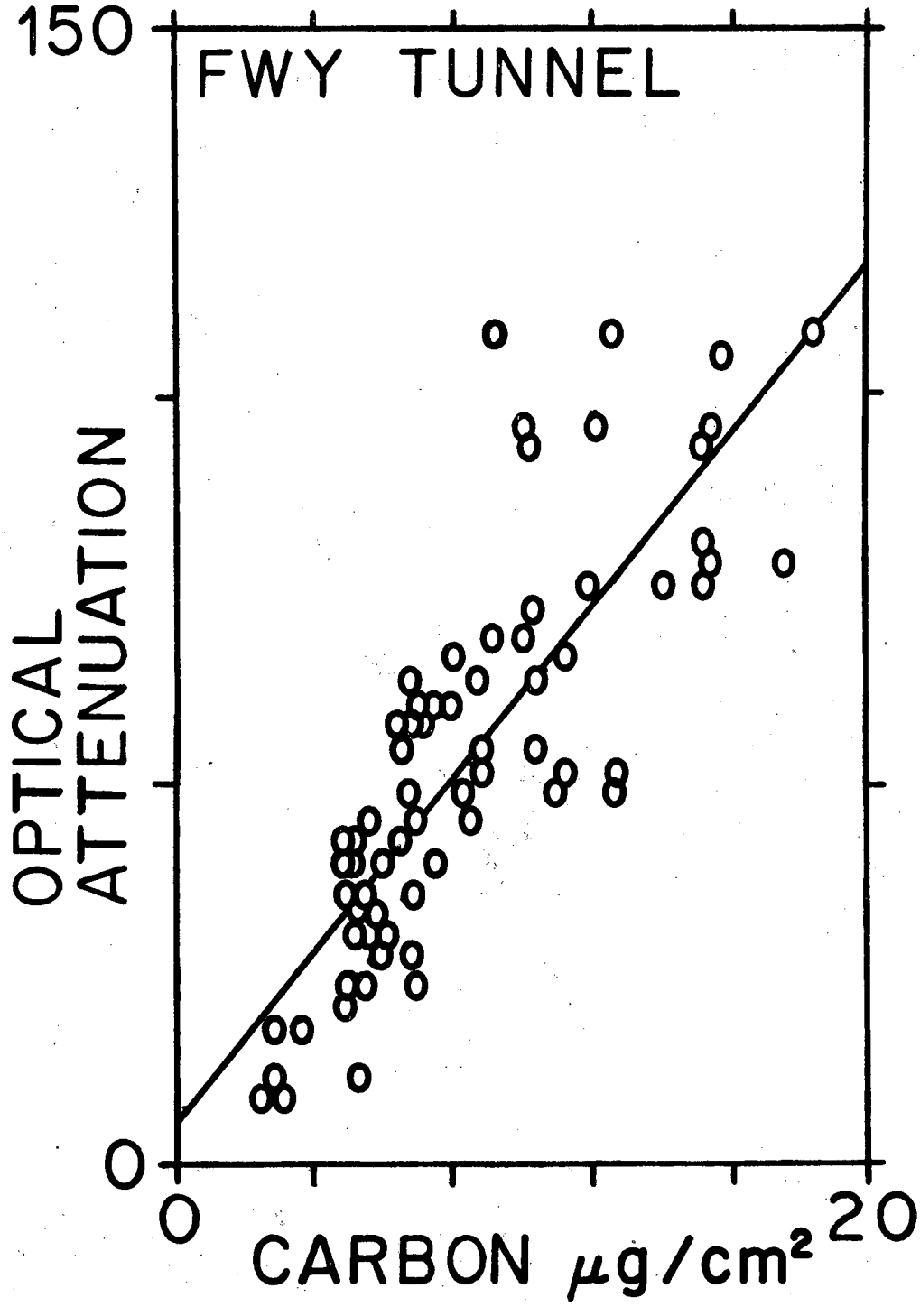

XBL 788-9882

Figure 2. Optical attenuation versus carbon loading for samples of vehicle exhaust particulates obtained in the vent bore of a freeway tunnel. Least-squares fit line shown.

$$\sigma_T = (ATN/C)_T = \frac{\sum_i ATN_i}{\sum_i C_i} = \frac{\sum_i \sigma_i C_i}{\sum_i C_i} \qquad (6)$$

In other words, the specific attenuation of an ambient sample is an average of the specific attenuations of all its components, weighted according to the mass of carbon they each contribute.

Secondary material will not contain a "graphitic" component and therefore should not appreciably increase the total optical attenuation; its value of σ is very small. However, it does increase the total mass of carbon, and will therefore reduce the graphitic-to-total-carbon fraction and dilute the specific attenuation of the ambient sample. This is seen in Equ. (6) as the addition of secondary contributors, is, where σ_{is} is zero but C_{is} is non-zero. The presence of large amounts of secondary carbonaceous particulate material in the ambient aerosol will have the effect of reducing the specific attenuation of ambient samples relative to that of source samples.

Results

Results on source samples. We first present quantitative support for the assumption of Equ. (2) that the optical attenuation of a particulate sample collected on a filter (i.e., the degree of its dark coloration) is proportional to the total carbon loading. This occurs if the "graphitic" soot component, responsible for the coloration, constitutes a constant fraction of the total amount of particulate carbon. Figure 1 shows results from one series of samples taken from a small diesel engine under identical load and speed conditions. The correlation between optical attenuation and total carbon loading is extremely good ($r = 0.99$) even up to heavy loadings, giving a constant specific attenuation of $\sigma = 5.6$. In contrast, Fig. 2 shows the results for a number of freeway tunnel samples spanning a wide range of traffic conditions. Although a similar correlation obviously exists, it is clear that the specific attenuation of these samples shows a greater variability (ranging from $\sigma = 3.75$ to $\sigma = 12.5$). We postulate that this is due to a varying fraction of "graphitic" soot to total particulate carbon in the mix of exhaust, depending on the mix of vehicles and driving conditions. Similar results have been obtained for the other sources: in all cases, samples of different loadings taken under identical source conditions show good correlation, while samples of mixed composition show more variability.

Results on ambient samples. In view of the variability of specific attenuation shown by source samples, the uniformity of results obtained from ambient samples is remarkable. Figure 3 shows optical attenuation vs. carbon loading for the samples collected at Berkeley, Fremont, Anaheim, and Argonne. All the graphs have the same scale of axes, enabling direct comparison and determination of the following very important results.

1. There is a strong correlation ($r > 0.85$) between optical attenuation and total suspended particulate carbon mass at every site.

2. The mean specific attenuation, i.e., the coefficient of this proportionality, is virtually identical at each site.

Discussion

Source and Ambient Samples' Specific Attenuation Results

The diesel source results show that the method of optical attenuation can indeed be used as an accurate quantitative measure of total particulate carbon mass for samples from individual sources under constant operating conditions, i.e., a presumed constant fraction of "graphitic" soot to total particulate carbon. The freeway tunnel results show that the net value of σ_T for an aerosol derived from many sources can vary according to the mix of contributions (C_i) and characteristics (σ_i) of each source. The ambient air contains material from a very large number of primary and secondary sources covering the entire spectrum of "graphitic" content (i.e., of σ); if the patterns of daily input remain approximately constant, the net composition of our 24-hour samples may also remain constant. This, we believe, is the basic explanation for the results obtained from the ambient sampling program. Result (1) shows that for a particular site it is possible to estimate the amount of total suspended particulate carbon with a root mean square error of 25% by means of the very simple measurement of optical attenuation. Furthermore, this is true independent of season, meteorology, or conventional air pollution indicators. This remarkable result implies that the fraction of "graphitic" soot to total particulate carbon is approximately constant under all circumstances studied.

The specific attenuation distribution of samples collected during summer pollution episodes in Anaheim is virtually identical to that of samples collected in Berkeley on extremely clear winter days, or in Argonne in winter, although the loading of these samples varied widely (from 2.9 μg C/m^3 to 52.4 μg C/m^3). Because the specific attenuation σ reflects only the aerosol's fractional "graphitic"

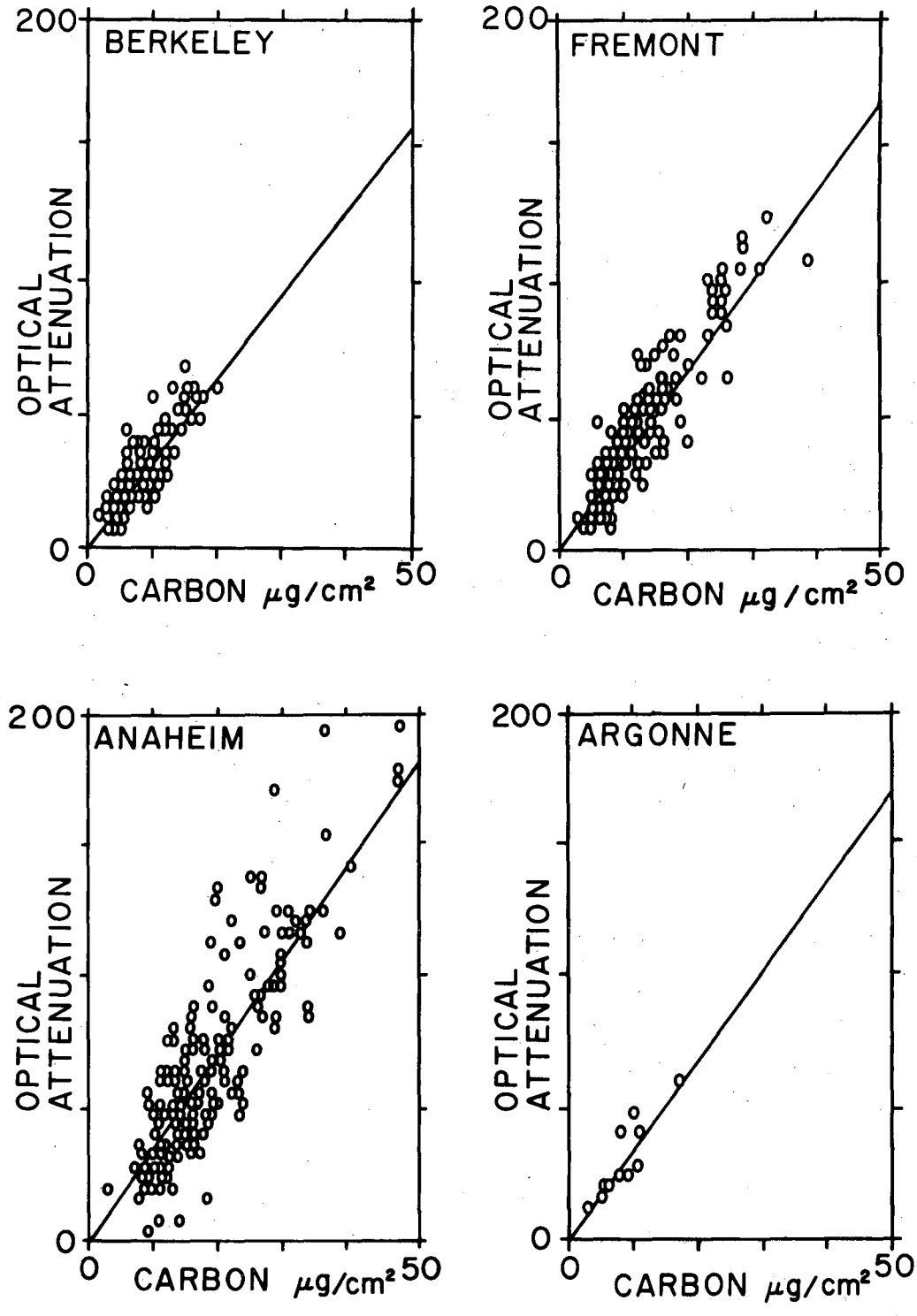

XBL 788-9886

Figure 3. Optical attenuation versus particulate carbon loading for ambient samples collected at Berkeley, Fremont, Anaheim, and Argonne. Least-squares fit line shown. Note same scale of axes on graphs.

composition, this result implies that the fraction of "graphitic" soot to total carbon in all these locations is approximately equal and constant.

The range of values of specific attenuation measured on ambient samples is overlapped by the range measured on source samples. This implies that the "graphitic" fraction of the ambient aerosol is similar to that of a representative mixture of primary emissions.

Secondary Particulate Carbon

The category of secondary carbon includes particulates formed from precursor gases in gas-to-particle conversion reactions in the atmosphere. Most of the proposed reactions responsible for the formation of secondary organic particles involve ozone as a reactant. If ozone-related atmospheric reactions were a substantial contributor of secondary particulate carbonaceous material in the ambient aerosol, we would expect larger contributions of this material on days characterized by higher ozone concentrations. This secondary material cannot contain a "graphitic" component and so would have a low specific attenuation, thereby diluting the total ambient aerosol's attenuation. The specific attenuation of the ambient aerosol on days characterized by high ozone levels would be expected to be lower than on days with low ozone levels.

Figure 4 shows the distribution of specific attenuation of ambient samples from all sites taken together, subdivided according to peak hour ozone concentration. Clearly, there is little indication that high-ozone days are characterized by aerosols of strongly diluted attenuation. Furthermore, the maximum correlation coefficients of peak hour ozone concentration and specific attenuation at any individual site or all samples taken together are only $r = 0.24$ and $r = 0.11$ respectively. This places a rather low limit on the maximum importance of secondary carbonaceous particulates formed in ozone-related atmospheric reactions.

Figure 5 shows the average diurnal cycles of specific attenuation for samples collected at the same time of year in Berkeley (relatively clean conditions, average particulate carbon loading, 5.7 $\mu g/m^3$) and Riverside, California (severe air pollution conditions, 33.2 $\mu g/m^3$ average particulate carbon loading). These cycles, averaged over many days, are essentially identical in form and magnitude in spite of very different atmospheric chemical conditions at the two sites, including an average peak 1-hr ozone concentration of 240 ppb in Riverside vs. < 30 ppb in Berkeley. Certainly there is no evidence for the dilution of the specific attenuation of the Riverside aerosol relative to the Berkeley aerosol

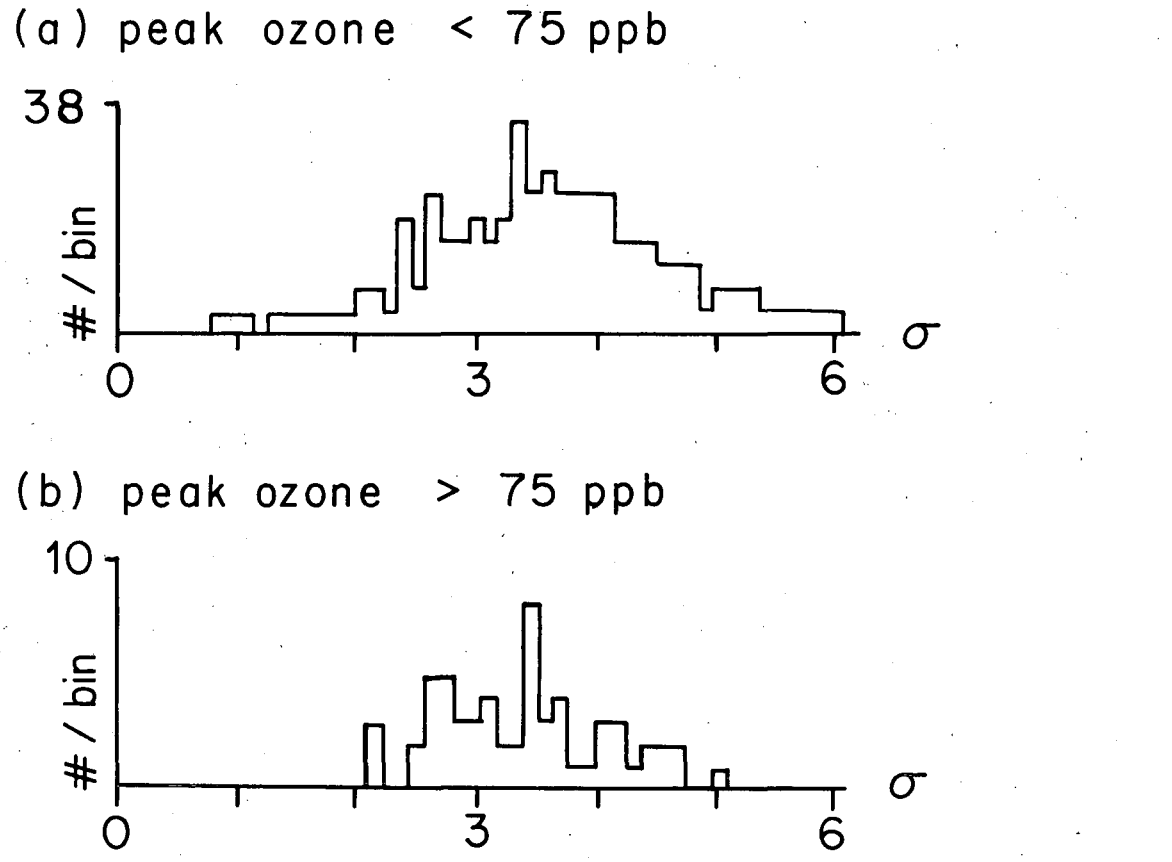

XBL 788-10619

Figure 4. Distribution of values of specific attenuation of ambient particulate samples, subdivided according to peak hour ozone concentration.

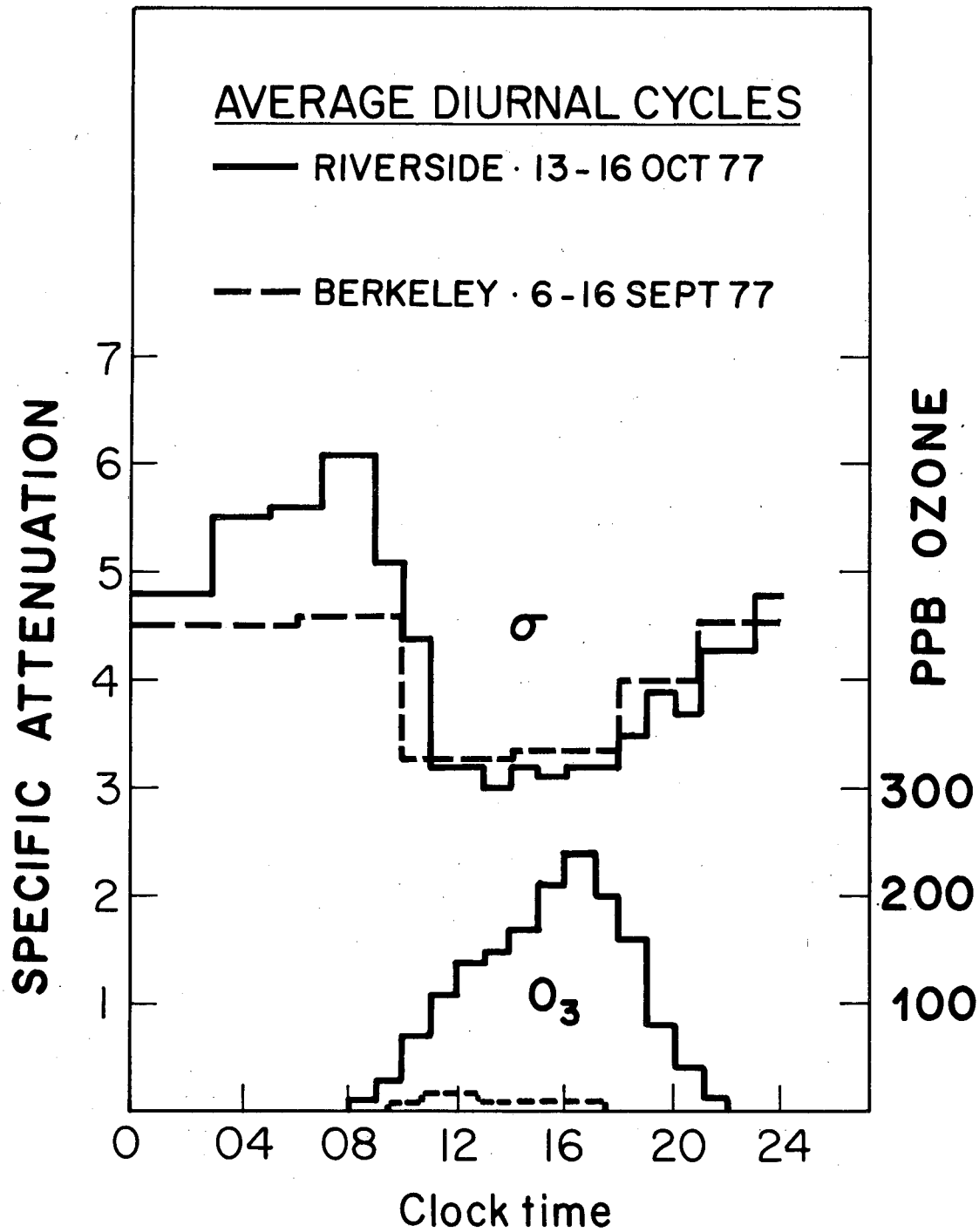

XBL 788-9884

Figure 5. Average diurnal cycles of specific attenuation and ozone concentration at Berkeley and Riverside.

that would be expected if high ozone levels were associated with significant production of secondary particulate carbon.

Conclusions

We have demonstrated that the optical attenuation technique is a valid semi-quantitative method for detection of the "graphitic" soot component of ambient aerosols, and that this component is an approximately constant fraction of the total suspended carbonaceous particulate loading under the atmospheric conditions so far encountered at widely differing sites. We find that this "graphitic" fraction of the ambient aerosol is comparable to that of representative source emissions. We also find a lack of evidence for the substantial production of carbonaceous particulates from gaseous precursors in atmospheres characterized by high ozone levels. Unless we can find secondary reaction mechanisms (1) that are not accompanied by ozone formation, (2) that are independent of location, season, or meteorology, and (3) whose contribution to the total ambient aerosol mass is linked to the primary particulate loading (in order to maintain a constant composition fraction), the results obtained from our ambient sampling programs so far indicate that primary particulates constitute a major fraction of the ambient carbonaceous aerosol in the two California air basins we have studied.

References

1. H. Rosen, A.D.A. Hansen, L. Gundel, and T. Novakov, "Identification of the graphitic carbon component of source and ambient particulates by Raman spectroscopy and an optical attenuation technique," Proceedings, Conference on Carbonaceous Particles in the Atmosphere, Lawrence Berkeley Laboratory, Berkeley, California (in press).
2. H. Rosen, A.D.A. Hansen, L. Gundel, and T. Novakov, "Identification of the optically absorbing component in urban aerosols," Appl. Optics 17, 3859 (1978).
3. P.K. Mueller, R.W. Mosley, and L.B. Pierce, "Carbonate and non-carbonate carbon in atmospheric particulates," in Proceedings of the Second International Clean Air Congress (New York, Academic Press, 1971).

Optical Attenuation: A Measurement of the Absorbing Properties of Aerosol Particles

H. Rosen and T. Novakov

The optical attenuation technique (described in detail elsewhere in this report) appears to be a direct measure of the absorbing component of aerosol particles and is apparently insensitive to its scattering properties. This has been demonstrated by noting that most of the mass of the aerosol responsible for scattering can be removed by solvent extraction or heat treatment procedures without appreciably affecting the optical attenuation measurement.[1] It has also been shown that addition of the order of one monolayer of nonabsorbing particles to the filter substrate does not give an appreciable optical attenuation. From a theoretical point of view, these results are not obvious, since it is unclear why the backscattered radiation from nonabsorbing particles should not make a significant contribution to the optical attenuation measurement. This is especially true where the absorbing component represents only a small fraction of the aerosol mass. In this paper we will present a simple theoretical model which accounts for all these observations and points out the critical role of the filter substrate as an almost perfect diffuse reflector in the technique. Similar considerations may also apply to the opal glass method used by Weiss et al.[2]

For this model calculation, we will assume that the particles and the filter media can be treated independently and consider the geometry shown in Fig. 1. A similar treatment, where the light beam is first incident on the particles, gives identical results. After the light beam passes through the filter medium, it is incident on the particles with an intensity, I_0. The particles forward scatter a fraction of the incident light, backward scatter a fraction, and absorb a fraction. These components in the low loading limit are respectively given by $n_s\sigma_F I_0$, $n_s\sigma_B I_0$, and $n_A\sigma_A I_0$, where n_s is the number of scattering aerosol particles per unit area, n_A is the number of absorbing aerosols per unit area, σ_F is the forward scattering cross section, σ_B is the backward scattering cross section, and σ_A is the absorption cross section.

Since the optical attenuation technique only measures the forward scattering light, it would seem as if the backscattered light would be lost to the system and would contribute to the attenuation. However, the filter, in our method, is almost a perfect reflector. Under these circumstances, the backscattered light

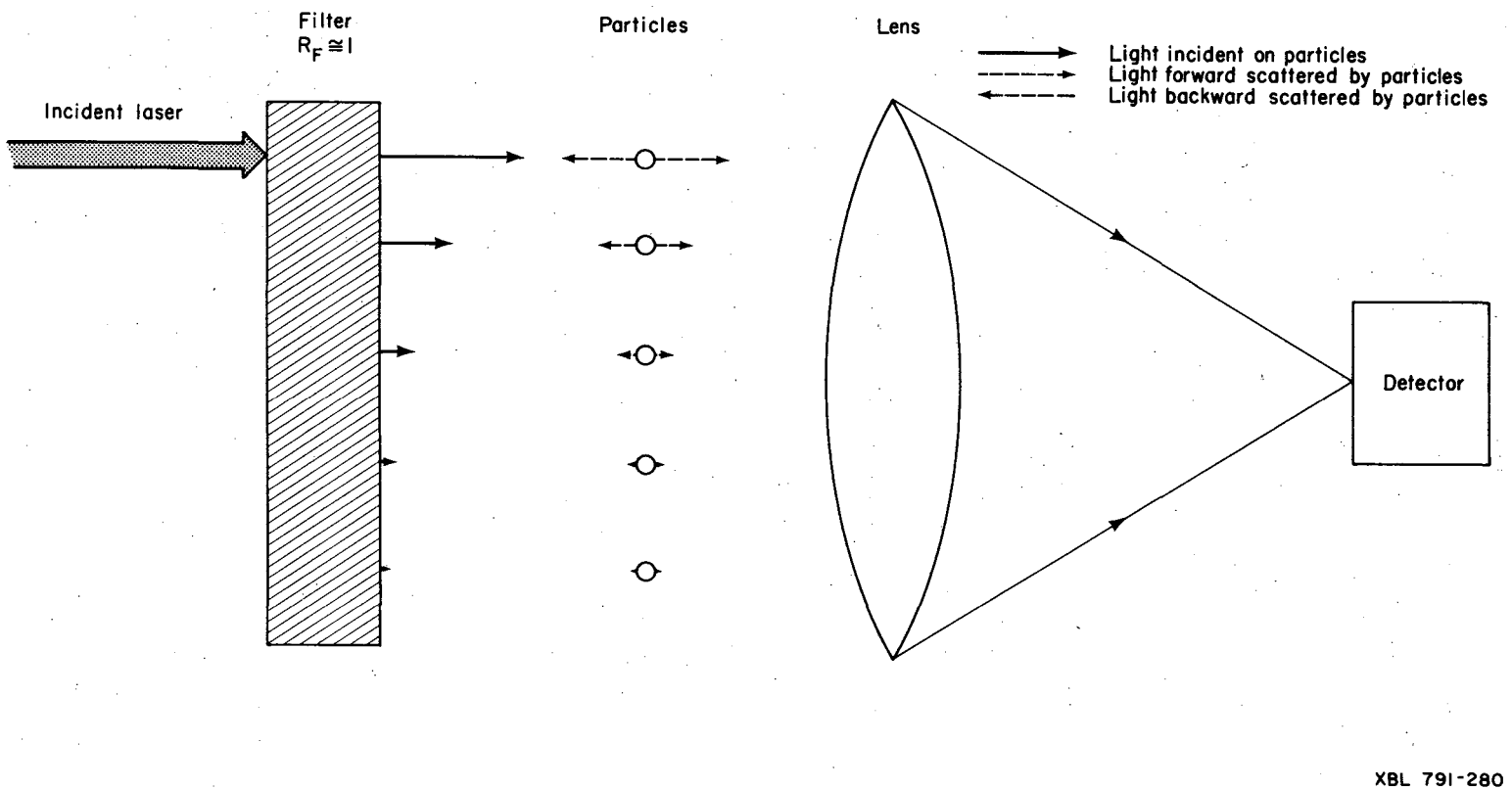

Figure 1. Schematic of experimental arrangement used for model calculation.

will be reflected in the forward direction and will again be incident on the particles. This process will continue until almost all the backscattered radiation is collected by the optics and therefore does not contribute to the optical attenuation. This result can be put in mathematical form, where I is the light detected by the collection optics and R_F is the reflectivity of the substrate.

$$I = I_0(1 - n_s\sigma_b - n_A\sigma_A) + I_0(1 - n_s\sigma_B - n_A\sigma_A)n_s\sigma_B R_F \qquad (1)$$

$$+ I_0(1 - n_s\sigma_B - n_A\sigma_A)n_s^2\sigma_B^2 R_F^2 + \ldots I_0(1 - n_s\sigma_B - n_A\sigma_A)n_s^n\sigma_B^n R_F^n$$

$$= I_0 \frac{(1 - n_s\sigma_B - n_A\sigma_A)}{(1 - n_s\sigma_B R_F)} .$$

Consider several limits. Where $R_F \simeq 0$, which normally would be considered an ideal substrate, Equ. (1) reduces to

$$I = I_0(1 - n_s\sigma_B - n_A\sigma_A) .$$

Under these conditions the backscattered radiation will contribute significantly to the optical attenuation and make the technique unsuitable for exclusively measuring the absorbing properties of the aerosol. In our method, however, $R_F \simeq 1$ and Equ. (1) becomes

$$I = I_0(1 - \frac{n_A\sigma_A}{1 - n_s\sigma_B}) .$$

Or the optical attenuation in the low loading limit is

$$ATN = I_0 - I = \frac{I_0 n_A\sigma_A}{1-n_s\sigma_B} .$$

From this expression it is clear that a nonabsorbing aerosol will make no contribution to the optical attenuation; this is consistent with our experimental results. The magnitude of the optical attenuation is somewhat dependent on the scattering properties of the aerosol; however, in the low loading limit, this effect is small. For example, if the substrate has 50% coverage, and if the scattering cross section of the particles, σ_s, is twice the particle area, then $n_s\sigma_s \simeq 1$. If σ_B is about 20% of σ_s (the maximum value measured by Charlson and his coworkers[3]), then

$$1 - n_s\sigma_B \simeq .8 ;$$

so that even for this rather high loading, the error in the absorption measurement due to scattering of the aerosol is only about 20%. This treatment is only approximate since it assumes that the scattering properties of the particles are not affected by the filter substrate and neglects the penetration of the particles into the substrate. Future analysis will try to evaluate the significance of these effects.

References

1. H. Rosen, A.D.A. Hansen, L. Gundel, and T. Novakov, "Identification of the optically absorbing component in urban aerosols," Appl. Optics 17, 3859 (1978).
2. R.E. Weiss, A.P. Waggoner, R.J. Charlson, D.L. Thorsell, J.S. Hall, and L.A. Riley, "Studies of the optical, physical, and chemical properties of light absorbing aerosols," Proceedings, Conference on Carbonaceous Particles in the Atmosphere, Lawrence Berkeley Laboratory, Berkeley, California (in press).
3. R. Weiss, R.J. Charlson, A.P. Waggoner, M.B. Baker, D. Covert, D. Thorsell, and S. Yuen, "Application of directly measured aerosol radiative properties to climate models," in Atmospheric Aerosols: Their Optical Properties and Effects, NASA Report CP-2004.

Identification of the Optically Absorbing Component in Urban Aerosols*

H. Rosen, A.D.A. Hansen, L. Gundel, and T. Novakov

Aerosol particles may play a significant role in modifying the local and global climate; therefore it is important to study the optical properties of these suspended particulates. The overall effect of aerosol particles in heating or cooling the earth's surface depends critically on the relative magnitude of their scattering and absorption coefficients.[1,2] In the past the effects of aerosols were thought to be due almost entirely to their scattering properties, but more recently it has been realized that the absorptivity of these particles is large. Therefore much more attention has been given to the imaginary index of refraction in heat balance calculations as well as in visibility degradation.[3,4] To model the effects of fossil fuel combustion on climate and visibility, it is important to establish the nature of these absorbing species. We will describe the application of Raman spectroscopy and an optical attenuation technique to show that the high optical absorptivity of urban particulates and particles produced directly from various combustion sources is due to "graphitic" carbon, one component of combustion-produced soot, which also contains a complex mixture of organics.

Raman spectroscopy is a highly selective method of analysis, which was not applied until recently to the characterization of air pollution particulates.[5-7] The technique can often be used to make unambiguous identifications since different chemical species have characteristic vibrational modes and therefore characteristic Raman spectra. The Raman spectroscopy apparatus uses a Coherent Radiation argon ion laser producing 1 W of power at 514 nm. The laser beam is focused by a 75-mm focal length cylindrical lens to a spot .06 mm × 2 mm on the sample surface via a small mirror, and the backscattered radiation is collected and imaged by an f/1 lens onto the slit of a 1-m Jarrell Ashe double monochromator equipped with two 1180-grooves/mm gratings blazed at 5000 Å. The output of the spectrometer is detected by an FW130 photomultiplier cooled to -20°C and used in a photon-counting mode. The pulses, after appropriate shaping, are counted and displayed on a multichannel analyzer. A computer-controlled grating drive made by RKB, Inc., allows a given spectral region to be scanned many times and added to the memory of the multichannel analyzer, greatly improving the signal-to-noise ratio. In order to minimize heating effects, the highly absorbing

samples used in these experiments are rotated at 1800 rpm by a motor, which increases the area illuminated by the laser beam by a large factor with almost no loss in signal level. The focal spot of the laser is located approximately 5 mm below the axis of rotation so that the effective illuminated area is an annulus of radius 5 mm and width 2 mm, resulting in the low power density of $\sim 1\ W/cm^2$.

The Raman spectra between 900 and 1950 cm^{-1} of ambient, automobile exhaust, and diesel exhaust particulates are compared with the spectra of activated carbon and polycrystalline graphite in Fig. 1. It is evident that the spectra of activated carbon, diesel exhaust, automobile exhaust, and the ambient sample are very similar, with the positions of the two Raman modes coincident to within $\pm 10\ cm^{-1}$, the estimated experimental error. The ambient sample was collected as part of the RAPS program in St. Louis, Missouri; however, the same Raman modes are also evident in every urban sample studied, including samples collected in Buffalo, New York, and Berkeley, Fremont, and Anaheim, California. Koenig et al.[8] have studied the Raman spectrum of activated carbon and have identified the modes near 1600 cm^{-1} and 1350 cm^{-1} as being due to phonons propagating within "graphitic" planes. The close correspondence of the spectra in Fig. 1 indicates the presence of physical structures similar to activated carbon in both source and ambient samples. These graphitic species are formed directly in combustion, and throughout the text we shall use the term "graphitic" soot to describe them.

Urban and combustion source particulates collected on various filter media have a grey or black appearance. The "graphitic" species identified by Raman spectroscopy are the most likely cause of this coloration. To test this hypothesis, we have developed an optical attenuation technique to quantitatively measure various properties of the absorbing species. The optical attenuation apparatus compared the transmission of a 633-nm He-Ne laser beam through a loaded filter relative to that of a blank filter (Fig. 2). The loaded filters are placed in the beam with the loaded side towards the laser; after multiple scattering through the filter substrate, the light is collected by an f/1 lens and focused on a photomultiplier tube. The data presented in this paper were obtained from particles collected on Millipore or quartz fiber substrates, but

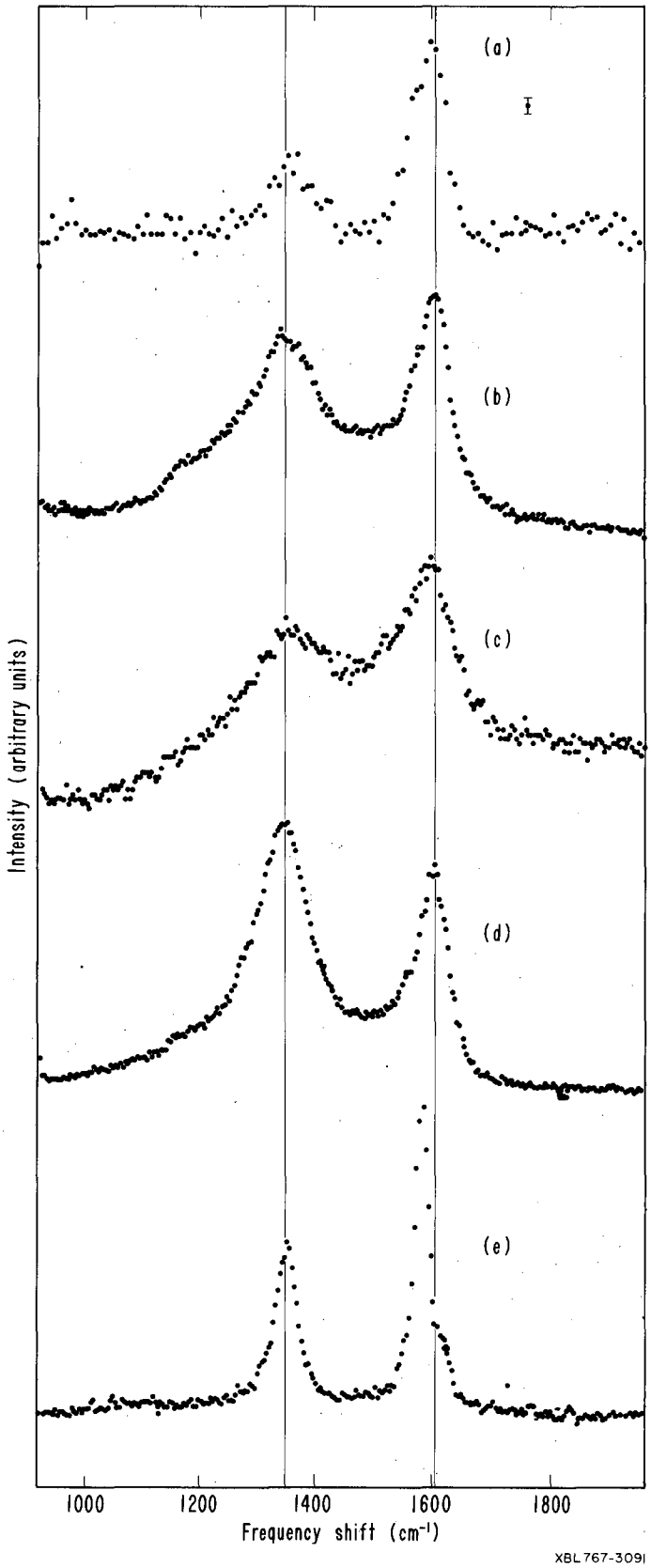

Figure 1. Raman spectra of a) ambient particulates, b) automobile exhaust particulates, c) diesel exhaust particulates, d) activated carbon, and e) polycrystalline carbon.

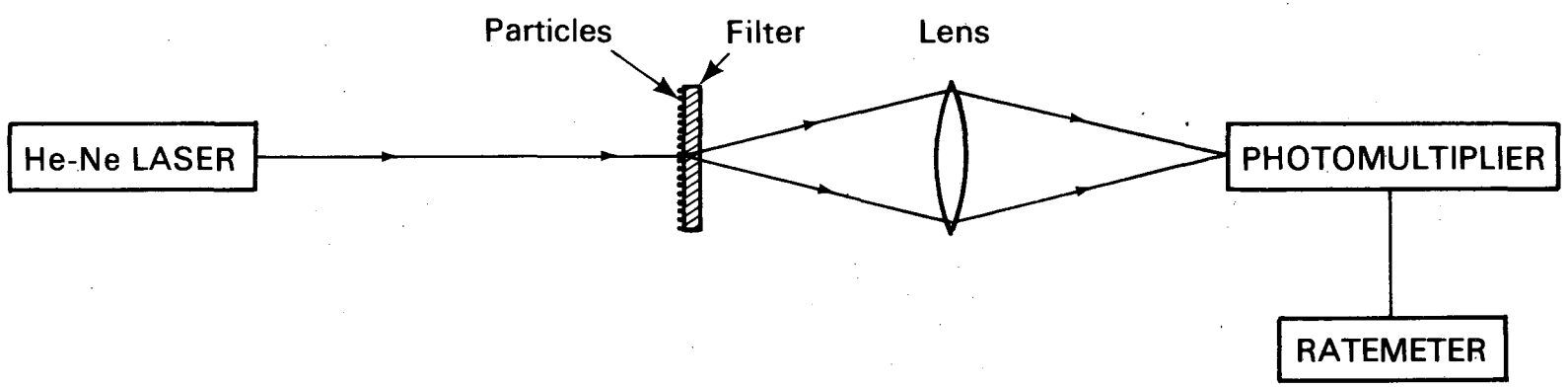

XBL 787-1361

Figure 2. Schematic of optical attenuation apparatus.

the optical attenuation measurement can be made with a wide variety of filter media. This technique is based on a principle similar to that of the opal glass method used by Weiss et al.[4] and measures the absorbing rather than the scattering properties of the aerosol (see theoretical discussion in "Optical Attenuation: A Measurement of the Absorbing Properties of Aerosol Particles," this report).

Using this apparatus we have studied the temperature stability and solubility of the absorbing species in ambient and source particulate samples. Our results show that these species have high temperature stability with only minimal oxidation up to 400°C[9] and are essentially insoluble in a wide variety of solvents (see Fig. 3).[4,9] We have also shown, using a spectrophotometer, that to within 20% over the visible spectral region, the optical attenuation has a $1/\lambda$ wavelength dependence characteristic of a constant imaginary index of refraction.[4,9]

All these results strongly suggest that the absorbing species in urban and source particulate samples is "graphitic" soot. A direct substantiation of this hypothesis is provided by comparing the integrated intensity of the 1600 cm^{-1} Raman mode with the optical attenuation of the same filter sample. These measurements have been done on acetylene soot samples, which were essentially pure carbon with only trace amounts of metallic impurities; highway tunnel samples; and ambient samples collected in Berkeley and Fremont in the San Francisco air basin and Anaheim in the Los Angeles air basin. The results shown in Fig. 4 indicate that within experimental error there is a direct correspondence between the optical attenuation and the Raman intensity or "graphitic" soot content for all samples studied, despite widely different chemical compositions (e.g., for a given optical attenuation, the Pb and Fe concentrations vary by more than a factor or 100). The only reasonable explanation is that the optical attenuation is due to the "graphitic" soot content of the collected particulates.

In summary, we have shown that the species responsible for the high optical absorptivity of particulate samples has high temperature stability in air, is insoluble in a variety of solvents, and absorbs uniformly throughout the visible region. We have also demonstrated that the amount of the absorbing species is directly proportional to the "graphitic" soot content as defined by Raman spectroscopy. All these results taken together indicate that the high optical absorptivity of ambient samples collected in urban environments and various source particulate samples is due to the "graphitic" component of the aerosol. The effects of these species on physical and chemical processes[10,11] in the atmosphere require further investigation.

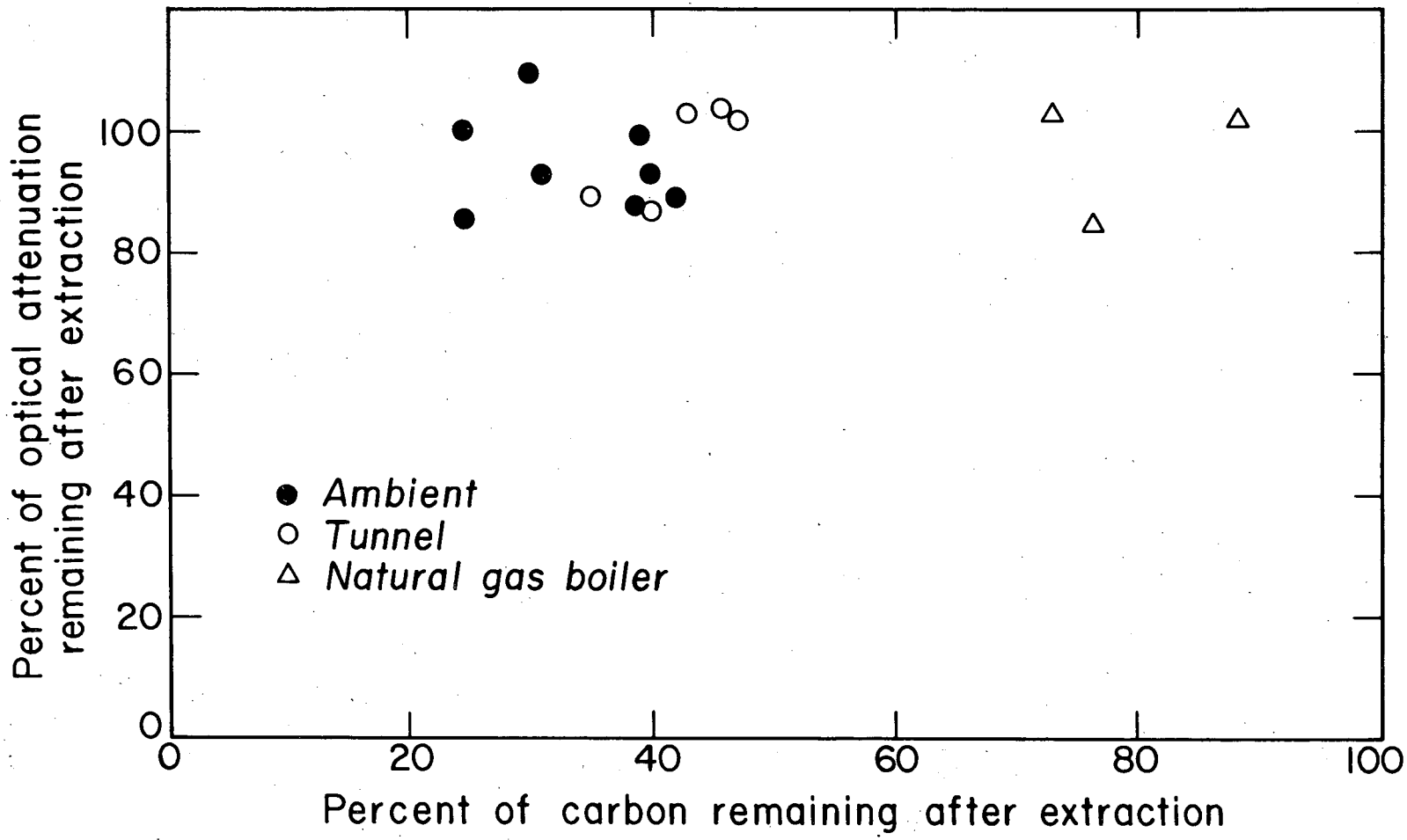

XBL 783-344

Figure 3. Plot of the percent of the optical attenuation remaining after successive Soxhlet extraction in benzene and a methanol-chloroform mixture as a function of the carbon remaining after extraction for various ambient and source particulate samples.

0 0 0 5 3 0 1 4 1 4

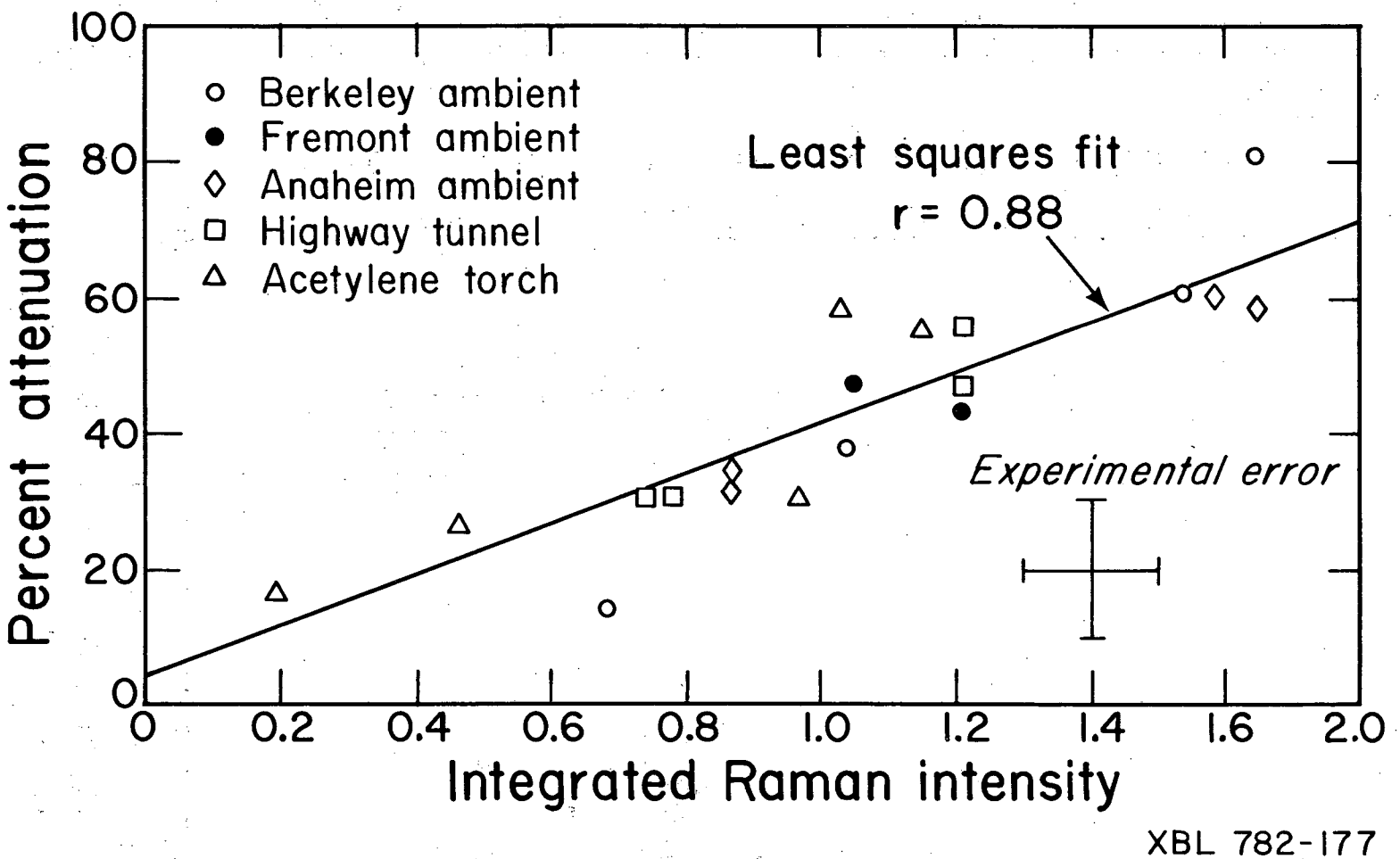

Figure 4. Plot of integrated Raman intensity of the 1600 cm^{-1} mode versus percent optical attenuation at 633 nm for ambient, acetylene soot, and tunnel samples.

References

1. P. Chýlek and J.A. Coakely, Jr., "Aerosols and climate," Science 183, 75 (1974).

2. R.A. Reck, "Aerosols in the atmosphere: Calculation of the critical absorption/backscatter ratio," Science 186, 1034 (1974).

3. W. Bach, "Global air pollution and climatic change," Rev. Geophys. and Space Phys. 14, 429 (1976).

4. R.E. Weiss, A.P. Waggoner, R.J. Charlson, D.L. Thorsell, J.S. Hall, and L.A. Riley, "Studies of the optical, physical, and chemical properties of light absorbing aerosols," Proceedings, Conference on Carbonaceous Particles in the Atmosphere, Lawrence Berkeley Laboratory, Berkeley, California (in press).

5. H. Rosen and T. Novakov, "Raman scattering and the characterization of atmospheric aerosol particles," Nature 266, 708 (1977).

6. H. Rosen and T. Novakov, "Identification of primary particulate carbon and sulfate species by Raman spectroscopy," Atmos. Environ. 12, 923 (1978).

7. J.J. Blaha, G.J. Rosasco, and E.S. Etz, "Raman microprobe characterization of residual carbonaceous material associated with urban airborne particulates," Appl. Spectrosc. 32, 292 (1978).

8. F. Tuinstra and J.L. Koenig, "Raman spectrum of graphite," J. Chem. Phys. 53, 1126 (1970).

9. H. Rosen, A.D.A. Hansen, L. Gundel, and T. Novakov, "Identification of the graphitic carbon component of source and ambient particulates by Raman spectroscopy and an optical attenuation technique," Proceedings, Conference on Carbonaceous Particles in the Atmosphere, Lawrence Berkeley Laboratory, Berkeley, California (in press).

10. T. Novakov, S.-G. Chang, and A.B. Harker, "Sulfates as pollution particulates: Catalytic formation on carbon (soot) particles," Science 186, 259 (1974).

11. S.-G. Chang, R. Brodzinsky, R. Toossi, S.S. Markowitz, and T. Novakov, "Catalytic oxidation of SO_2 on carbon in aqueous suspensions," Proceedings, Conference on Carbonaceous Particles in the Atmosphere, Lawrence Berkeley Laboratory, Berkeley, California (in press).

*This article has been published in Applied Optics 17, 3859 (1978).

PHYSICAL AND CHEMICAL CHARACTERIZATION: CHEMICAL

Characterization of Source and Ambient Particulate Samples by Solvent Extraction

L.A. Gundel, G.E. Mason, and T. Novakov

Since polar organic extracts of ambient particulates have been shown to be direct-acting mutagens,[1-6] it is important to understand the chemical and physical processes which lead to the association of oxidized organic compounds with ambient particulates. Considerable effort has been directed toward demonstrating that photochemical reactions can account for the formation of aerosol-phase polar organics from gas-phase reactive hydrocarbons,[7] and that polar compounds in ambient particulates result from such photochemical processes.[8,9] It has been postulated[8,9] that concentrations of polar compounds as carbon correlate with indicators of photochemical activity such as ozone concentration, whereas concentrations of nonpolar compounds as carbon and elemental carbon do not correlate with ozone concentration. If substantial concentrations of polar compounds are associated with ambient particulates collected during nonphotochemical atmospheric conditions, alternative mechanisms for generation of polar aerosol particulates must exist.

In this project we are attempting to answer the following questions:

1. How does particulate matter collected under nonphotochemical conditions (Berkeley, winter) compare with particulate matter collected in the Los Angeles Basin during photochemical episodes when characterized by solvent extraction? Of particular interest here is the ratio of polar to nonpolar carbon ("secondary" to "primary") for each condition.

2. How do ambient particulates compare with particulate material collected from various combustion sources, when characterized by the same solvent extraction technique?

3. What processes may contribute to the transformation of combustion-generated particulates to account for the difference in polarity between carbonaceous compounds associated with combustion sources and ambient particulates?

4. Does solvent extraction with carbon determination of the extracts allow recovery of all the carbon removed during extraction? This may affect conclusions based on previous work.[9-11]

Analytical Strategy and Experimental Details

The solvent extraction method was chosen to allow direct comparison with results available from studies of particulates collected in the Los Angeles Basin.[9-11] The analytical strategy previously applied to samples obtained in

the Los Angeles Basin[9-11] is based on several assumptions. First, benzene extraction followed by extraction with the methanol-chloroform mixture removes all organic material from the filter, leaving "elemental" carbon. The next assumption is that cyclohexane removes only "primary" or source-related organics from the particulate sample. This assumption is based on early work[9] which showed no correlation between cyclohexane-extractable carbon and ozone level for samples collected during a photochemical episode; whereas the difference between total extracted carbon and cyclohexane-extracted carbon showed a positive correlation with ozone level. The difference has been attributed to polar compounds originating in photochemical reactions, which are "secondary" transformations of less polar primary gaseous compounds. In a Los Angeles episode (July, 1975), "primary," "secondary," and "elemental" carbon fractions all correlated positively with ozone level.[10,11] Another assumption of the "primary"/"secondary"/"elemental" carbon breakdown is that all carbon removed by solvent extraction is recovered in the extract. Our results prove that this is not so.

Samples were collected on prefired (800°C) quartz filters using a high volume sampler at 40 SCFM. Sampling time for ambient samples was typically 24 hr. For sources the sampling time varied with the output of the source; for example, Caldecott Tunnel samples gave loadings of 40 μg C cm^{-2} in about 20 min. Filter samples were stored at -5°C in aluminum foil and plastic bags. The Soxhlet extraction procedure was identical in most respects to that used by B.R. Appel et al.[10,11] Using spectroquality solvents, one quarter of each filter was extracted in cyclohexane, while a different quarter was extracted in benzene for 6 hr followed by a methanol-chloroform (1:2 vv) mixture the next day. The three extracts were concentrated to 10 ml and 1 ml of each was allowed to evaporate to dryness before carbon determination by combustion. Carbon was also measured for portions of the filter at all stages of extraction. This is an addition to the analytical strategy,[10] which permits comparison of the carbon content of each extract with the carbon lost by the filter during extraction.

Comparison of Berkeley and New York City Particulates with Los Angeles Particulates

The application of this solvent extraction method to ambient particulates collected in Berkeley and New York City allows a comparison with ambient particulates collected during a photochemical smog episode in the Los Angeles basin[10,11] and with combustion sources. We have adopted the formalism used by those workers to differentiate between source-related carbon ("primary") and particulate carbon formed by photochemical processes ("secondary"). In this formalism

total soluble C = benzene-soluble C + methanol-chloroform-soluble C = total organic C

"primary" C = cyclohexane-soluble C = nonpolar C

"secondary" C = total soluble C - "primary" C = polar C

"elemental" C = total C - total soluble C = graphitic C

Figure 1 presents the results obtained by carbon measurements of the evaporated extracts and the extracted ambient filters. Similar data are also presented for typical particulate sources, representing vehicle traffic in a highway tunnel, traffic in a parking garage, diesel passenger buses, and a natural gas boiler.

Several observations can be made from the data shown in Fig. 1. The major finding is that particulate matter in Berkeley, collected during low ozone conditions, appears to contain appreciable amounts of "secondary" or polar carbon. The "primary," "secondary," and "elemental" breakdown is very similar to that reported for Los Angeles.[10,11] Roughly half the total carbon in Berkeley particulate samples is recovered in successive solvent extraction with benzene and the methanol-chloroform mixture, with about one-seventh of the total carbon recoverable in cyclohexane. The ratio of "secondary" to "primary" to "elemental" (S:P:E) for the Los Angeles samples is 40:17:43; that ratio is 38:13:49 for Berkeley particulates, averaged for winter and summer. There is no significant difference between winter and summer Berkeley samples (see Fig. 2). However, there appears to be slightly less "primary" carbon, and slightly less recoverable soluble carbon in Berkeley samples, compared with the Los Angeles samples. Winter particulates in New York show a pattern similar to that in Berkeley and Los Angeles, although they appear to contain less soluble carbon and more elemental carbon than either Los Angeles or Berkeley particulates.

Comparison of Source with Ambient Particulates

Use of the formalism which has been applied to photochemical episodes[9,10] shows that vehicle combustion sources produce particulates which contain more "primary" than "secondary" material (Fig. 1). The "primary" component is significantly larger for vehicle sources than Berkeley ambient samples (17-32% compared with 13%). The sources we measured contain 11-19% "secondary" C compared with average Berkeley ambient samples, where "secondary" C is 38%. Highway tunnel traffic and traffic in a parking garage produce similar particulates when characterized by solvent extraction, with S:P:E ratios of 16:32:52 and 18:23:58 respectively. Diesel buses produce a smaller fraction of recoverable soluble

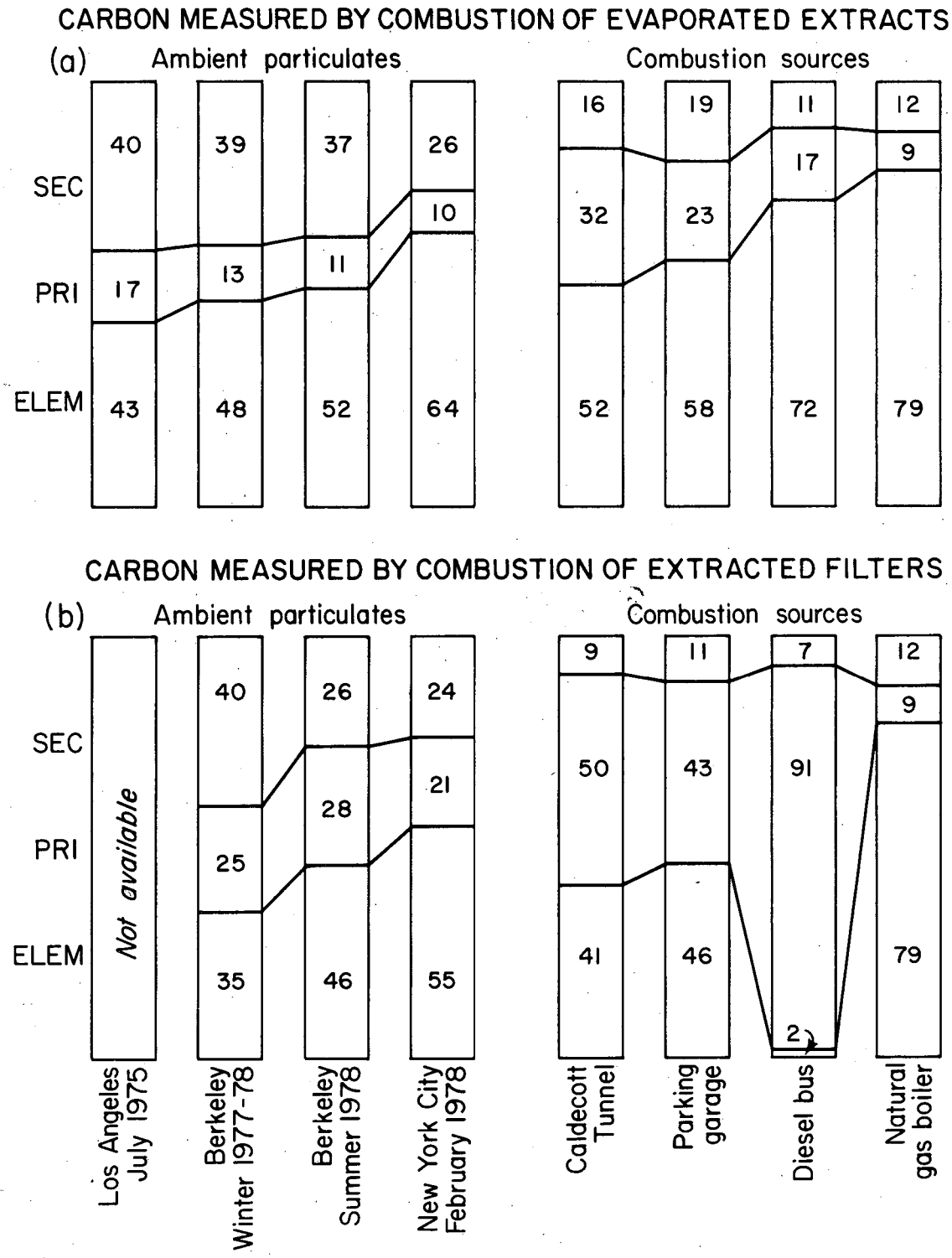

Figure 1. Characterization of particulate matter by selective solvent extraction and carbon determination. Results expressed as percentage of total original carbon. As applied to any filter sample, the formalism is SEC = "secondary" = polar carbon; PRI = "primary" = nonpolar carbon; ELEM = "elementary" = insoluble carbon.

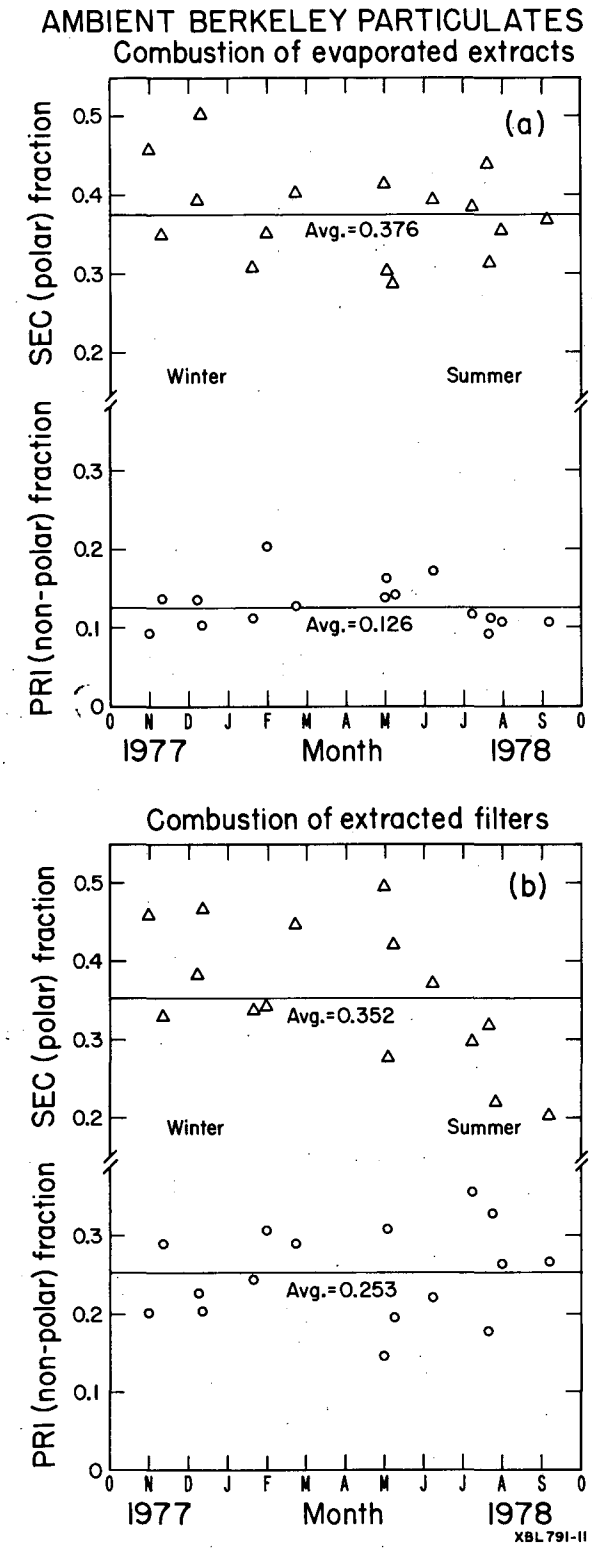

Figure 2. Variation of "primary" (nonpolar) and "secondary" (polar) carbon during one year (1977-1978) for ambient particulates collected in Berkeley, California. a) Carbon measured by combustion of evaporated extracts; b) carbon measured by combustion of extracted filters.

organic material than the tunnel or garage, as do samples collected from a natural gas boiler exhaust.[11] Although our results may be affected by the difficulties associated with source sampling, they indicate that ambient samples contain more "secondary" or polar carbon than source samples, and that vehicle traffic and ambient particulates may contain a similar fraction of total soluble carbon. We have demonstrated that ambient particulate carbon collected under nonphotochemical conditions is similar to the particulate carbon collected during a photochemical episode, but both differ from sources when characterized by solvent extraction.

Comparison of Carbon in Extracts to Carbon Lost by Filters During Extraction

The results presented so far have been based on measurement of the carbon content of the evaporated extracts. The amount of carbon recovered in the extracts can be compared with the amount lost by the filter samples during extraction, since the carbon content of the filters can be measured directly by combustion. This provides another method with which to characterize ambient and source particulates. The lower part of Fig. 1 contains these results. Again, a clear difference can be seen between ambient and source samples. Compared with ambient particulates, sources show much larger fractions of carbon lost by treatment of the filter with cyclohexane ("primary" carbon), whereas ambient particulates show more loss of polar carbon ("secondary" carbon). Significantly less carbon remains on the filter after extraction ("elementary" carbon) than predicted by combustion of the evaporated extracts, for both source and ambient particulates. Amounts of carbon remaining after extraction with benzene and methanol-chloroform ("elementary" carbon), appear to be similar for ambient particulates and particulates collected from a highway tunnel and parking garage.

"Secondary":"primary":"elemental" ratios are different when determined by these two methods. For example, Berkeley particulates give 38:13:49 by combustion of evaporated extracts and 35:25:40 by combustion of extracted filters. The major difference is that less carbon is recovered in the cyclohexane extract than is lost by the filter during the extraction. Table 1 shows the ratio of carbon measured by evaporation of extracts to carbon lost by the extracted filters for Berkeley ambient samples and for several sources. For cyclohexane and benzene, evaporation of extracts recovers 60-70% of the carbon lost by the extracted filter. Methanol-chloroform extraction yields more carbon than has been lost by the filter, and this is not due to blank problems. The nonpolar extracts appear to lose volatile carbon, as is expected for adsorbed low boiling hydrocarbons. Since losses in the actual evaporation of the 1-ml aliquot have been shown to be

minimal,[10] volatilization is probably occurring during the extraction, since the boiling points of both cyclohexane and benzene are higher than those of many aliphatic hydrocarbons likely to be present as adsorbed species. The most extreme case of this loss of volatile material occurs with diesel particulates, where only 18% of the carbon lost by the filter during cyclohexane extraction is present in the evaporated extract. The gain of carbon in the extract during methanol-chloroform extraction may be due to reaction of methanol with reactive polar compounds such as carboxylic acids and alcohols, so that esters and ethers are formed which contain one more carbon atom per molecule than the parent compounds. The gain in carbon during methanol-chloroform extraction may not completely offset the loss during benzene extraction, so that the total recoverable extracted carbon is underestimated. "Elemental" carbon, the difference between original and extracted carbon, is therefore overestimated by this method; for ambient Berkeley samples, this overestimate is close to one-third of the carbon remaining on the filter.

Table 1. Ratio of carbon content of evaporated extracts to carbon content of extracted filters. Effect on secondary to primary (S/P) ratios.

	Cx	Bz	MC	Elem	S/P extract	S/P filter	Number of samples
Ambient Particulate							
Los Angeles	a	—	—	—	2.3	—	12
Berkeley	0.52±.16	0.69±.15	1.10±.39	1.28±.24	3.0	1.6	16
New York	0.42±.14	0.65±.02	1.09±.23	1.16±.06	2.8	0.87	2
Combustion Sources							
Caldecott Tunnel	0.63±.14	0.74±.14	1.56±.46	1.25±.24	0.52	0.17	6
Parking garage	0.56±.14	0.67±.03	1.50±.20	1.24±.02	0.83	0.27	3
Diesel bus	0.18±.11	0.24±.07	2.68±.47	32±2	0.67	0.07	2

[a]Not available.

Direct measurement of carbon removed by combustion of extracted filters appears to be more accurate than measurement of carbon in evaporated extracts. The latter measurement suffers from loss of volatile material and reaction of the sample with solvent, but these processes do not affect the carbon remaining on the filter. Another possible problem with the extracts is contamination, causing addition of carbon from solvents, glassware, and transfer operations, although these errors have been included in the blank corrections.

Solubility of Heavy Elements and the Question of Particle Loss During Extraction

A possible problem with direct measurement of carbon on the filters is physical loss of particles during solvent extraction, as small fiber particles can sometimes be observed in the methanol-chloroform extracts.[10,11] We have attempted to assess this problem by following the concentrations of selected heavy elements by XRF analysis of several sections of a tunnel filter after each step of the extraction. For this sample the average carbon fraction lost was 0.53; lead, 0.44; Br, 0.97. However, only small fractions of Cr (0.06), Cu (0.00), and Fe (0.11) were removed. C, Pb, and Br appear to be removed by solubilization, but the low losses of Cr, Cu, and Fe indicate that particle loss during extraction is small, certainly $\leq$ 10%. These findings on the high solubility of lead and bromine are consistent with the results of other workers on the occurrence of lead in polar extracts of ambient particulates.[5] We find that losses of Pb and Br in benzene alone are $\leq$ 5% in this experiment; losses of the other metals are even smaller. Our results are consistent with the dissolution of PbBrCl[12] or $PbBrCl \cdot NH_4Cl$[12] in methanol accompanied by no more than 10% physical particle loss during extraction. Thus, solubility characterization of particulates by measurement of carbon loss from extracted filters is possible.

Adsorption of Volatile Organic Species onto Quartz Filters During Hi-Vol Sampling

With this understanding of the limits of the extraction and carbon measurement techniques, it is possible to use them to address a sampling problem. The high efficiency of quartz fiber filters for particle collection has long been established. Another concern is the extent to which organic vapors may be adsorbed onto the filter itself or onto atmospheric soot during collection, so that soluble carbon measurements do not reflect ambient particulate composition but may include sampling artifacts. To explore the filter gas pickup problem, we collected ambient particulates for 24 hours in Berkeley using two filters in series, with all other hi-vol operations as normal. The downstream filter showed carbon loading equivalent to 11% of the upstream, particle-loaded filter. The top filter showed a typical ambient S:P:E distribution, but benzene removed all the carbon from the lower filter, and roughly 70% was recovered in the extract. Cyclohexane removed $\sim$ 70% of the carbon with only 3% recovery in the extract. This result implies that hydrocarbons are being trapped on the clean filter to a small extent. The source could be ambient air or outgassing from the particulate material on the upper filter. The volatilization of the lower filter cyclohexane extract is very

similar to the behavior of ambient cyclohexane extracts, suggesting that part of the cyclohexane-soluble carbon may be due to a sampling artifact.

Conversion of "Primary" to "Secondary" Carbon Under Nonphotochemical Conditions

The results presented so far have shown that ambient particulates contain more polar ("secondary") and less nonpolar ("primary") carbon than source particulates. The ratio of "secondary" (S) to "primary" (P) carbon for ambient and source particulates is given in Table 1. For carbon measured in evaporated extracts, ambient samples give S/P close to 3.0, while vehicle combustion sources have S/P < 0.85. For carbon measured by combustion of extracted filters, S/P ratios follow the same pattern. Coupled with these source-ambient differences is the fact that S/P ratios for ambient particulates do not depend on the ozone concentration, implying that the highly polar character of organic compounds associated with particulates is not related to the presence of a photochemically reactive atmosphere. These observations lead us to suggest several possible explanations:

1. Oxidation of reactive hydrocarbons and other organic compounds in homogeneous or heterogeneous reactions, such as oxidation of adsorbed compounds while they are associated with soot, in mechanisms which appear to be unrelated to the photochemical activity of the atmosphere as indicated by the ozone concentration.

2. Replacement of nonpolar compounds adsorbed on soot by polar compounds which are less volatile during dilution of combustion effluent into the atmosphere or during the residence time of combustion-generated particles in the ambient air.

3. Addition of polar aerosol compounds into the atmosphere from natural sources, such as marine air or fog,[13] in high enough concentration to dilute anthropogenic source particulates.

4. Direct emission of polar compounds such as plasticizers into the atmosphere,[14] followed by adsorption onto soot.

5. Replacement of nonpolar compounds adsorbed on soot or on the filter fibers by polar compounds (sampling artifact).[15]

6. Reaction of atmospheric oxidant gases with compounds adsorbed on soot or filter fibers during sampling (sampling artifact).[16]

We have initiated experiments to transform combustion particulates into their more polar ambient counterpart so that we can deduce some of the contributing processes. Preliminary results indicate that hi-vol sampling does not lead to substantial replacement of nonpolar by polar compounds, nor do ambient gases oxidize a large fraction of adsorbed nonpolar compounds during sampling. So far

we have no data concerning the possibility of dilution effects or soot-catalyzed oxidation of reactive hydrocarbons.

Summary and Conclusions

Particulates collected under nonphotochemical conditions (Berkeley and New York City) appear very similar to particulates collected during a photochemical episode in the Los Angeles Basin when characterized by solvent extraction. There appears to be no substantial seasonal variation in S:P:E ratios for Berkeley samples. "Secondary" to "primary" (polar to nonpolar) ratios based on extracts are close to 3 for all ambient particulates but less than 1 for source particulates.

We suggest that the significant differences between ambient and source samples may be due to chemical and physical transformation processes which do not require a photochemically active atmosphere.

We have also found that a substantial amount (30-40%) of nonpolar carbonaceous material associated with source and ambient particulates is lost by evaporation during extraction with cyclohexane and benzene, implying that earlier measurements[9-11] of total mass or carbon content of these extracts do not reflect the total amount of material extracted.

References

1. Y.Y. Wang, R.E. Talcott, R.S. Sawyer, S.M. Rappoport, and E.T. Wei, "Direct acting mutagens in automobile exhaust," Cancer Lett. 5, 39 (1978).
2. J.N. Pitts, Jr., D. Grosjean, T.M. Mischke, V.F. Simon, and D. Poole, "Mutagenic activity of airborne particulate organic pollutants," Toxicology Lett. 1, 65 (1977).
3. R. Talcott and E. Wei, "Airborne mutagens bioassayed in Salmonella typhimurium," J. Natl. Cancer Inst. 58, 449 (1977).
4. B. Commoner, P. Madyastha, A.J. Bronsdon, and A.J. Vithayathil, "Environmental mutagens in urban air particulates," J. Toxicol. and Environ. Health 4, 59 (1978).
5. J.M. Daisey, M.A. Leyko, M.T. Kleinman, and E. Hoffman, "The nature of the organic fraction of the New York City summer aerosol," Ann. N.Y. Acad. Sci. (in press).
6. J.N. Pitts, Jr., K. van Cauwenberghe, D. Grosjean, J. Schmid, D. Litz, W. Belser, G. Knudson, and P. Hinds, "Chemical transformations of polycyclic aromatic hydrocarbons in real and simulated atmospheres and their biological implications," paper presented at the Third International Symposium on Polycyclic Aromatic Hydrocarbons, Battelle Laboratories, Columbus, Ohio, October 25-27, 1978.
7. D. Grosjean, "Aerosols," in Ozone and Other Photochemical Oxidants (National Academy of Sciences—National Research Council, Committee on Medical and Biological Effects of Environmental Pollutants, Washington, DC, 1977), Ch. 3.

8. D. Grosjean, "Solvent extraction and organic carbon determination in atmospheric particulate matter: The organic extraction-organic carbon analyzer (OE-OCA) technique,"Anal. Chem. 47, 797 (1975).

9. B.R. Appel, P. Colodny, and J.J. Wesolowski, "Analysis of carbonaceous materials in southern California atmospheric aerosols," Environ. Sci. Technol. 10, 359 (1976).

10. B.R. Appel, E.M. Hoffer, M. Haik, S.M. Wall, E.L. Kothny, R.L. Knights, and J.J. Wesolowski, Characterization of Organic Particulate Matter, Final Report to California Air Resources Board, Contract No. ARB 5-682 (1977).

11. B.R. Appel, E.M. Hoffer, E.L. Kothny, S.M. Wall, M. Haik, and R.L. Knights, "Analysis of carbonaceous material in southern California atmospheric aerosols," Environ. Sci. Technol. 13, 98 (1979).

12. K. Habibi, "Characterization of particulate matter in vehicle exhaust," Environ. Sci. Technol. 7, 223 (1973).

13. W.R. Barger and W.D. Garrett, "Surface active organic material in air over the Mediterranean and over the Eastern Equatorial Pacific," J. Geophys. Res. 81, 3151 (1976).

14. W. Cautrells and K. van Cauwenberghe, "Fast quantitative analysis of organic compounds in airborne particulate matter by gas chromatography with selective mass spectrometric detection," J. Chromatog. 131, 253 (1977).

15. H. Della Diorentina, F. de Wiest, J. De Graene, "Determination per spectrometrie infrarouge de la matière organique nonvolatile associée aux particles en suspension dans l'air-II. Facteurs influencant l'indice aliphatique," Atmos. Environ. 9, 517 (1975).

16. J.N. Pitts, Jr., K.A. van Cauwenberghe, D. Grosjean, J.P. Schmid, and D.R. Fitz, "Atmospheric reactions of polycyclic aromatic hydrocarbons: facile formation of mutagenic nitro derivatives," Science 202, 515 (1978).

Characterization of Particulate Amines

L.A. Gundel, S.-G. Chang, M. Clemenson, S.S. Markowitz, and T. Novakov

Introduction

In addition to nitrate and ammonium species,[1] a large fraction of the nitrogen associated with ambient particulate matter occurs in two or more chemically reduced forms.[2] These reduced species, N_x, have been tentatively identified[2] as amine, amide, and possibly nitrile species by means of X-ray photoelectron spectroscopy (ESCA or XPS). For simplicity and in the absence of a more rigorous term, we shall refer to these reduced species as particulate amines or N_x. N_x species occur in combustion-generated and ambient particulates, and species with similar ESCA spectra and thermal behavior in vacuum can be produced by reaction of soot or graphite with NH_3.[3]

Both ESCA and traditional analytical methods have helped characterize particulate nitrogen, but their results for NH_4^+, N_x, and NO_3^- do not agree.[4] Whereas ESCA samples are subject to volatility losses in high vacuum, especially for NO_3^-, wet methods may modify the chemical composition of the samples by reactions such as hydrolysis, so that the technique affects the results. To reconcile the existing information and to further characterize particulate amines, we have used a new nondestructive nitrogen determination,[5,6] proton activation analysis (PAA), in conjunction with ESCA for ambient particulate samples, before and after solvent extraction.[4] ESCA has also been used for the characterization of evaporated solvent extracts.

Chemical Characterization of Particulate Nitrogen

ESCA has proved to be a very useful tool in identifying the variety of nitrogen species associated with ambient particulates, and its use has been extensively reviewed.[7-9] The following observations about ambient particulate nitrogen are based on ESCA measurements on silver filter samples from several locations (Los Angeles, St. Louis, and Berkeley); the experimental evidence has been presented earlier[4,7-9] and will not be repeated here.

1. Besides the expected salts — ammonium sulfate $[(NH_4)_2SO_4]$ and ammonium nitrate (NH_4NO_3) — which are relatively stable in vacuum, a more volatile ammonium species, probably ammonium chloride (NH_4Cl) or adsorbed NH_3, is often associated with ambient particulate matter.

2. Particulate amines (N_x) typically account for up to half of the total nitrogen as determined by ESCA.

3. Nitrate nitrogen is typically much less abundant than ammonium nitrogen. The nitrate species are more volatile in vacuum than NH_4NO_3, indicating that adsorbed nitric acid may be present. Wet methods tend to find much more (3-5x) nitrate than ESCA.[4] Besides the volatility of HNO_3, artifact nitrate on glass fiber filters[10] can account for some of this difference.

4. ESCA determination of total reduced nitrogen ($NH_4^+ + N_x$) agrees with determination of NH_4^+ by wet methods.[4] Since N_x is often more abundant than NH_4^+ in ambient samples, there is a serious discrepancy which is consistent with the conversion of N_x to NH_4^+ during the analytical procedure[11] to determine NH_4^+.

5. Based on studies of winter aerosol samples from Berkeley, California,[12] ESCA inventories nitrogen as 25% nitrate, 25% ammonium, and 50% N_x. Indirect evidence[13] supports the existence of N_x by showing that nitrate and ammonium cannot account for all nitrogen associated with ambient particulates. The average deficiency is 25%. Other evidence for N_x comes from the detection of amides[14] in ambient particulates by high resolution mass spectrometry.

Solubility Behavior of Particulate Nitrogen

A series of ambient particulate samples collected on silver filters during autumn and winter in Berkeley, California, have been washed with water and organic solvents. PAA and ESCA analyses have been performed after each step. Static extraction with distilled deionized water at room temperature for 2 hours removed a large fraction of the original nitrogen, as shown in Table 1. Further sequential Soxhlet extraction with benzene followed by methanol and chloroform (1:2 vv) removed only a small fraction of the remainder. Nitrogen remaining on the filter accounts for between 2 and 25% of the initial nitrogen. Water-washing of all winter 1977-78 samples (Table 2) changes the nitrogen-to-carbon ratio from 0.32±0.26 to 0.040±0.020. For comparison we find that untreated vehicle exhaust collected in a highway tunnel has a nitrogen-to-carbon ratio lower than untreated ambient particulates (0.046±0.010). The ESCA results in Fig. 1 show the effect of water washing on one of the samples (Dec. 1977). The other samples exhibit similar behavior except they contain less nitrate. The nitrate peak occurs at binding energy close to 407 eV, NH_4^+ close to 402 eV, and N_x close to 400 eV. The reduced nitrogen peaks have been resolved into contributions from NH_4^+ and N_x by comparison with standards. The untreated particulate material contains roughly equivalent amounts of ammonium, particulate amine, and nitrate species, with total nitrogen equal to 5.0 μg m^{-3}. After water washing, the remaining nitrogen is N_x. It can be seen from Table 1 that 4.8 μg m^{-3} of the initial nitrogen has been removed by water extraction.

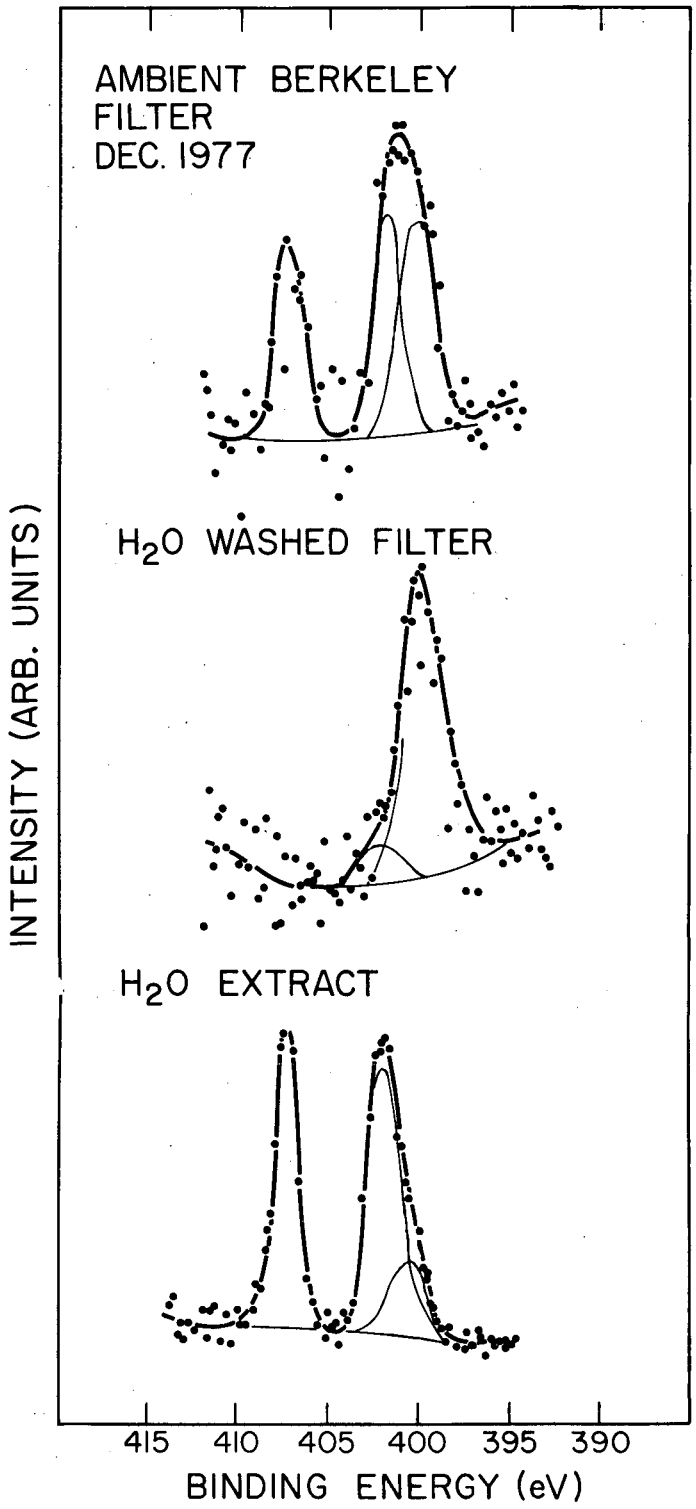

XBL 783-405A

Figure 1. ESCA spectra in the nitrogen region for ambient particulate material collected in December, 1977, in Berkeley, California. Binding energy for nitrogen species: NO_3^-, 407 eV; NH_4^+, 402 eV; N_x, 400 eV. Top: untreated particulate material. Middle: H_2O-washed ambient particulate on Ag. Bottom: dried H_2O extract.

Table 1. Solubility behavior of ambient particulate nitrogen. PAA results ($\mu g/m^3$).

	Haze episode	Overcast	Moderate haze	Sunny
Date	5 Nov 76	9-12 Dec 77	30 Jan-1 Feb 78	19-23 Jan 78
Duration, hr	6	72	48	96
Total weight loading[a]	229[b]	71	49	22
Total N	8.9[c]	5.0	2.2	0.67
N after H_2O wash[d,e]	4.6	0.23	0.08[f]	0.17
	(0.52)	(0.05)	(0.04)	(0.25)
N after H_2O, Bz, MC wash[g]	0.89	0.22	0.05	0.17
	(0.10)	(0.04)	(0.02)	(0.25)
Total C[h]	40.9	8.28	9.31	5.93
C after H_2O wash[e,i]	na	4.26	3.97[f]	3.69
		(0.51)	(0.43)	(0.62)
C after H_2O, Bz, MC wash	na	0.83	na	na
		(0.10)		

[a]Net mass loading, except as noted.

[b]TSP

[c]Drop of 14% compared with measurement made 6 months earlier.

[d]Static extraction — 2 hours with deionized H_2O at 20°C except as indicated.

[e]Numbers in parentheses give the fraction of initial total nitrogen.

[f]Static extraction — 2 hours with deionized H_2O at 80°C.

[g]Bz = benzene, MC = methanol + chloroform (1:2 v:v).

[h]Total C by combustion (LBL). Prefired quartz hi-vol filters were used for collection.

[i]Numbers in parentheses give the fraction of initial carbon.

The chemical speciation of the evaporated extract may be expected to reflect the initial speciation; however, as seen from Fig. 1, the extract contains much less N_x than NH_4^+ and shows a higher NO_3^--to-NH_4^+ ratio. These findings suggest two interpretations. First, assuming that all nitrogen removed in water washing appears in the dried extract, N_x present in the untreated extract has been converted to NH_4^+ during the extraction procedure or during evaporation. Hydrolysis of amides would convert N_x to NH_4^+, and we shall discuss this further. The second observation, that more nitrate appears in the extract than in the untreated sample, implies that nitrate present in the untreated sample is quite volatile, and that a substantial fraction of the original nitrate is lost in the ESCA spectrometer. From the dependence of the nitrate peak intensity on X-ray and vacuum exposure time (Fig. 2), we can estimate the original NO_3^- intensity. It is important to note that the nitrate associated with the ambient sample is more volatile in vacuum than expected for a salt such as NH_4NO_3. The water extraction has changed

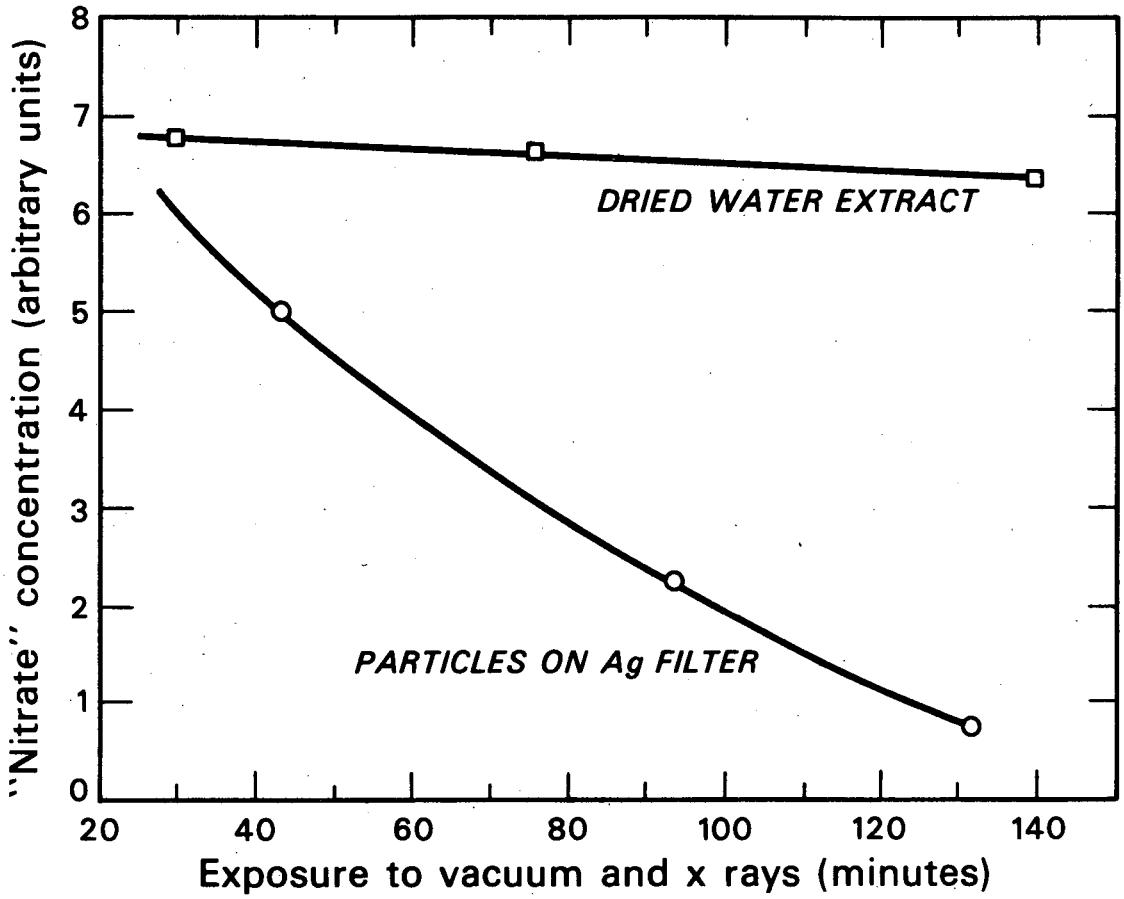

XBL 787-1273

Figure 2. Dependence of the nitrate peak intensity on high vacuum and X-ray exposure time during ESCA. Top curve: dried extract. Lower curve: untreated ambient particulate sample (December, 1977; Berkeley, California).

the chemical composition of the sample, so that conclusions based on methods employing extraction may characterize the original particulate material inaccurately.

Table 2. Effect of water washing on December 1977 ambient particulates.[a,b]

	Ambient	H_2O extract[c]	Extract-ambient	H_2O-washed ambient
NH_4^+ as N	1.4	2.3	+0.9	0.0[d]
fraction	0.28	0.47		0.0
N_x as N	1.7	0.7	-1.0	0.2
fraction	0.34	0.14		1.0
NO_3^- as N	1.9[e]	1.8	-0.1	0.0
fraction	0.38	0.39		0.0
Total nitrogen ($\mu g\ m^{-3}$)	5.0	4.8	-0.2	0.2

[a]9-12 December 1977 Berkeley particulate on Ag filters (Table 1). Total nitrogen in $\mu g\ m^{-3}$.
[b]Speciation is based on integrated areas under curves shown in Fig. 1. Total nitrogen is from PAA except for H_2O extract. H_2O extract total nitrogen is the difference between ambient total N before and after H_2O washing.
[c]Values for N are based on the assumption that all N removed by H_2O appears in the evaporated extract.
[d]ESCA results in Fig. 1 may show a small amount of NH_4^+.
[e]The volatility correction is calculated from results presented in Fig. 2.

N_x species can be hydrolyzed during H_2O extraction and thus converted to NH_4^+. The expected reaction, illustrated for particulate amides, is

$$R\text{-}\underset{\underset{O}{\|}}{C}\text{-}NH_2 + H_3O^+ \rightarrow R\text{-}\underset{\underset{O}{\|}}{C}\text{-}OH + NH_4^+ \ .$$

ESCA distinguishes amide (N_x) from NH_4^+; and, indeed, the ratio of N_x to NH_4^+ is smaller in the extract than in the ambient sample, as mentioned previously. Amine salts would appear in the extract as N_x. In Table 2 we present nitrogen speciation for the Berkeley sample from December, 1977, whose ESCA spectra were shown in Fig. 1. Total nitrogen loadings derive from PAA and speciation from ESCA, with volatility corrections for NO_3^- in the untreated sample based on vacuum behavior of nitrate in ESCA. We have assumed that all nitrogen removed from the sample during water extraction is retained in the evaporated extract so that the concentrations of dissolved species can be expressed in $\mu g\ m^{-3}$. The fact that NO_3^- concentrations for the untreated sample and the extract agree within 0.1 $\mu g\ m^{-3}$ provides a self-consistency check. We note that <u>more</u> NH_4^+ appears in the extract than was present on the untreated sample; <u>less</u> N_x appears in the extract than was

present on the untreated sample. The N_x deficiency in the extract (1.0 μg m^{-3}) matches the surplus in NH_4^+ (0.9 μg m^{-3}). These results provide evidence which is consistent with amide hydrolysis.

Removal of N_x by dissolution in water without hydrolysis can occur when N_x species are soluble stoichiometric compounds such as amines. Our results indicate that about half the original N_x is removed by hydrolysis and the other half by dissolution, as expected for a mixture of amine, amide, and nitrile functional groups. Some of the species may be present as stoichiometric compounds and others may occur as surface species.

Summary

Our principal results can be summarized as follows:

1. A large fraction of N_x (85%) originally present in ambient particulate matter can be removed by water extraction (whereas NH_4^+ and NO_3^- are completely removed).

2. Compared with the untreated sample, NH_4^+ concentration in the extract increases by approximately the same amount as the N_x concentration decreases. We attribute this behavior to the hydrolysis of amide groups.

Extraction of particulate material with water may chemically change the nitrogen species so that the chemical composition of the extract is not representative of the original sample. Therefore, analytical methods based on extraction may give erroneous results. The conversion of particulate amides to NH_4^+ during extraction may yield NH_4^+ concentrations which are too high.

References

1. G.M. Hidy, et al., Characterization of Aerosols in California (ACHEX), Rockwell International Science Center Report SC524.2SFR (1974).

2. T. Novakov, P.K. Mueller, A.E. Alcocer, and J.W. Otvos, "Chemical composition of Pasadena aerosol by particle size and time of day. III. Chemical states of nitrogen and sulfur by photoelectron spectroscopy," J. Coll. Interface Sci. 39, 225 (1972).

3. S.-G. Chang and T. Novakov, "Formation of pollution particulate nitrogen compounds by NO-soot and NH_3-soot gas-particle surface reactions," Atmos. Environ. 9, 495 (1975).

4. B.R. Appel, J.J. Wesolowski, E. Hoffer, S. Twiss, S. Wall, S.-G. Chang, and T. Novakov, "An intermethod comparison of X-ray photoelectron spectroscopic (ESCA) analysis of atmospheric particulate matter," Intern. J. Environ. Anal. Chem. 4, 189 (1976).

5. M. Clemenson, S.S. Markowitz, and T. Novakov, "Determination of low-Z elements in atmospheric aerosol particles by nuclear reactions," in Atmospheric Aerosol Research, Annual Report 1976-77, Lawrence Berkeley Laboratory Report LBL-6819.

6. M. Clemenson, T. Novakov, and S.S. Markowitz, "Determination of nitrogen in atmospheric aerosols by proton activation analysis," Anal. Chem. (in press).

7. T. Novakov and S.-G. Chang, "ESCA in environmental chemistry," in Advances in Analytical Chemistry, D. Natusch, ed. (American Chemical Society, Washington, D.C., 1977).

8. T. Novakov, S.-G. Chang, and R.L. Dod, "Application of ESCA to the analysis of atmospheric particulates," in Contemporary Topics in Analytical and Clinical Chemistry, D.M. Hercules, ed. (New York, Plenum, 1977), Vol. 1.

9. T. Novakov, R.L. Dod, S.-G. Chang, "Study of air pollution particulates by X-ray photoelectron spetroscopy," Z. anal. Chem. 282, 287 (1976).

10. C.W. Spicer and P.M. Schumacher, "Interferences in sampling atmospheric particulate nitrate," Atmos. Environ. 11, 873 (1977).

11. M.W. Weatherburn, "Phenol-hypochlorite reaction for determination of ammonia," Anal. Chem. 39, 971 (1967).

12. C.D. Hollowell, R.L. Dod, R.D. Giauque, G.W. Traynor, and T. Novakov, "Characterization of winter air pollution episodes," in Atmospheric Aerosol Research, Annual Report 1976-77, Lawrence Berkeley Laboratory Report LBL-6819.

13. C.W. Spicer, "Photochemical atmospheric pollutants derived from nitrogen oxides," Atmos. Environ. 11, 1089 (1977).

14. D.R. Cronn, R.J. Charlson, R.L. Knights, A.L. Crittenden, and B.R. Appel, "A survey of the molecular nature of primary and secondary constituents of particles in urban air by high resolution mass spectrometry," Atmos. Environ. 11, 929 (1977).

0 0 0 0 5 3 0 1 4 2 6

ATMOSPHERIC CHEMISTRY: LABORATORY STUDIES

SO_2 Oxidation by Water Droplets Containing Combustion Nuclei

W.H. Benner, H. Rosen, and T. Novakov

Particulate sulfate composes a significant fraction of the total suspended particulate matter in urban air and is thought to play an important role in visibility reduction as well as being a health hazard. The relative importance of currently known reaction mechanisms for SO_2 oxidation in the ambient atmosphere has not been decided. Recently, increased attention has been directed to reaction pathways involving liquid water. One reaction pathway which shows promise is the soot-catalyzed aqueous oxidation of SO_2.

Evidence in our laboratory has shown that the oxidation of sulfurous acid (which can be produced by hydrolysis of SO_2) to $SO_4^=$ by an aqueous suspension of soot is fairly rapid.[1] Extrapolation of the sulfurous acid oxidation results to the atmosphere indicates that this reaction pathway may be an important source of $SO_4^=$. In this paper, we report preliminary results of a laboratory study in which water droplets having soot nuclei were exposed to SO_2 in a fog chamber. This chamber study is thought to simulate a common tropospheric process — the condensation of water vapor onto nuclei to form fogs, plumes, and clouds in the presence of SO_2. Preliminary results of our experiments indicate that fog droplets containing soot nuclei are a very effective system for the oxidation of SO_2 to $SO_4^=$.

Experimental

A diagram of the experimental system is shown in Fig. 1. A flowstream of combustion particles (soot particles) was humidified and subsequently cooled so that water vapor condensed onto the particles. The resultant fog droplets were drawn into a fog chamber and exposed to SO_2.

Soot particles from several types of sources were drawn through the system:

1. A propane diffusion flame ($\sim$ 125 ml/min propane) was produced by plugging the air holes in a Bernz-o-matic torch nozzle. Soot particles from this flame were forced into a 5-m^3 polyethylene bag that had previously been inflated with filtered room air. The particles were permitted to coagulate in the bag for several hours, after which the bag was connected to the fog generator. For the remaining sources, the soot particles were collected from an 8 cm diam × 40 cm high stainless steel chimney into which the flames were introduced (Fig. 1).

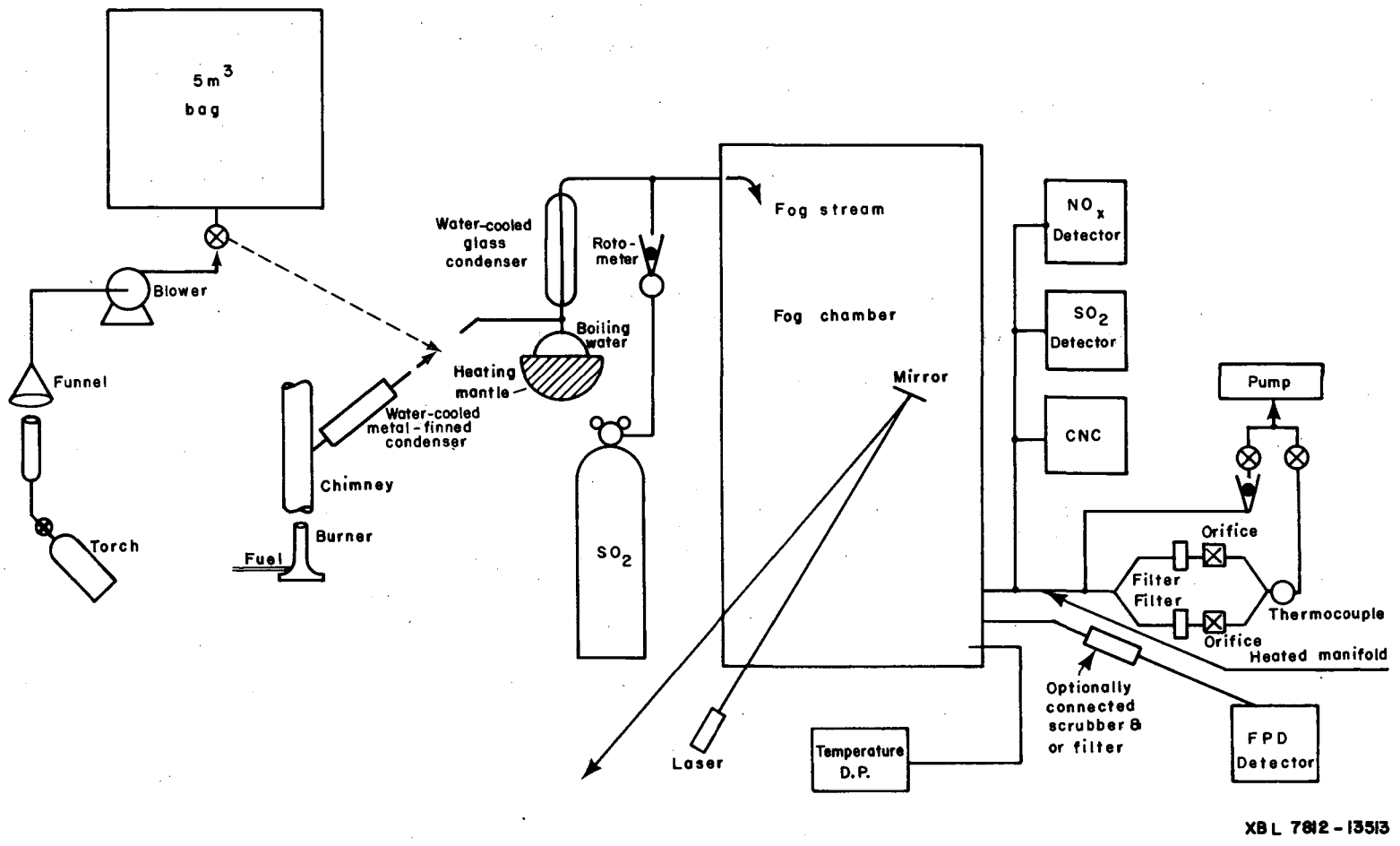

Figure 1. Diagram of the experimental system used to study the oxidation of SO_2 in fog droplets.

2. A propane diffusion flame was produced as in (1) above.

3. A natural gas diffusion flame was produced by covering the air holes in a Fisher Bunsen burner and was introduced into the chimney.

4. A natural gas premixed (fuel and air mixed before burning) flame from a Bunsen burner was introduced into the chimney.

Soot particles were optionally drawn through the fog generator or introduced directly into the fog chamber. Fog was produced by introducing water vapor from a flask of boiling water into a flowstream of particle-laden gases and subsequently cooling the humidified gases in a glass water-cooled distillation condenser (Fig. 1). When combustion particles were withdrawn directly from the chimney, an additional metal-finned water-cooled condenser for cooling the combustion gases was placed in the flowstream between the chimney and the humidifier. The resultant fog droplets were $\sim$ 10 μm in diameter, as measured by sedimentation rates in the chamber. A mixture of 100 ppm SO_2 in N_2 could be introduced into the stream of fog droplets by a rotameter and valve. The resultant mixture of gases and particles was drawn into the top of a 60 cm deep × 91 cm wide × 122 cm high fog chamber. The chamber was constructed from 1.9-cm thick plywood with one of the 91 cm × 122 cm sides constructed from 1.9-cm thick plexiglass. The inside surface of the fog chamber was covered with a moisture-resistant paint.

Air samples were removed from the chamber through several closely spaced sampling ports located near the floor of the chamber. Two in-line 2.5-cm diam stainless steel filters were connected to one of the sampling ports by means of a 1.9-cm diameter brass pipe Y. The Y and filters were heated by an electrical heating tape. Calibrated critical orifices were used to control the rate at which chamber air was drawn through the filters. Normally, identical orifices were used with the two filters, and particles from the chamber were collected simultaneously on a prefired quartz fiber filter and a 1.2-μm pore Millipore filter. The temperature of the air which passed through the filters was monitored by a thermocouple located downstream from the critical orifices and the temperature was maintained at 50°C to prevent liquid water from being collected on the filters. This precaution avoided the possibility of chemical reactions involving liquid water taking place on the filter media.

An SO_2-specific monitor (Thermal Electron Co.) was connected to the heated manifold via a Teflon sampling tube. A dew-point sensor (thermoelectrically cooled mirror, General Eastern Corp.) was attached to a second sampling port. Chamber temperature was measured by a thermocouple. Formation of particulate $SO_4^{=}$

in the chamber was monitored by filter analysis and/or flame photometry. A sulfur-specific flame photometric detector (FPD) (Model 285, Meloy Inst.) was attached to a third sampling port on the fog chamber. The instrument was modified slightly so that an air sample passed through only 10 cm of 0.32-cm diam tubing before it entered the FPD. A diffusion scrubber was optionally inserted in the inlet line of the FPD. The use of an SO_2/H_2S diffusion scrubber (lead peroxide as the adsorbate) has been described in the literature as a selective way to remove sulfur gases from an air stream containing SO_2, H_2S, and particles.[2] The particles pass through the scrubber; if they contain sulfur, they are detected by the FPD. The Meloy instrument suffers from CO_2 interference, i.e., if CO_2 and SO_2 are present in an air sample, the CO_2 decreases the response to SO_2. This problem is particularly severe when the analyzer is used to measure sulfur in combustion gases which are characteristically enriched in CO_2. A new type of diffusion scrubber was designed to overcome the CO_2 interference problem. A 0.64 cm diam × 19 cm long tube was constructed from 100-mesh stainless steel screening. This mesh tube was positioned axially inside a 1.7 cm × 19 cm long glass tube and sealed to the glass tube with appropriate tube fittings. The space between the mesh tube and the glass tube was filled with 8-20 mesh Ascarite (Matheson-Coleman and Bell Co.). The Ascarite diffusion scrubber was capable of decreasing the CO_2 concentration in room air from 330 ppm to < 0.5 ppm and lowered the CO_2 concentration in the chamber gases to 22 ppm from a presumably high value. The Ascarite scrubber was capable of removing 99%+ of SO_2 from an air stream containing 5 ppm SO_2. This scrubber was also found to remove from the chamber sulfur-containing gases which were not removed by lead peroxide scrubbers.

By placing a 2.5-cm diam quartz fiber filter and the Ascarite scrubber in the sampling line of the FPD, gaseous and particulate sulfur were removed from the sample stream. The difference in FPD response with and without the filter in line is assumed to be due to particulate sulfur. A pressure drop associated with the filter was not responsible for this difference in FPD response because the same difference was observed when a larger filter was used. The lower limit of detection for particulate sulfur was 0.2 ppb as SO_2 or 0.8 μg $SO_4^{=}/m^3$. It has also been reported in the literature that the sensitivity of the FPD to particulate sulfur is dependent on the sulfur species and the temperature of the FPD burner.[2] For example, at temperatures in excess of about 100°C, H_2SO_4 is vaporized, and as much as 90% of this vapor is lost by reaction with metal parts in the FPD and escapes detection. Ammonium sulfate is not as easily vaporized, and the FPD shows

a greater response to ammonium sulfate than to equal concentrations of H_2SO_4. The sulfate concentrations as indicated by the FPD may be as low as 10% of the actual concentration because of the vaporization problem since the sulfate species is possibly H_2SO_4. This response factor must be kept in mind when extrapolating the results of this work to the ambient atmosphere. Attempts are being made to overcome the vaporization problem and to determine the sulfate species produced.

The extent to which the fog droplets filled the chamber was determined by shining a 1-mW He-Ne laser beam through the plexiglass window to a mirror on the opposite chamber wall. By siting along the reflected beam, crude measurements of light scattered in the forward direction by the particles and droplets were made. The beam was also used to probe the extent to which the fog filled other parts of the chamber.

Particulate samples collected on prefired quartz fiber filters (baked at 800°C for 12 hr) were analyzed for total combustion carbon. The CO_2 evolved from the combusted sample was detected by gas chromatography. The total carbon per m^3 was then calculated from the CO_2 value and the volume of air drawn through the filter. Particulate samples collected on Millipore filters were analyzed by X-ray fluorescence (XRF) in a few cases for elements having $Z > 14$, but were normally analyzed only for sulfur. Electron spectroscopy (ESCA) was used to show that the sulfur was primarily sulfate. The light-absorbing properties of the filtered particles was determined by directing a 1-mW He-Ne laser beam through a loaded Millipore filter. By comparing the light transmitted by clean and loaded filters, a percent transmission value was calculated. From the percent transmission the optical attenuation, $-100 \ln I/I_0$, was calculated.[3]

To determine if combustion nuclei were encapsulated with liquid water, a small impactor, designed from a 2.5-cm diam plastic in-line filter holder, was used to collect fog droplets. A 22-gauge hypodermic needle was inserted through the center of the inlet to the filter holder and sealed in place with epoxy cement. The needle extended to within several mm of the grill, which normally supports the filter in such a filter holder. A small circle of gummed label was stuck onto the center of the grill and served as the impaction surface. By trial and error, the velocity of air through the needle was adjusted so that fresh combustion particles were not collected by this impactor and the fog droplets were impacted. Examination of the impaction spots indicated that many droplets contained black nuclei.

Results and Discussion

Propane Soot Particles

An initial series of chamber runs was conducted in which combustion particles were drawn from the 5-m^3 bag into the fog generator and chamber. Filter samples of the particles were collected during these runs, but the FPD was not used. Figures 2 and 3 show the results of this series of runs. The presence of added SO_2 and fog increased the $[SO_4^=]$ in the chamber. An average of 5.6 μg $SO_4^=/m^3$ was observed in 18 soot-fog-SO_2 runs in which the $[SO_2]$ was between 70 and 120 ppb. In 8 background runs, i.e., soot and fog or soot alone, an average of 1.8 μg $SO_4^=/m^3$ was detected. Since the reaction time for the fog droplets was determined by the 15-min setting time, these results indicate a rather fast oxidation of SO_2 in the droplets.

Figure 2 shows that poor correlation ($r^2 = 0.25$) was obtained for the regression of total particulate carbon versus particulate $SO_4^=$. Soot particles, by definition, are composed of several components such as graphitic crystallites (source of black color) and various hydrocarbons. The amounts of either of these components varies with the type of soot, and it is therefore not surprising that the production of $SO_4^=$ was not well correlated with total particulate carbon.

A comparison of μg $SO_4^=$ versus the optical attenuation of the particles is presented in Fig. 3. Evidence from our laboratory has shown that the optical attenuation of filter deposits is proportional to the graphitic content of the particles.[4] Figure 3 thus shows that a relationship exists between the graphitic content of the particles and $SO_4^=$ formation which agrees with the SO_2 oxidation mechanism reported by Chang et al.[1]

An additional run was conducted in which propane diffusion flame particles were introduced into the fog chamber via the chimney. The results of this run are shown in Fig. 4 and are discussed later in this paper.

Natural Gas Soot Particles

In this series of experimental runs, the concentration of particulate $SO_4^=$ was monitored by the FPD. Filter samples of the particles were not collected. Figures 4 and 5 show the results of these runs. At t = 0 (Fig. 4), an equilibrium concentration of combustion nuclei existed in the chamber, and at this time the influent stream of particles was diverted through the fog generator. SO_2 was also introduced into the fog stream at this time. Initially, the fog droplets evaporated rapidly in the chamber. As the RH in the chamber increased, the lifetime of the droplets also increased so that the chamber was filled with fog in about 1-2 hr. At such a time, the chamber RH was ∿ 100% and the droplets did not

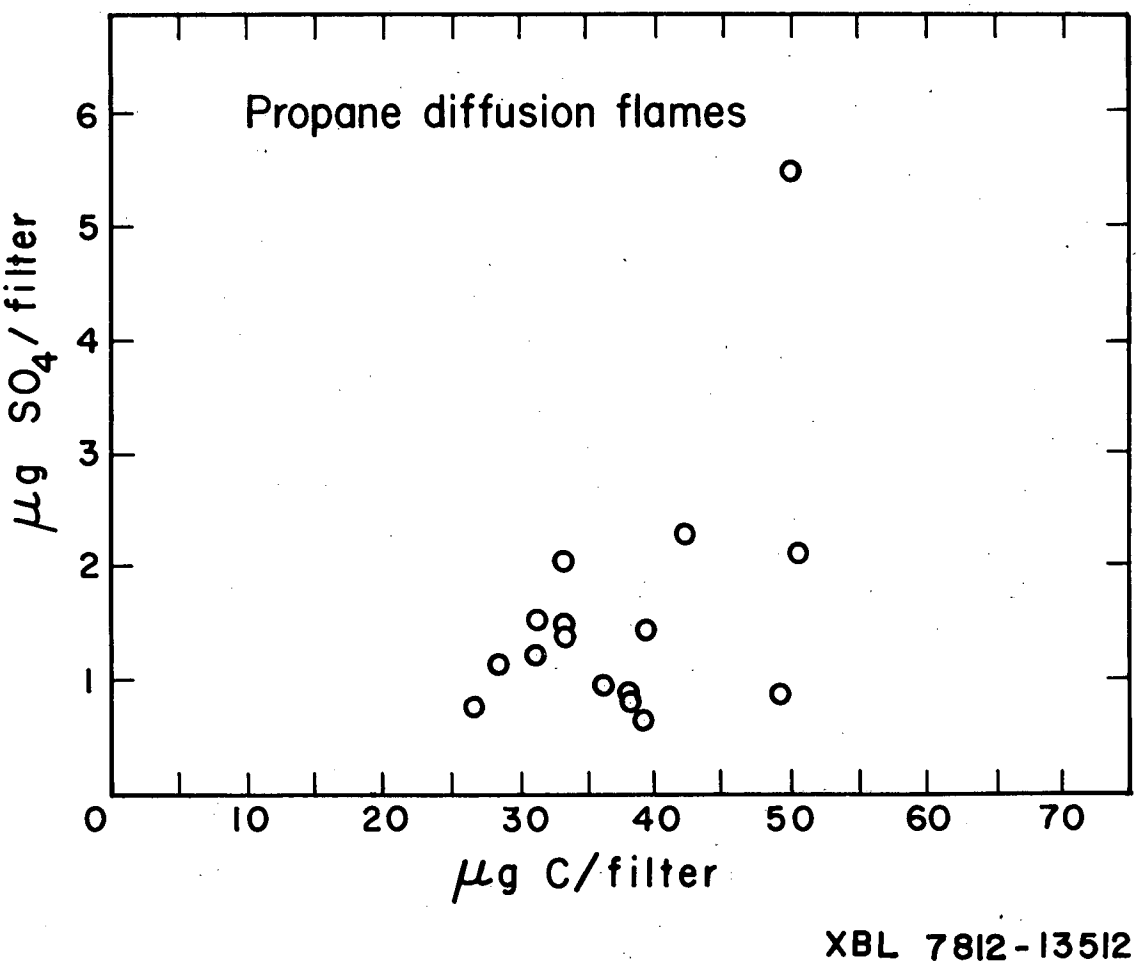

Figure 2. A plot of sulfate formed versus carbon loading for fog droplets containing propane soot nuclei. The correlation coefficient for the two parameters was $r^2 = 0.25$.

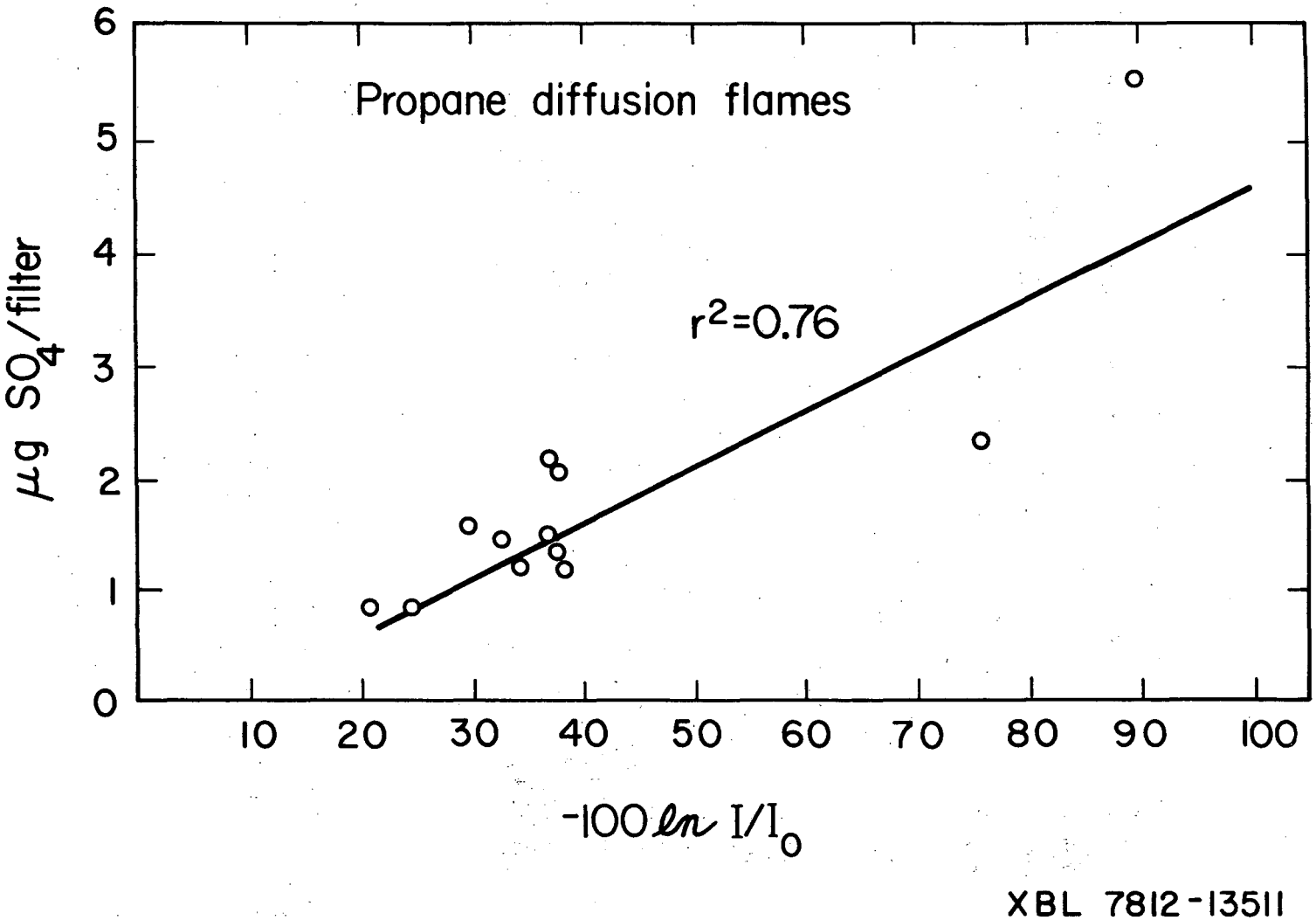

Figure 3. A plot of sulfate formed versus optical attenuation ($-100 \ln I/I_0$) for fog droplets containing propane soot nuclei.

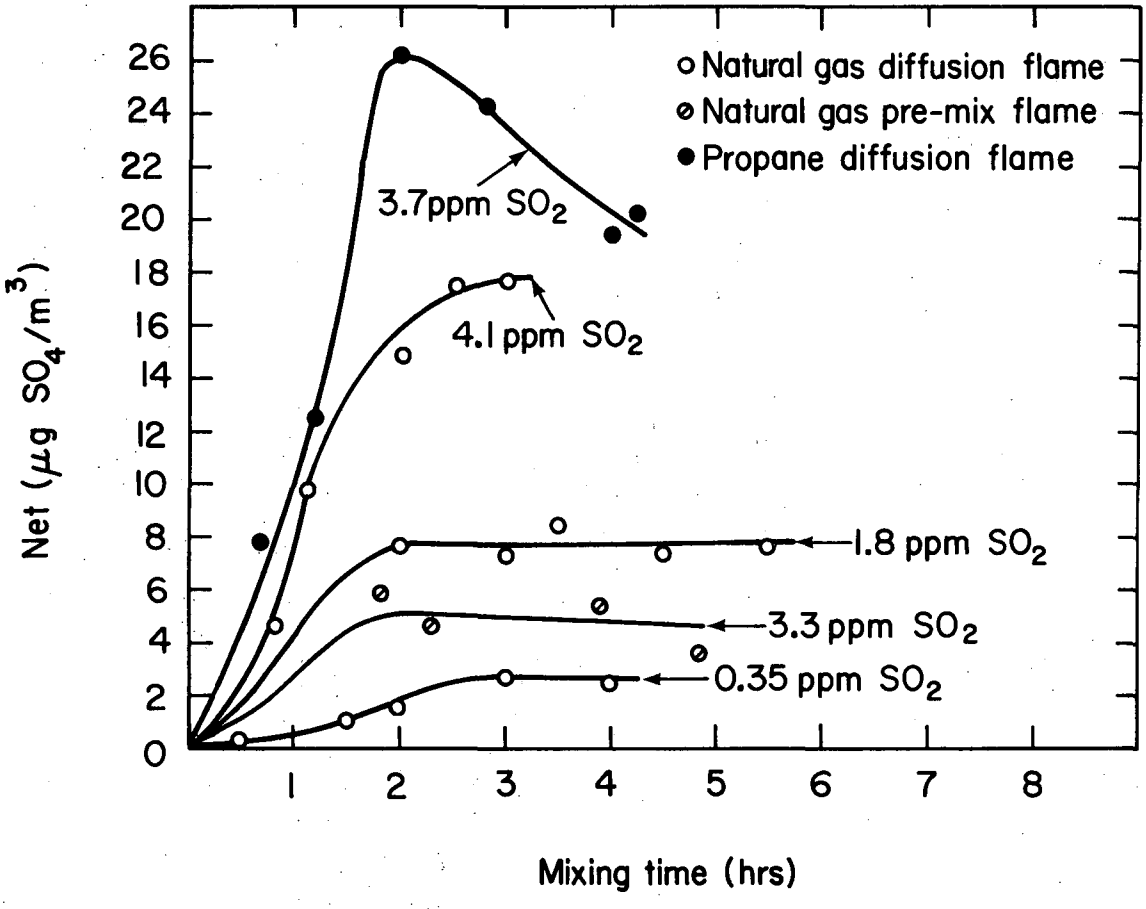

XBL 7812-13509

Figure 4. A plot of sulfate production versus mixing time in a chamber for fog droplets containing various types of nuclei. At t = 0, fog droplets and SO_2 were introduced into a chamber which had RH < 50% and a background concentration of SO_2.

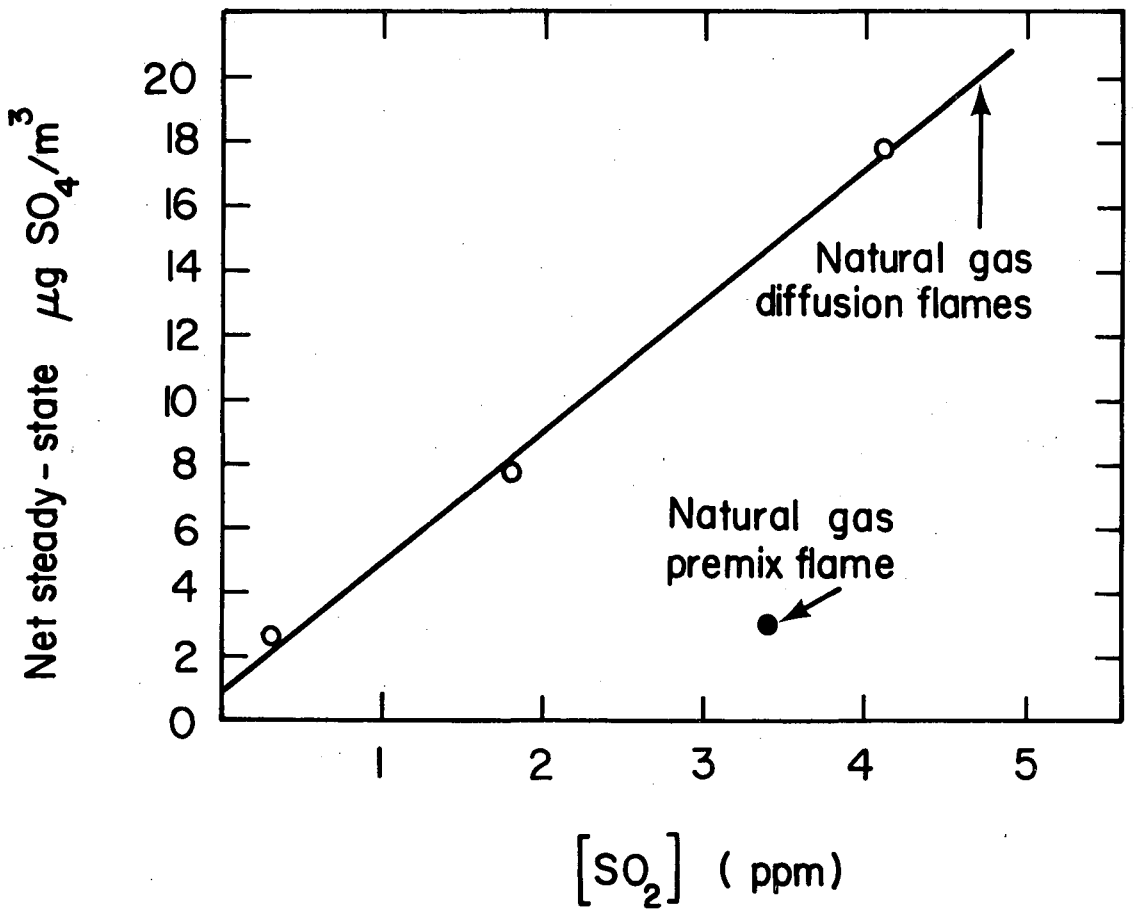

XBL 7812-13510

Figure 5. A plot of sulfate formed versus $[SO_2]$ for fog droplets containing natural gas combustion nuclei. The $[SO_4^{=}]$ was obtained from the net steady-state $[SO_4^{=}]$ presented in Fig. 4.

evaporate before they settled to the bottom of the chamber. Reaction time in the droplets was limited to evaporation time during the initial 1-2 hr period or to settling time of the droplets (∿ 15 min) after chamber RH was ∿ 100%. It is obvious from the curves in Fig. 4 that $SO_4^=$ was produced even when the droplet reaction time was shorter than 15 min.

In Fig. 5 the steady-state $[SO_4^=]$ for the runs in Fig. 4 are plotted versus the steady-state $[SO_2]$. The linear regression line drawn through the diffusion flame data points indicates a nearly linear dependence of $[SO_4^=]$ on $[SO_2]$. Previous investigations in our laboratory have indicated that the oxidation mechanism for $SO_3^=$ in aqueous suspensions of soot is zero order with respect to $SO_3^=$.[1] The results reported here do not disprove the zero order mechanism since reaction rates were not measured. If one assumes a zero order reaction mechanism, the data reported here suggest that the oxidation of SO_2 in the droplet proceeds at a faster rate than the oxidation of $SO_3^=$ in aqueous suspensions of soot. The rate may be fast enough so that all of the SO_2 in the droplet is oxidized in less than 15 min (settling time of droplets). In the zero order mechanism, the same amount of $SO_4^=$ is produced after a fixed reaction time, for example, 15 min, regardless of the initial $[SO_3^=]$. If, however, the reaction rate in fog droplets is rapid enough to oxidize <u>all</u> the $SO_3^=$ that was present initially, it would mistakenly appear that the amount of $SO_4^=$ produced was related to the initial $[SO_3^=]$. Investigation of the rate of reaction and the reaction mechanism for the oxidation of SO_2 in a soot-fog-SO_2 system is part of future plans.

In addition to the runs conducted with fog droplets containing natural gas diffusion flame particles, single runs were conducted with natural gas premixed-flame particles or propane diffusion flame particles. The results of these two runs are presented in Figs. 4 and 5. The premixed natural gas combustion particles produced a smaller equilibrium $[SO_4^=]$ than was expected for diffusion flame particles in a similar $[SO_2]$. This was presumably due to the fact that premixed flames are less sooty than diffusion flames.[5] The composition of the nucleus of a fog droplet appears to influence the oxidation of SO_2 in the experiments described here. The experimental run in Fig. 4, which was conducted with propane diffusion flame particles, supports the data in Figs. 2 and 3 and shows that soot particles, when encapsulated with liquid water, can oxidize SO_2. The experimental run with propane particles is thought to have the highest μg C/m^3 of all the runs in Fig. 4, judged by the density of the fog in the chamber. Thus the fact that the propane particle curve (3.7 ppm SO_2) rises above the natural gas diffusion particle curve (4.1 ppm SO_2) does not necessarily indicate that propane soot particles oxidize SO_2 more effectively than natural gas soot particles.

Evidence in our laboratory indicates that a large fraction of the particles in urban atmospheres are soot particles. These particles can act as sites for the condensation of water, and the lifetime of these droplets appears to be long enough to oxidize SO_2 to $SO_4^{=}$, even when the SO_2 concentration is low, i.e., several tens of parts-per-billion. Comparison of the relatively long reaction time permissible in natural fogs to the 15-min reaction time in the fog chamber strongly suggests that oxidation of SO_2 by soot particles encapsulated with liquid water is an important tropospheric reaction.

The following conclusions were drawn from the data reported in this paper:

1. Soot can act as a nucleus for the condensation of water.
2. SO_2 is oxidized in the soot-fog-SO_2 system to form $SO_4^{=}$.
3. The presence of liquid water and soot in the system is very important.
4. The production of $SO_4^{=}$ is poorly correlated with total particulate carbon, but more strongly correlated with the graphitic content of the particles.
5. Dense fogs could be produced with natural gas premixed and diffusion flame particles, but the fog containing the diffusion flame (sooty) particles appeared to oxidize SO_2 more efficiently.
6. The reaction appears to be rapid enough so that SO_2 oxidation in liquid droplets appears to be important in the ambient air.

References

1. S.-G. Chang, R. Brodzinsky, R. Toossi, S.S. Markowitz, and T. Novakov, "Catalytic oxidation of SO2 on carbon in aqueous suspensions," Conference on Carbonaceous Particles in the Atmosphere, Proceedings, Lawrence Berkeley Laboratory, Berkeley, California (in press).
2. J.J. Huntzicker, R.S. Hoffman, and C.-S. Ling, "Continuous measurement and speciation of sulfur-containing aerosols by flame photometry," Atmos. Environ. 12, 83 (1978).
3. A.D.A. Hansen, H. Rosen, R.L. Dod, W.H. Benner, and T. Novakov, "Optical characterization of ambient and source particulates," this report.
4. H. Rosen, A.D.A. Hansen, L. Gundel, and T. Novakov, "Identification of the optically absorbing component in urban aerosols," Appl. Optics 17, 3859 (1978).
5. A.F. Gaydon and H.G. Wolfhard, Flames, London, Chapman and Hall, 1970.

Kinetics and Mechanism of the Reactions of NO_x with SO_2 in Aqueous Solutions

S.B. Oblath, S.S. Markowitz, T. Novakov, and S.-G. Chang

The oxides of nitrogen (NO_x) and sulfur dioxide (SO_2) are common and abundant air pollutants. The gas-phase interaction of NO_x and SO_2 has been widely studied[1-4]; but so far the reaction between NO_x and SO_2 after dissolution in water droplets has been overlooked by atmospheric chemists. It is important to investigate the reaction in an aqueous medium because such circumstances occur frequently in fogs, clouds, rain, plumes, and the human respiratory system. In addition, deliquescent and/or hygroscopic salts such as NH_4HSO_4, $(NH_4)_2SO_4$, and NaCl in atmospheric particulates can pick up liquid water at a low relative humidity.[5]

We have reviewed the literature[6-9] and found that many concurrent and consecutive chemical reactions can occur as a result of the interaction between NO_x and SO_2 in liquid water. The kinetics and mechanisms of these reactions have not been well characterized. Nevertheless, it has been demonstrated that the products of the reaction depend on the concentrations of reactants, temperature, and acidity of the solution. For example, sulfuric acid is produced and NO_x is regenerated in the well-known lead chamber process where the reaction is carried out at very low pH and high concentrations of reactants. On the other hand, species such as N_2O, hydroxylamine sulfonates, amine sulfonates, and sulfuric acid are produced if the reaction takes place in a slightly acidic or neutral solution.

The purpose of this study is to determine the products, kinetics, and mechanisms of reactions occurring in the NO_x-SO_2-$H_2O(\ell)$ system under realistic atmospheric conditions and to assess the impact of these reactions on air quality. Preliminary results have indicated that the interaction of NO_x and SO_2 in an aqueous medium could be a very important source of sulfate and N_2O formation in the atmosphere.

Nitrous (III) and nitric (V) acids are produced in the aqueous phase after nitrogen oxides are absorbed into liquid water, and sulfurous (IV) acid is formed if SO_2 dissolves in water. The present study measured the reaction rate of nitrites with bisulfites in the pH region between 3 and 7 at 20°C. A mixture of sodium metabisulfite with sodium sulfite was used as the buffer solution for pH of 7, while potassium biphthalate and sodium hydroxide were used for pH of 5.5 and 4.5.

To study the dependence of the reaction rate on the nitrite and bisulfite concentrations, the initial concentrations of either nitrite or bisulfite were varied, while all other parameters, such as pH and temperature, were held constant. These kinetic experiments were carried out in an excess of bisulfite with respect to nitrite to keep the S(+4) concentrations nearly constant at the initial value throughout the course of the reaction. The concentration of nitrite was monitored spectrophotometrically during the course of the reaction using either a Beckman DU (358 nm) or a Bausch and Lomb Spectronic 20 (356 nm). Because the rate of disappearance of nitrite changes many orders of magnitude over the range of pH studied, the initial concentrations of the reactants are adjusted for the selected pH region. The typical initial conditions for pH = 7 were: nitrite, 0.01-0.02 M; bisulfite, 0.10-0.30 M; and sulfite, 0.10-0.25 M. The initial conditions for pH of 5.5 or 4.5 were: nitrite, 0.001-0.003 M; and bisulfite, 0.02-0.05 M.

The results of the experiments for pH of 7, 5.5, and 4.5 are shown in Figs. 1-6. The linear relationship between the logarithm of the nitrite concentration and the reaction time (Figs. 1, 3, and 5) indicates that the reaction rate is first order with respect to the nitrite concentration in all three pH regions. The bisulfite dependence on the reaction rate is illustrated by the logarithmic plot of $(d \ln [NO_2])/dt$ vs. $[HSO_3^-]$ (Figs. 2, 4, and 6). The slope of the line represents the reaction order of bisulfite, which is 2, 1.1, and 1 for pH of 7, 5.5, and 4.5 respectively.

We have also carried out a series of experiments to study the overall stoichiometry of the reaction at 20°C. In these experiments, similar initial concentrations of bisulfite and nitrite were employed. The sulfite concentration was determined by addition of excess iodine to quench the reaction and by back-titration with thiosulfate. The nitrites were determined by visible spectrophotometry at 356 nm. The results are 2.5, 2.1, and 1.5 bisulfite per nitrite molecule reacted at pH of 7, 4.5, and 3 respectively.

Further studies to determine the dependence of the reaction rate on species such as sulfate and sulfite are being investigated. The reaction rate was found to be independent of the sulfate concentration at a pH of 7. An increase in sulfite concentration appears to slow down the rate of disappearance of nitrite.[8] This may be due to a change in pH on addition of the sulfite.

These experimental results support the belief that there are several concurrent processes involved. The following diagram illustrates those reaction processes which have been indicated in the literature.[6-9]

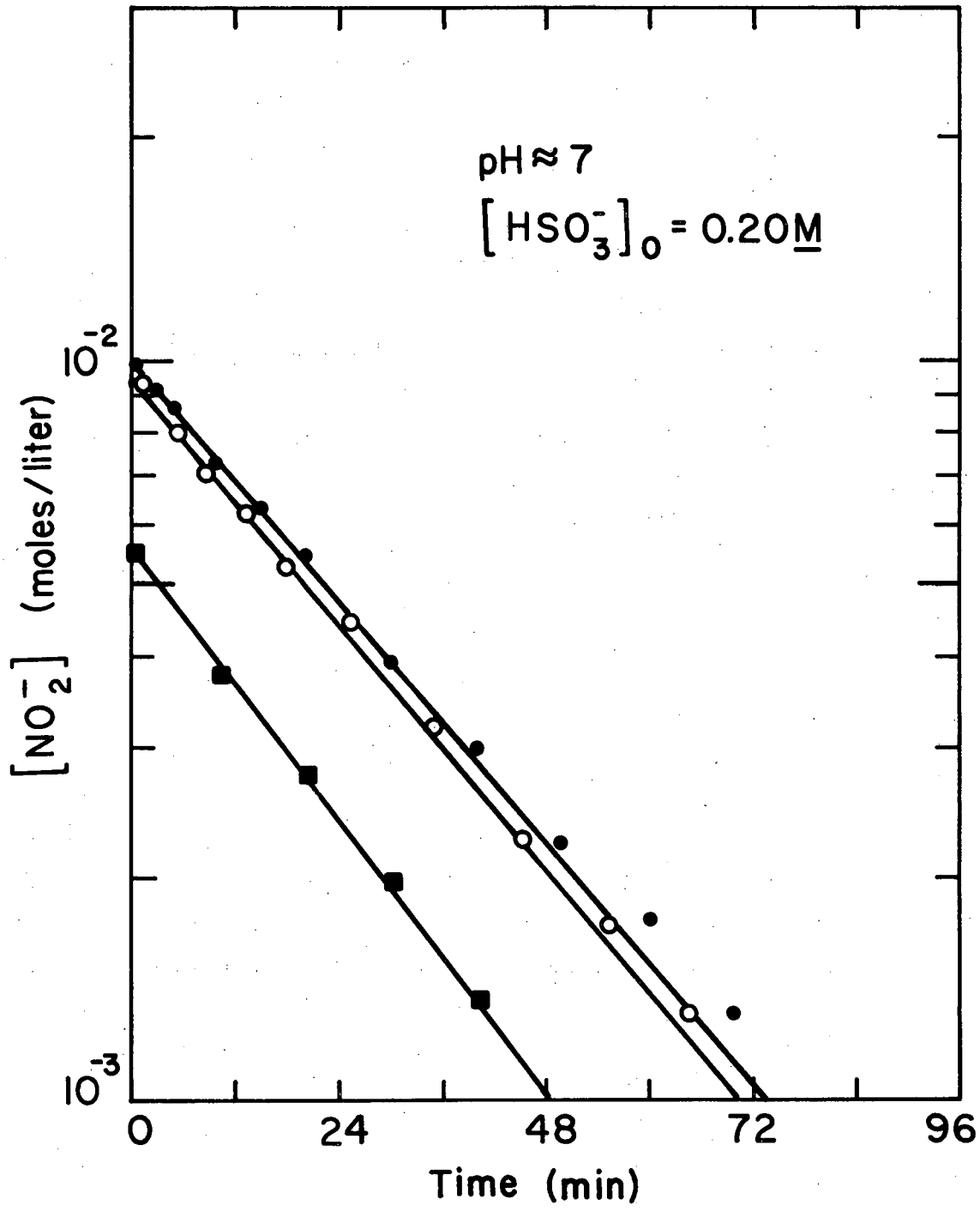

XBL 7812-13384

Figure 1. Nitrite concentration as a function of reaction time for various initial concentrations of nitrite for pH = 7. The initial bisulfite concentration is 0.20 M.

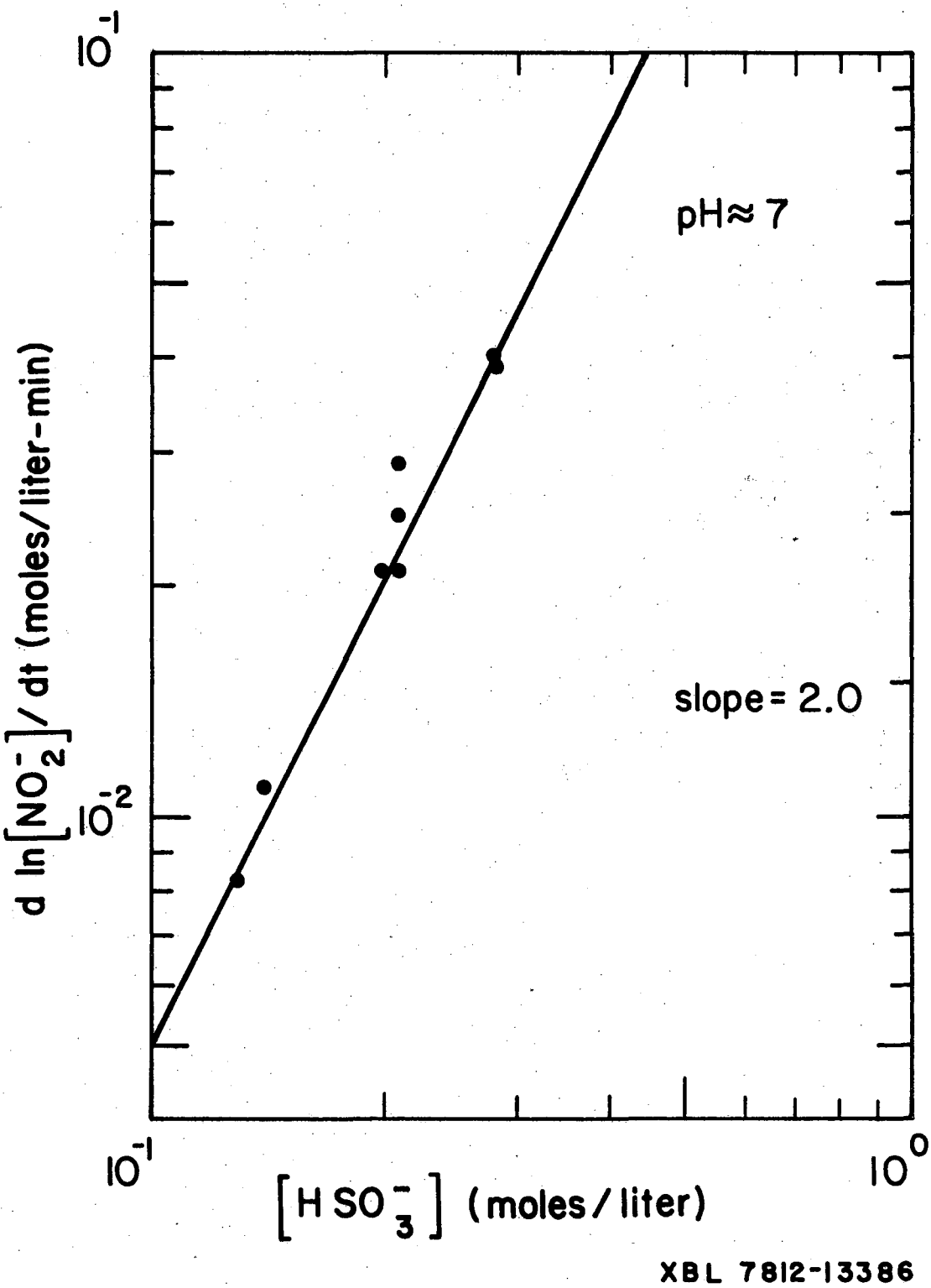

Figure 2. A plot of d ln[NO_2^-]/dt versus bisulfite concentration for pH = 7.

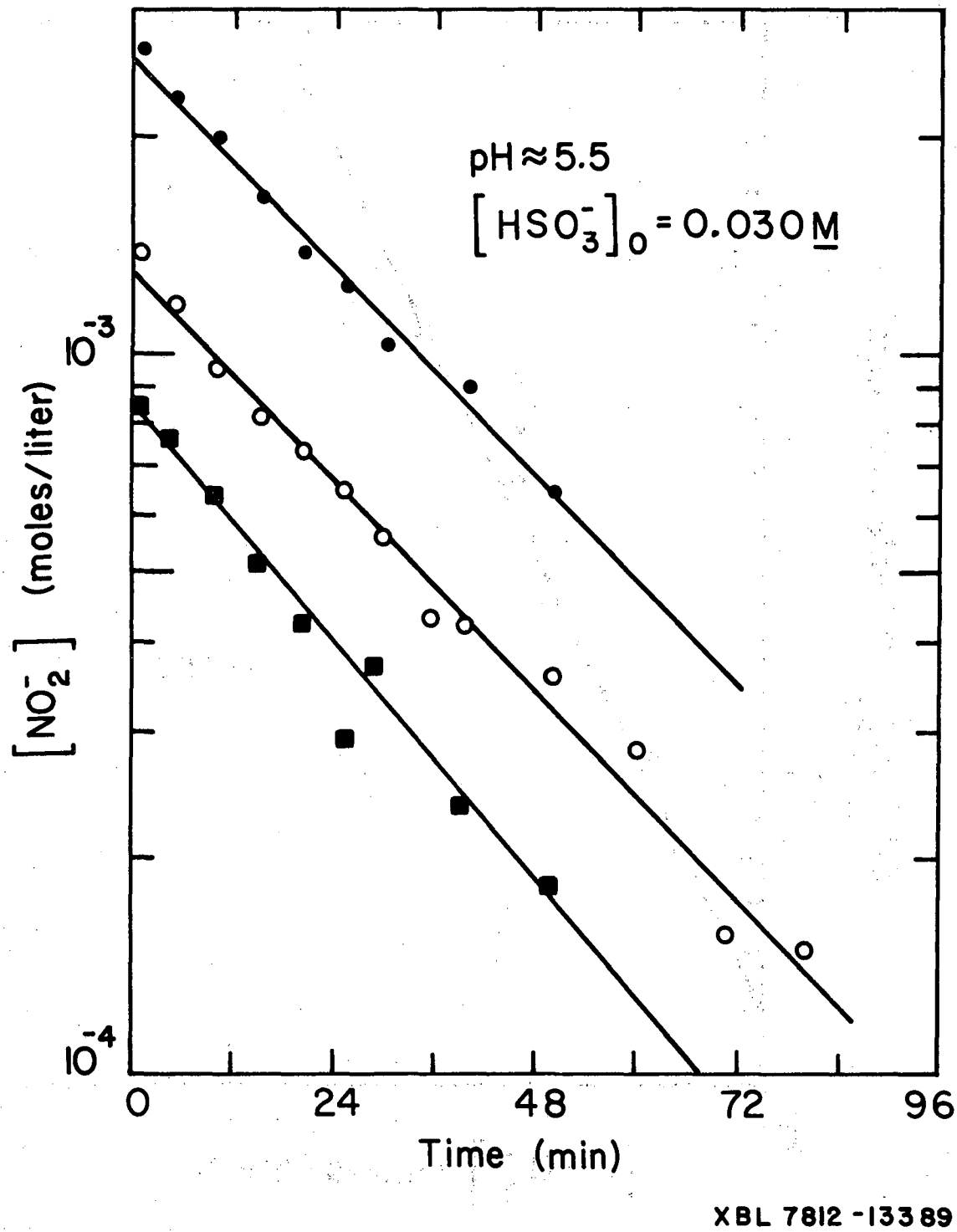

Figure 3. Nitrite concencentration as a function of reaction time for various initial concentrations of nitrite for pH = 5.5. The initial bisulfite concentrations are 0.030 M.

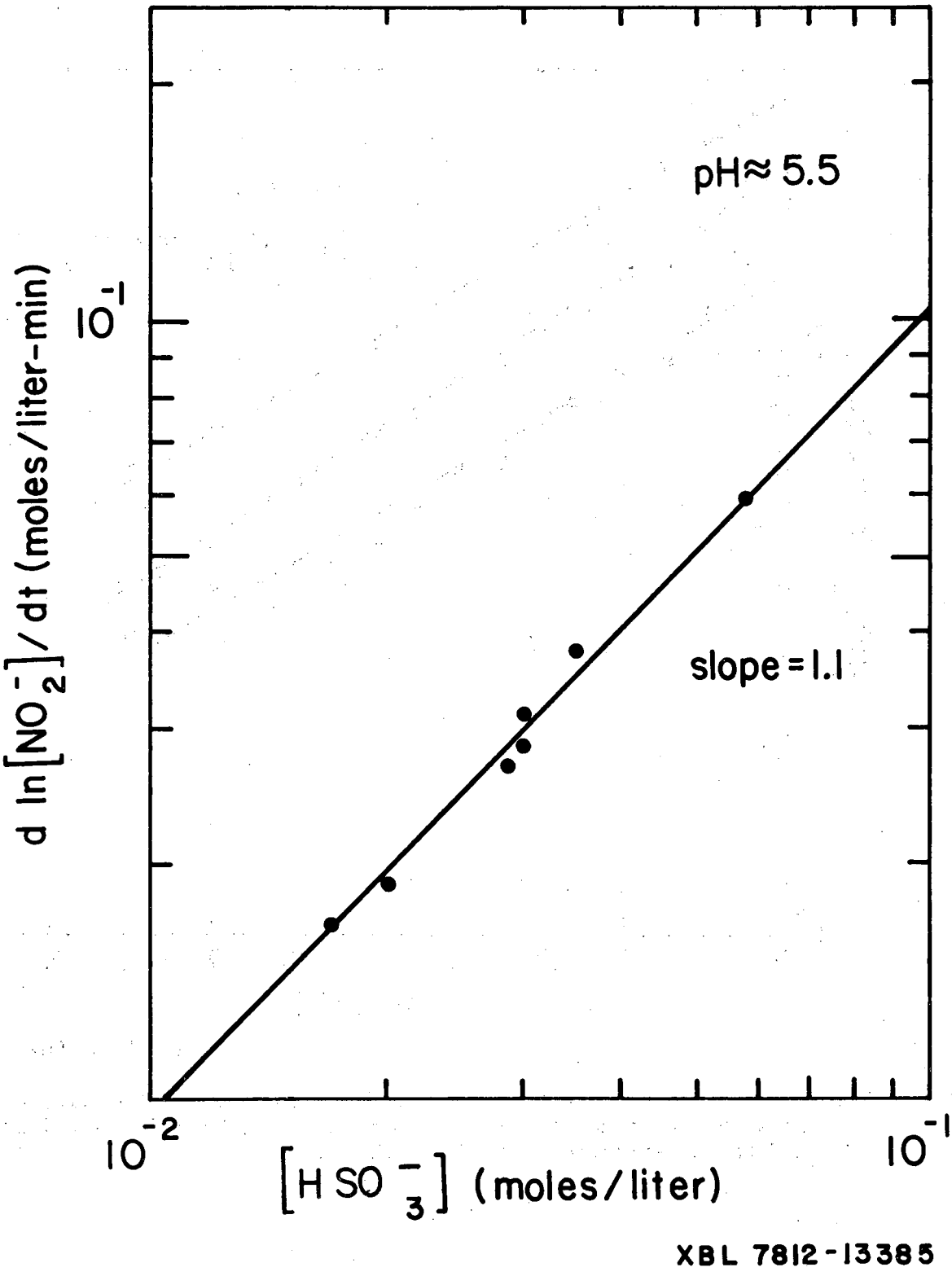

XBL 7812-13385

Figure 4. A plot of d ln[NO_2^-]/dt versus bisulfite concentration for pH = 5.5.

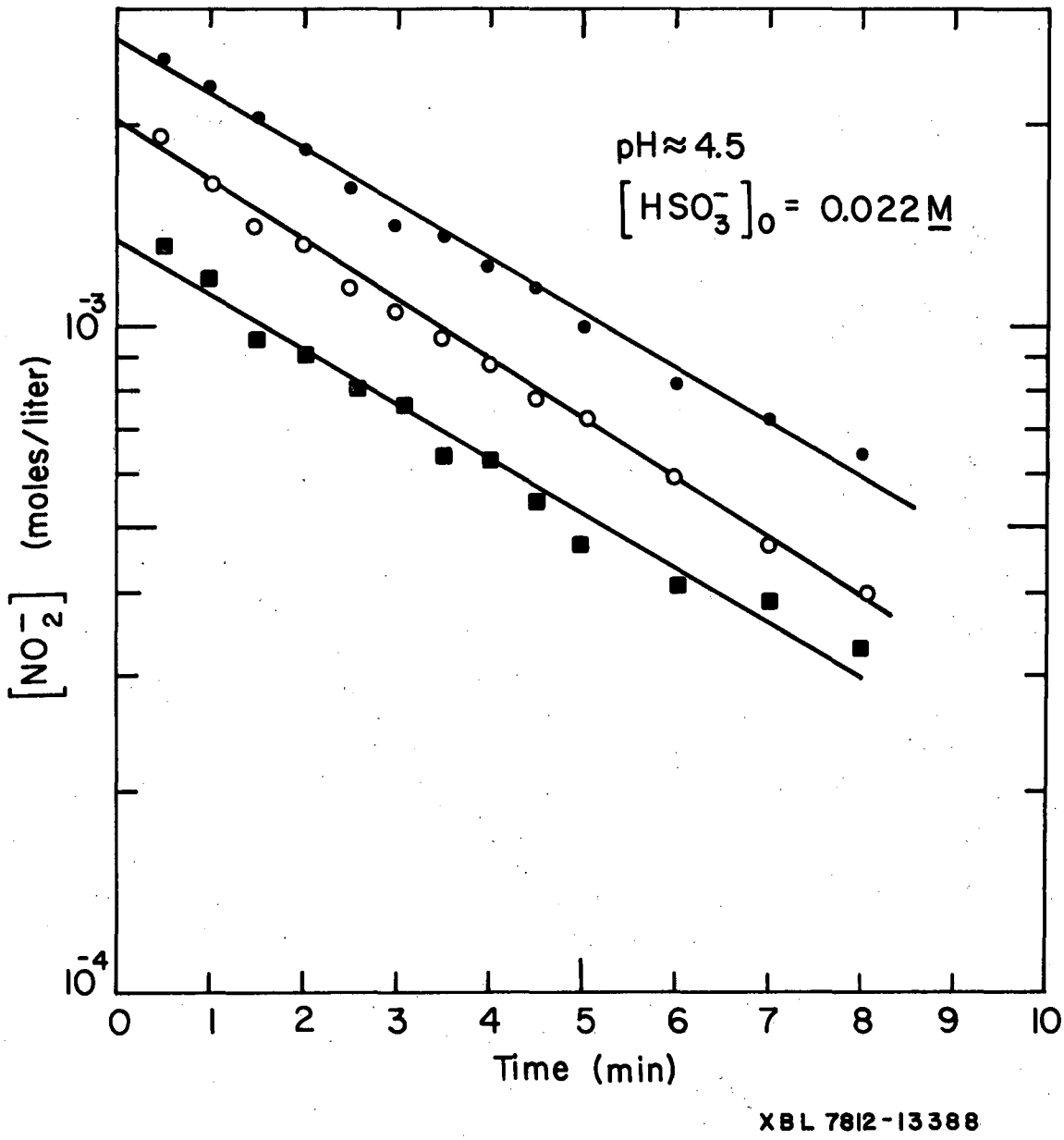

Figure 5. Nitrite concentration as a function of reaction time for various initial concentrations of nitrite for pH = 4.5. The initial bisulfite concentrations are 0.022 M.

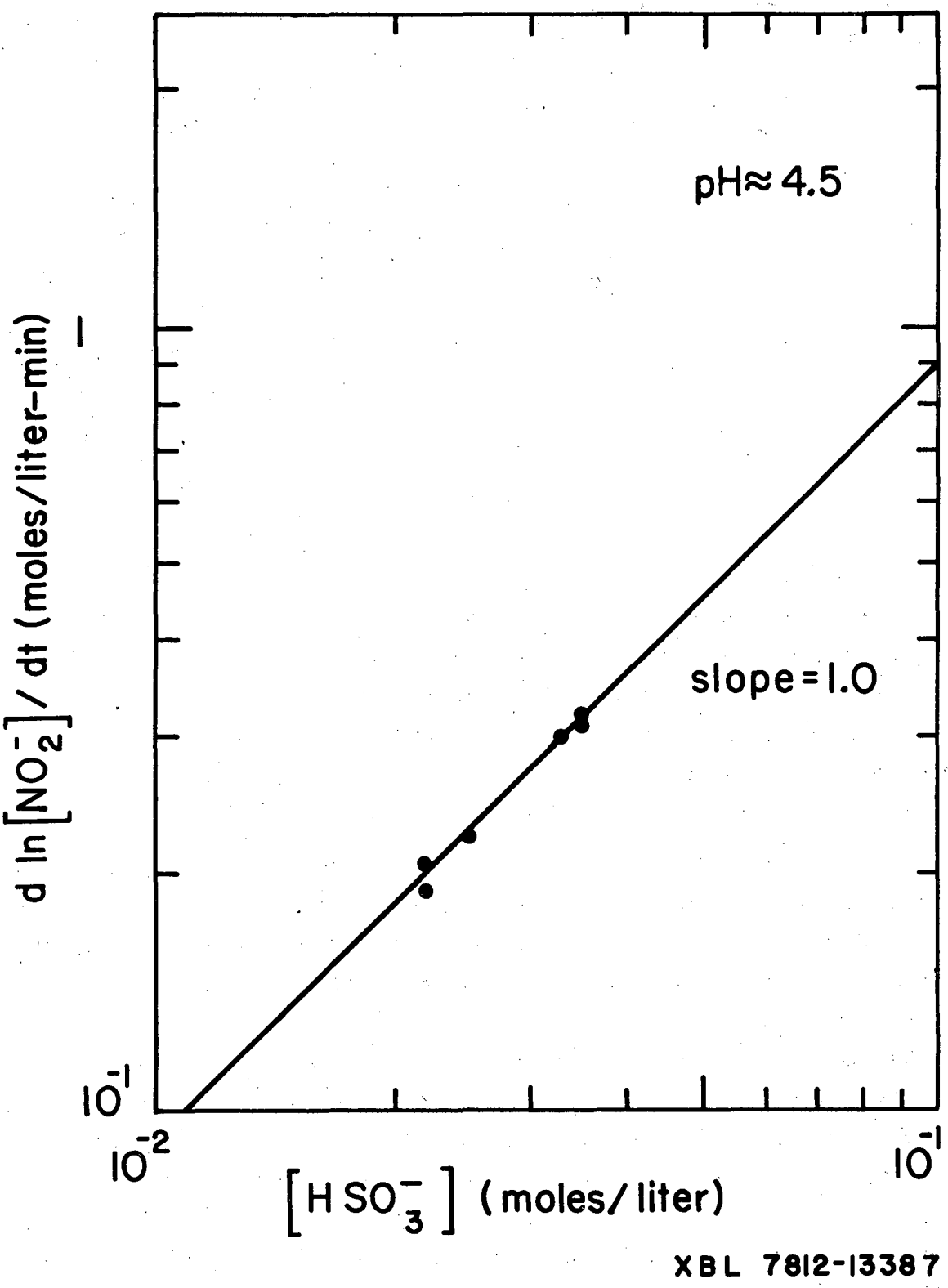

Figure 6. A plot of the d ln[NO_2^-]/dt versus bisulfite concentration for pH = 4.5.

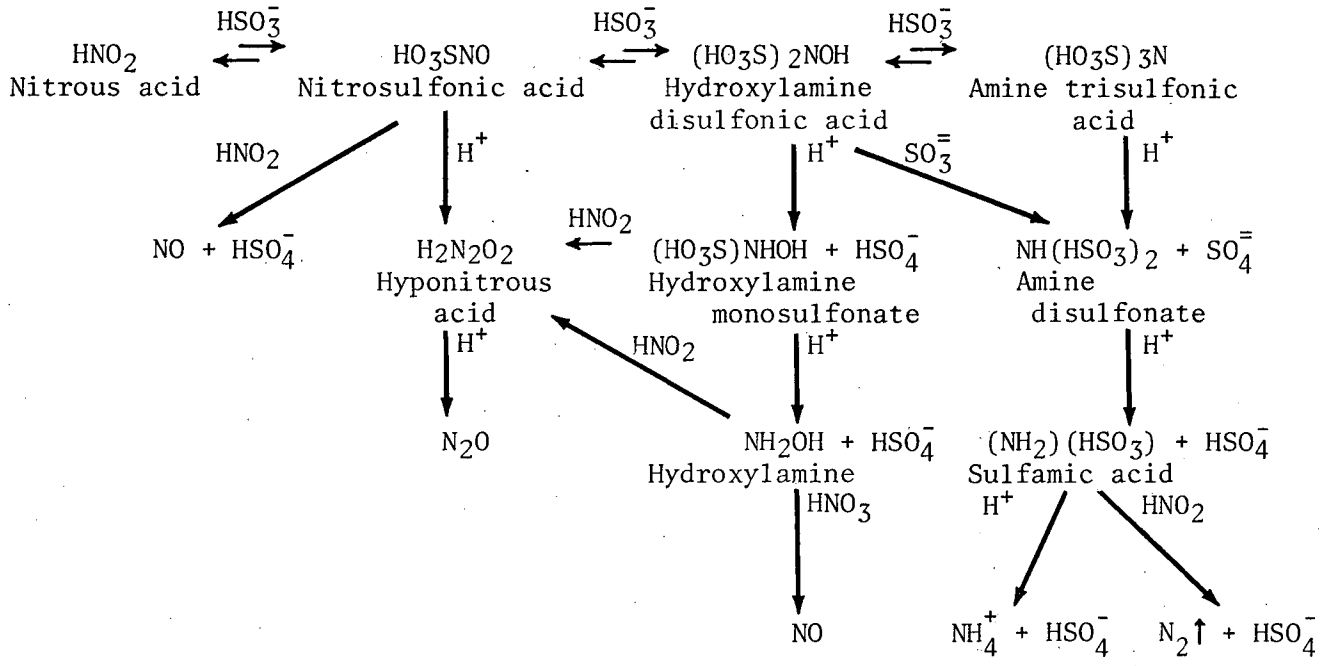

Nitrous acid and bisulfite react to form nitrosulfonic acid, which then continues along one or more of three reaction paths:

1. Further sulfonation to produce hydroxylamine disulfonate and amine trisulfonate. These can hydrolyze to form sulfuric acid and reduced nitrogen species.
2. Hydrolysis to form sulfuric acid and hyponitrous acid. The latter decomposes to produce nitrous oxide.
3. Reaction with nitrous acid to yield sulfuric acid and nitric oxide.

The extent to which these three different processes will contribute to the system depends on the pH, temperature, and concentration of nitrite and bisulfite species. It is believed that process 1 favors a neutral or mildly acidic solution; processes 2 and 3 are expected to become increasingly important as the pH of the solution decreases.

Our experimental results appear to indicate that process 1 is the major process even at a pH as low as 4.5. The contributions from processes 2 and 3 are observed at a pH of 3 under the conditions of this investigation.

Further experiments are currently being carried out to determine the effect of the sulfite concentration and the pH on the reaction rate. The results of these experiments will enable us to elucidate a mechanism which is consistent with all the experimental data.

References

1. N.A. Renzetti and G.J. Doyle, "Photochemical aerosol formation in sulphur dioxide-hydrocarbon systems," Int. J. Air Pollut. 2, 327 (1960).

2. P. Urone, H. Lutsep, C.M. Noyes, and J.F. Parcher, "Static studies of sulfur dioxide reactions in air," Environ. Sci. Technol. 2, 611 (1968).

3. A.P. Altshuller and J. Bufalini, "Photochemical aspects of air pollution: A review," Environ. Sci. Tech. 5, 39 (1971).

4. J.G. Calvert, F. Su, J.W. Bottenheim, and O.P. Strausz, "Mechanism of the homogeneous oxidation of sulfur dioxide in the troposphere," Atmos. Environ. 12, 197 (1978).

5. R.J. Charlson, D.S. Covert, T.V. Larson, and A.P. Waggoner, "Chemical properties of tropospheric sulfur aerosols," Atmos. Environ. 12, 39 (1978).

6. F. Raschig, Schwefel und Stickstoffstudien (Verlag Chemie, Berlin, 1924).

7. W. Latimer and J. Hildebrand, Reference Book of Inorganic Chemistry (New York, Macmillan, 1951), p. 208.

8. V.F. Seel and H. Knorre, "Die Umsetzung von Nitrit mit Hydrogensulfit in Hydrogensulfit-sulfit-Pufferlösungen," Z. anorg. allg. Chem. 313, 70 (1961).

9. W. Duecker and J. West, eds., The Manfacture of Sulfuric Acid, American Chemical Society Monograph Series No. 144 (1959).

Kinetics and Mechanism for the Catalytic Oxidation of SO_2 on Carbon in Aqueous Suspensions

R. Brodzinsky, S.-G. Chang, S.S. Markowitz, and T. Novakov

Introduction

Soot particles, in addition to being a major constituent of the ambient particulate burden,[1-4] are a catalytically and surface chemically active material. For example, Novakov et al.[1,5] have shown by photoelectron spectroscopy that SO_2 oxidation to sulfate can be catalyzed by combustion-generated soot particles. They reached the following conclusions:

1. Soot-catalyzed oxidation of SO_2 is more efficient at a higher humidity.
2. The oxygen in air plays an important role in SO_2 oxidation.
3. Soot-catalyzed oxidation exhibits a saturation effect.
4. The saturation level of sulfate produced is probably related to such properties of soot particles as size, active surface area, and adsorbed surface oxygen.
5. The sulfate produced on soot particles is water soluble and contributes to the acidification of the solution.
6. SO_2 can be oxidized on other types of graphitic carbonaceous particles, such as ground graphite particles and activated carbon.

Although these authors have shown that the soot-catalyzed oxidation of SO_2 is more efficient in prehumidified air rather than dry air, the specific role of water was not made clear in their experiments. The effects of liquid water are important because it may condense on the soot particles in plumes, and soot particles may encounter liquid water in their passage through fogs and clouds. Also, hygroscopic and deliquescent materials associated with soot particles may hold significant amounts of liquid water, even at a comparatively low relative humidity.[6]

We have recently extended research on the role of soot particles as catalysts for SO_2 oxidation by studying the effect of liquid water on the soot-catalyzed reaction.[7] In this paper, we present a reaction rate law and propose a reaction mechanism for the catalytic oxidation of SO_2 on soot particles in an aqueous suspension.

Experimental Methods and Results

The reaction was studied in systems containing various concentrations of sulfurous acid and suspended carbonaceous particles. The carbon concentrations used in the suspensions ranged from 0.005% to 0.32% by weight, and the sulfurous acid concentration ranged from 1.5×10^{-4} M to 1.00×10^{-3} M. The concentration of sulfurous acid was monitored, using iodometric titrations during the course of the reaction. The concentration of sulfuric acid was followed by the turbidimetric method in selected runs. Soots produced by the combustion of acetylene, natural gas, and a diesel engine were collected by impinging the effluent into water. They were found to be efficient catalysts.

Figure 1 shows the typical reaction curves of the oxidation of H_2SO_3 by dissolved oxygen in aqueous suspensions of soot particles collected from acetylene and natural gas flames. The reaction occurs in two steps. The rate of the initial disappearance of H_2SO_3 is so fast that it could not be followed by the analytical technique used. The second process is characterized by a much slower linear reduction of H_2SO_3. The results obtained with these combustion-produced soots were essentially reproduced (Fig. 2) by suspensions of similar concentrations of activated carbon[8] (Nuchar-C190, a trademark of West Virginia Pulp and Paper Co.; elemental composition shown in Table 1). Figure 2 also shows that there is a mass balance between the sulfurous acid consumed and the sulfuric acid produced. Since it is difficult to reproducibly prepare soot suspensions, suspensions of Nuchar were used as a model system.

Table 1. Elemental composition of Nuchar C-190 (% by weight).

C	74.7	K	0.091	Ni	0.001
O	23.6	Al	> 0.055	Cl	< 0.001
H	0.9	Ti	0.016	As	0.0004
N	0.1	Mn	0.013	Br	0.0004
Ca	0.221	Cr	0.002	Rb	0.0004
S	> 0.166	Cu	0.002	Zr	0.0004
Si	> 0.111	Zn	0.002	Pb	0.0004
Fe	0.117	Sr	0.002	Ga	0.0001

BET surface area = 550 m^2/g.
C,H,N: combustion; O: difference; other elements: X-ray fluorescence.

To investigate the reaction rate and mechanism, a series of experiments was done with Nuchar as a model catalyst. We previously reported[7] the effects of the

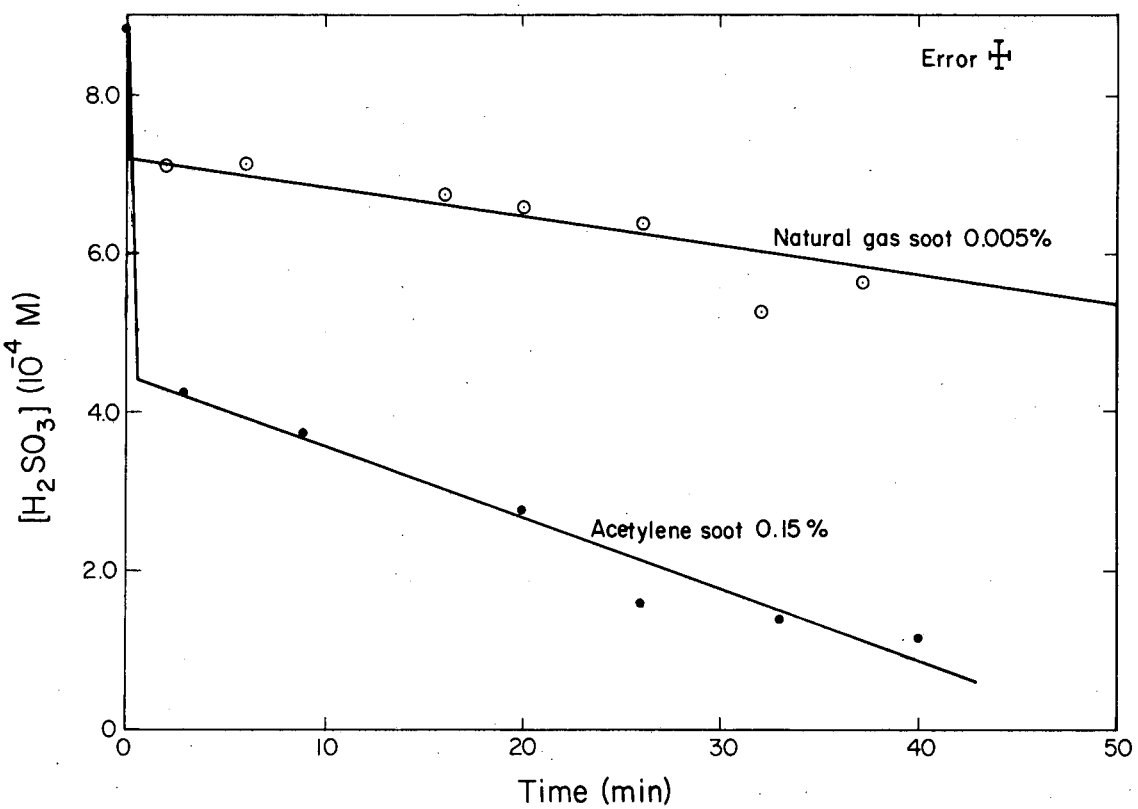

XBL7710-2065A

Figure 1. H_2SO_3 concentration as a function of time for acetylene and natural gas soot suspensions.

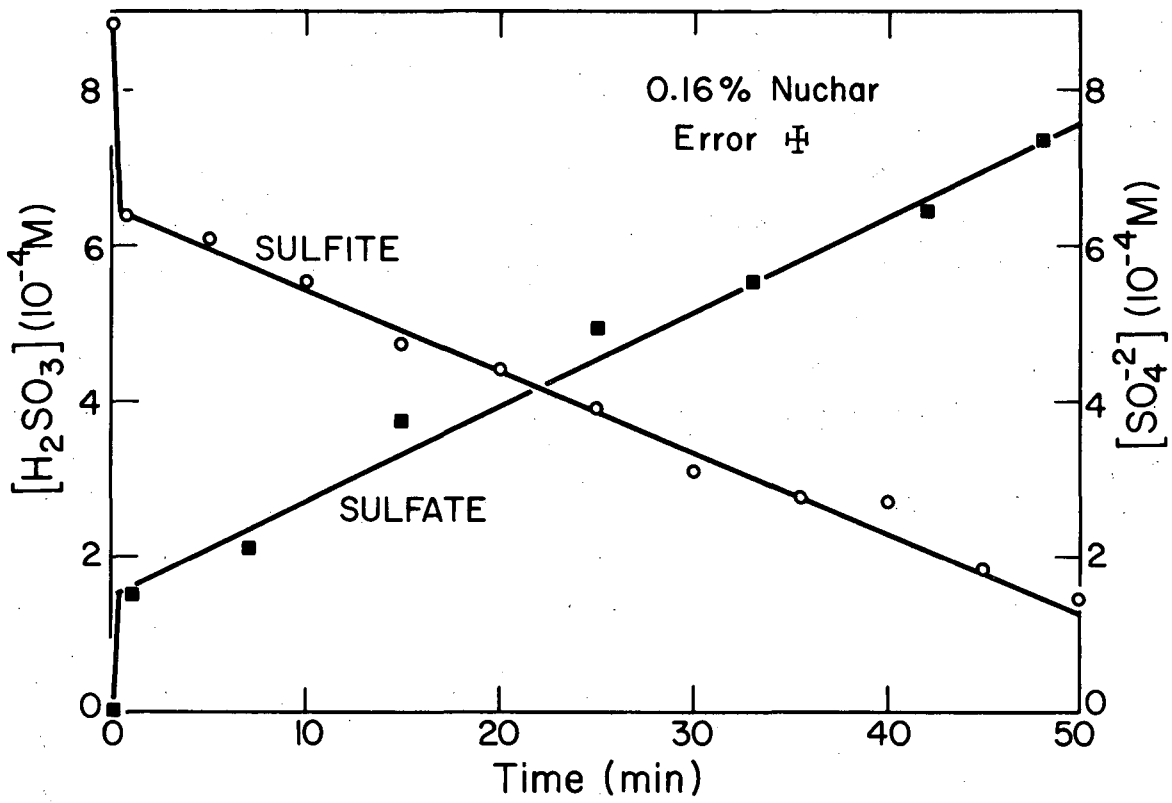

XBL 782-219

Figure 2. H_2SO_3 and H_2SO_4 concentrations as a function of time for activated carbon suspensions.

concentrations of carbon and sulfurous acid on the rate of oxidation of sulfurous acid. The amount of sulfurous acid oxidized, at a constant temperature, by the rapid first step process was found to be linearly proportional to the concentration of the carbon particles. A linear relationship was found between the half-life of the second process and both the reciprocal of the carbon concentration and the initial sulfurous acid concentration. This suggests a first order reaction with respect to the carbon catalyst concentration and zeroth order with respect to the sulfurous acid concentration under the conditions of the experiment (Nuchar, between 0.005% and 0.32% by weight; sulfurous acid, between 1.5×10^{-4} and 10^{-3} M; pH, between 1.5 and 7.5). Figure 3 shows the reaction curve at differing dissolved oxygen concentrations. The rate of reaction with respect to the concentration of dissolved oxygen was found to be a fractional order (0.69) (Fig. 4).

To assess the dependence of the SO_2 oxidation reaction on pH, a known volume of H_2SO_4 or NH_4OH was mixed into the sulfurous acid solution before adding Nuchar. This approach was used for low pH. High pH's were achieved using an NH_4OH-Na_2SO_3 solution. The pH of the solution decreased during the course of the reaction. The change in pH varied from 0.05 to 1.0 pH unit, depending on the initial pH of the solution: the larger the initial pH, the larger the change. The results, represented in Fig. 5, demonstrate that the reaction rate essentially does not depend on the pH of the aqueous suspension under the conditions of this investigation. This independence is very striking, as it differs from other heterogeneous reactions involving liquid water, which are dependent on the pH of the liquid water. The pH of these experiments — 1.45 to 7.5 — covers the range of atmospheric pH.

The reaction is accelerated by temperature, as may be seen from the results shown in Fig. 6. The activation energy is 11.7 kcal/mole between 5.5°C and 50°C (Fig. 7).

In summary, the reaction occurs in two steps — an initial rapid oxidation followed by a much slower one. The rate of the first process is too fast to follow. The reaction of the second process has the following characteristics:

1. The reaction rate is first order, zeroth order, and 0.69th order with respect to the concentration of carbon, sulfurous acid, and dissolved oxygen respectively.
2. The reaction rate is pH independent (between pH of 1.45 and 7.5).
3. The activation energy of the reaction is 11.7 kcal/mole.

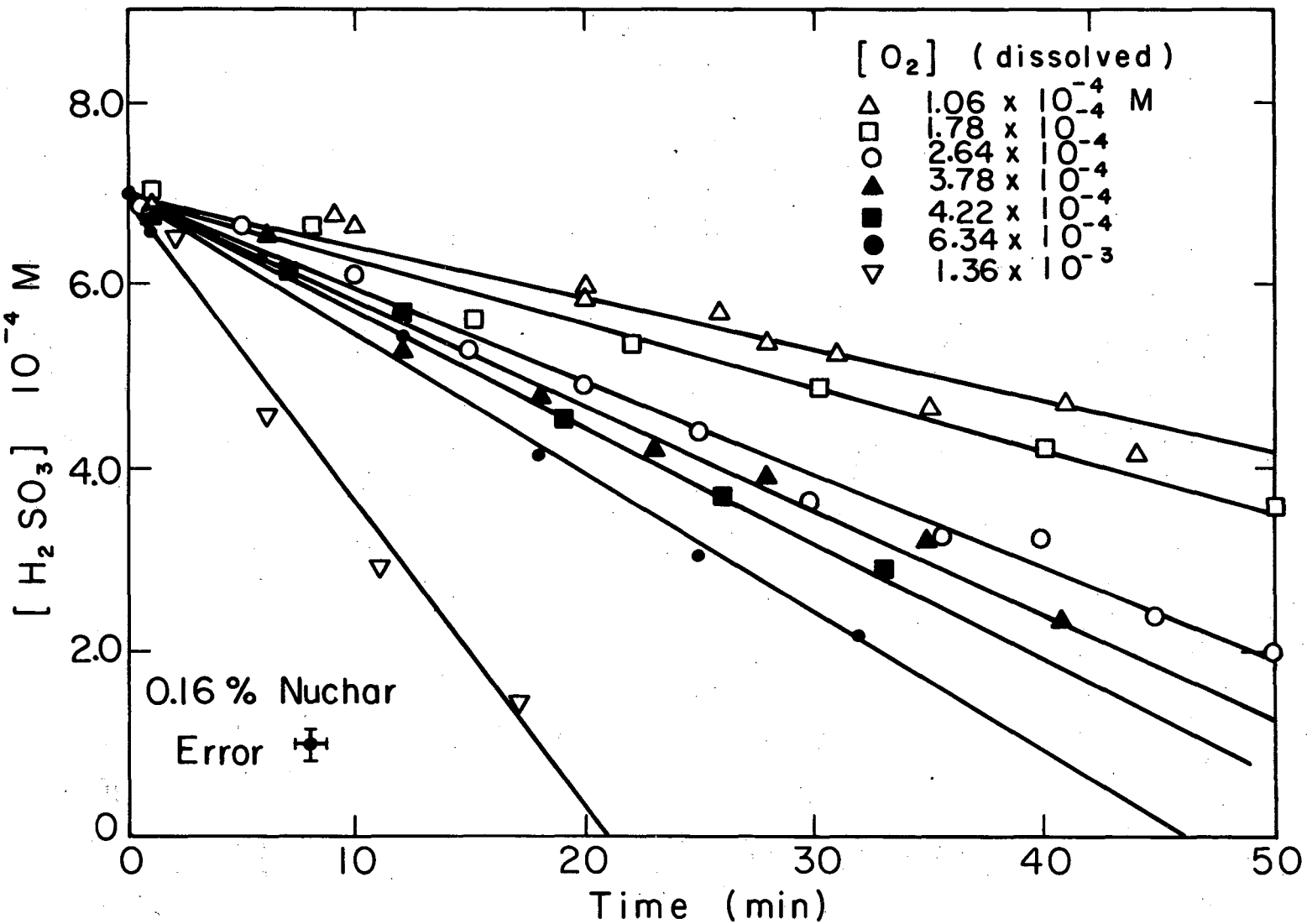

XBL782-299

Figure 3. H_2SO_3 concentration as a function of time for various concentrations of dissolved oxygen at a fixed activated carbon concentration of 0.16% by weight.

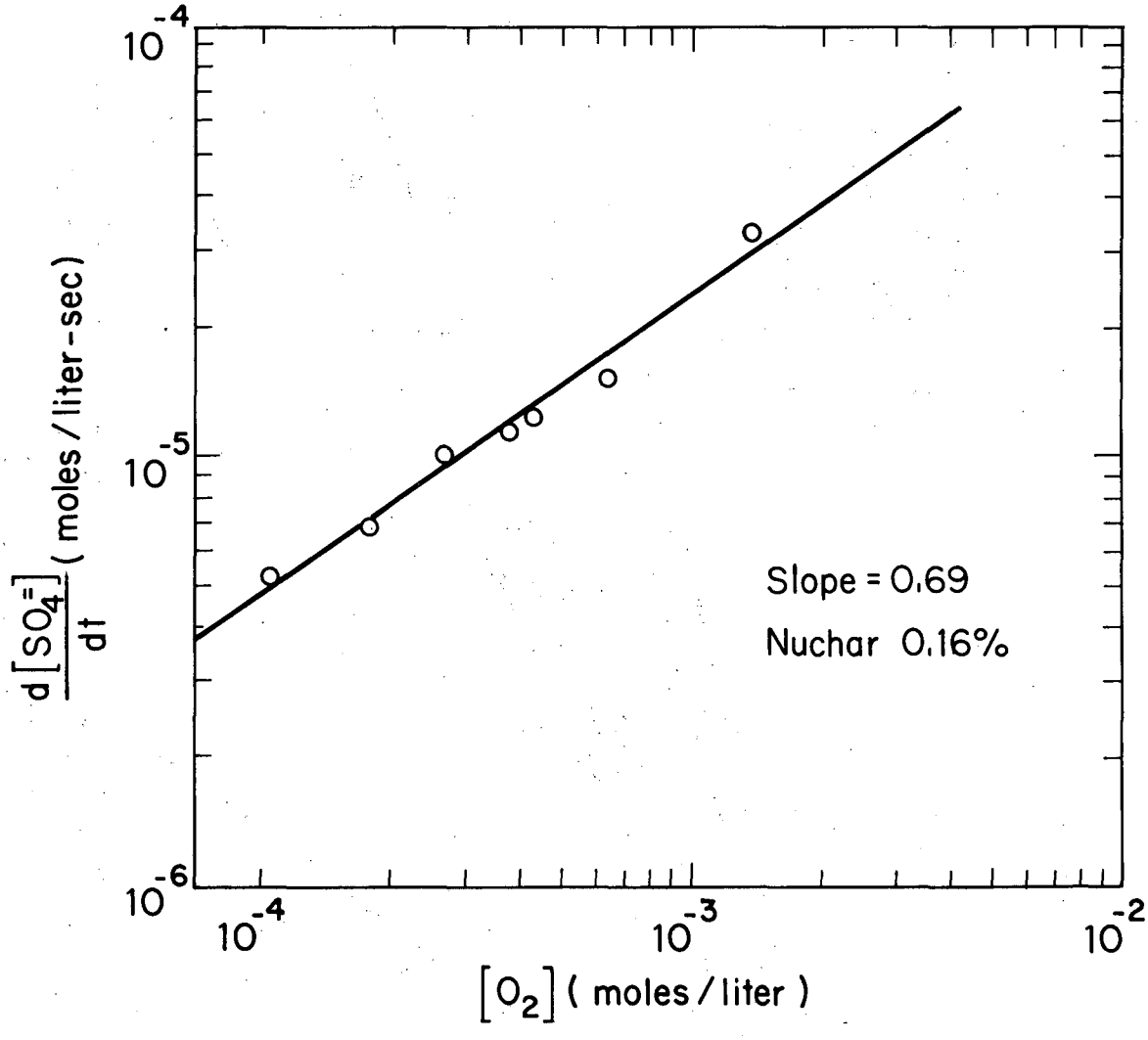

XBL 784-771

Figure 4. The rate of formation of sulfuric acid versus dissolved oxygen concentration at a fixed activated carbon concentration of 0.16% by weight.

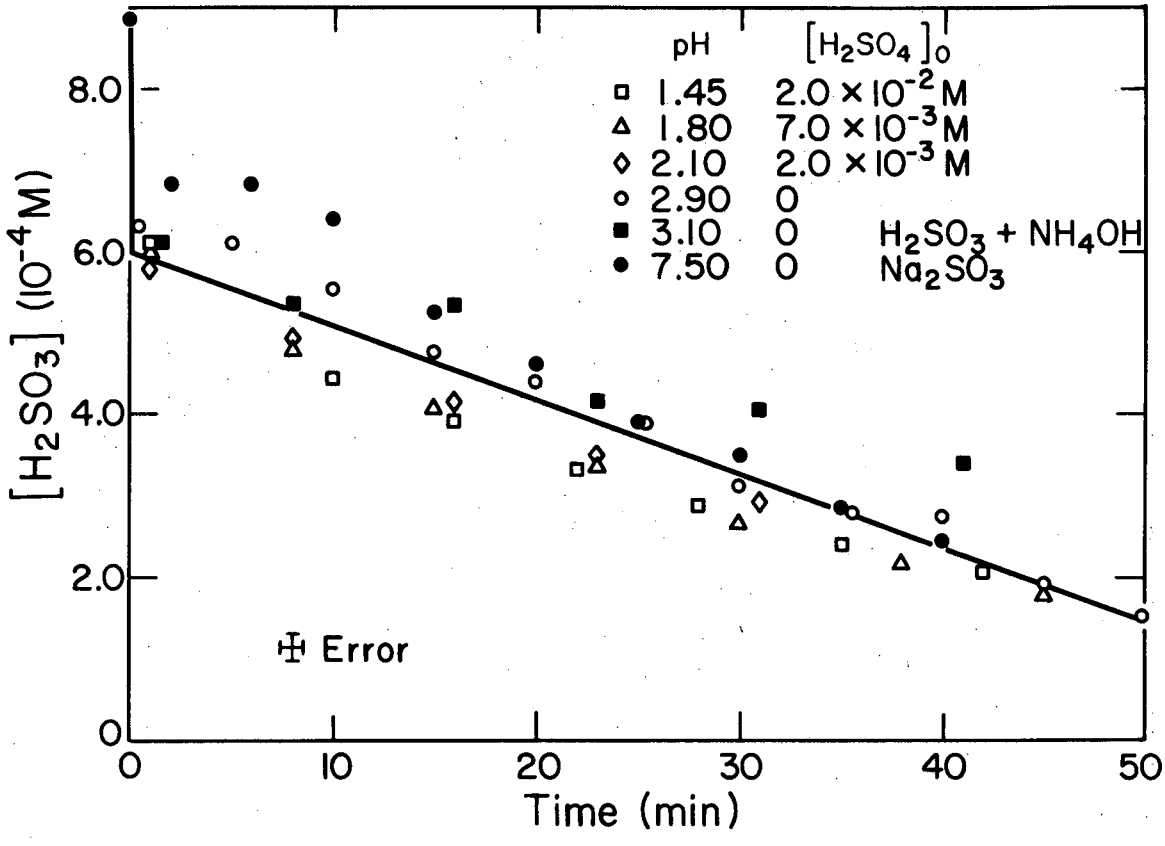

XBL 782-218

Figure 5. H_2SO_3 concentration as a function of time at an activated carbon concentration of 0.16% by weight at various pH values. The initial H_2SO_3 concentration was 8.85×10^{-4} M.

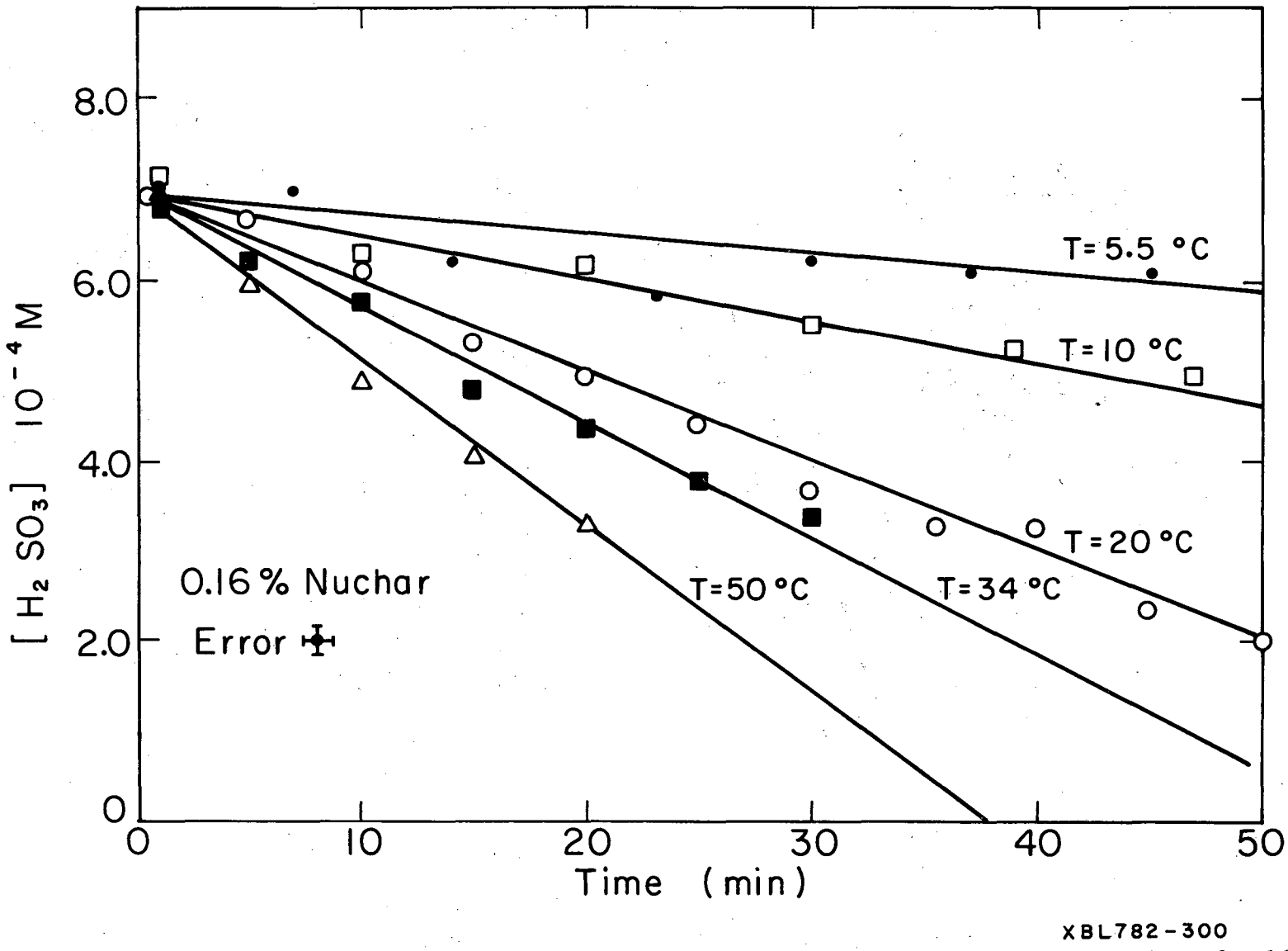

XBL782-300

Figure 6. H_2SO_3 concentration as a function of time at an activated carbon concentration of 0.16% by weight at various temperatures.

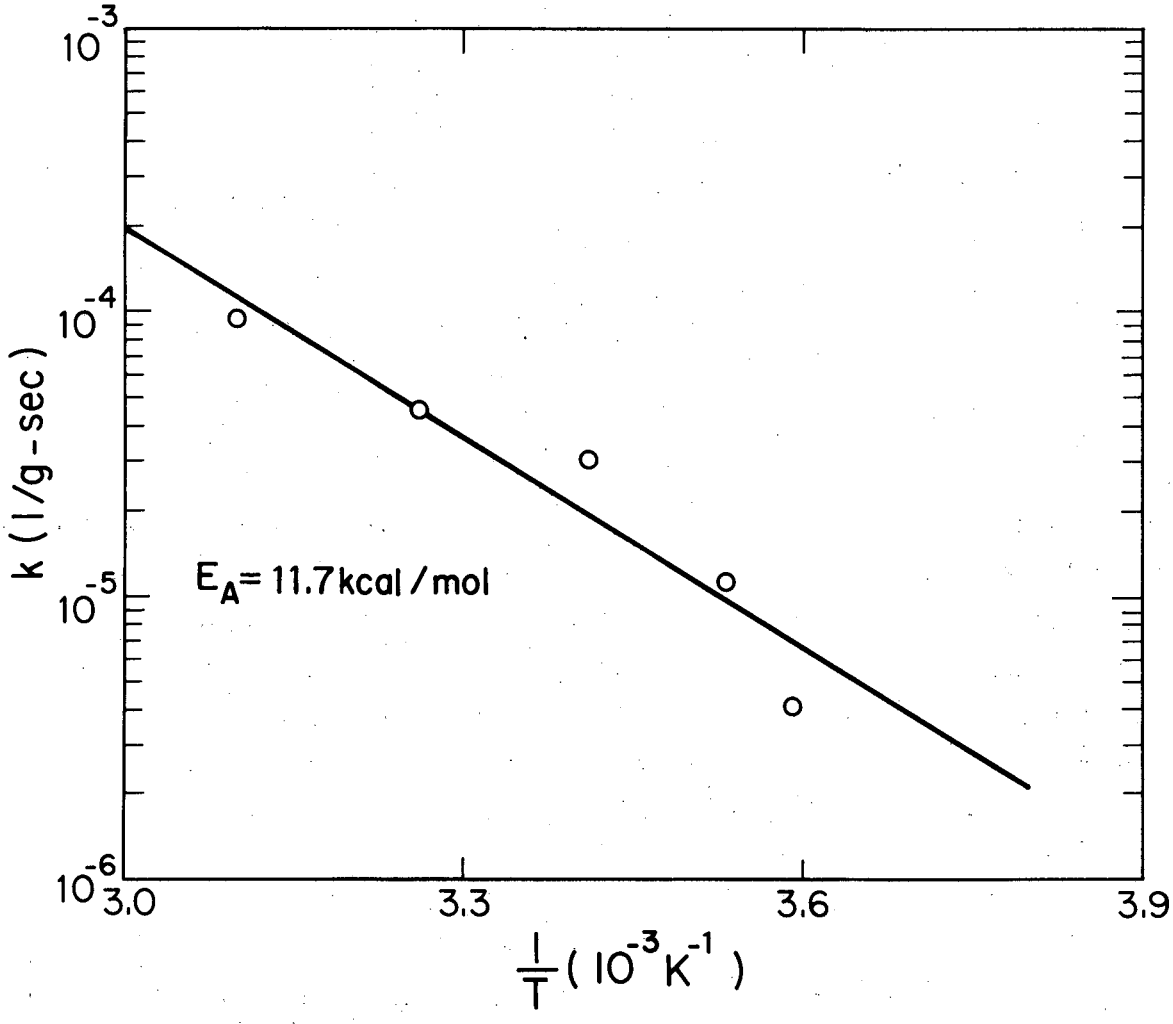

XBL 784-772

Figure 7. A plot of the rate constant versus the reciprocal of the reaction temperature (the Arrhenius equation). The activation energy is calculated to be 11.7 kcal/mole.

4. There is a mass balance between the consumption of sulfurous acid and the production of sulfuric acid.

Discussion

Based on the experimental results, we propose the following reaction mechanism:

$$C_x + O_2(\ell) \underset{k_{-1}}{\overset{k_1}{\rightleftharpoons}} C_x \cdot O_2(\ell) \tag{1}$$

$$C_x \cdot O_2(\ell) + Su \underset{k_{-2}}{\overset{k_2}{\rightleftharpoons}} C_x \cdot O_2(\ell) \cdot Su \tag{2}$$

$$C_x \cdot O_2(\ell) \cdot Su + Su \underset{k_{-3}}{\overset{k_3}{\rightleftharpoons}} C_x \cdot O_2(\ell) \cdot 2Su \tag{3}$$

$$C_x \cdot O_2(\ell) \cdot 2Su \xrightarrow{k_4} C_x + 2SuO \tag{4}$$

where C_x = soot, $O_2(\ell)$ = dissolved oxygen molecule, Su = sulfite species, and SuO = sulfate species.

Equation (1) indicates that dissolved oxygen is adsorbed on the soot particle surface to form an activated complex. This adsorbed oxygen complex then oxidizes the sulfurous acid to form sulfuric acid according to Equs. (2)-(4). If we assume that the reaction follows the condition of Langmuir adsorption equilibrium,[10] the rate of acid formation is:

$$\frac{d[SuO]}{dt} = 2k_4[C_x \cdot O_2(\ell) \cdot 2Su]$$

$$= 2k_4[C_x] \left\{\frac{K_1[O_2(\ell)]}{1 + K_1[O_2(\ell)] + K_W[H_2O] + K_{Su}[Su]}\right\}\left\{\frac{K_2[Su]}{1 + K_2[Su]}\right\}\left\{\frac{K_3[Su]}{1 + K_3[Su]}\right\}$$

where K_1, K_2, and K_3 are the equilibrium constants of reactions (1), (2), and (3) respectively. K_W and K_{Su} are the equilibrium constants of the adsorption of water and sulfite species on carbon particles respectively. If $k_2[Su] >> k_{-2}$ and $k_3[Su] >> k_{-3}$, the rate law simplifies to

$$\frac{d[SuO]}{dt} = 2k_4[C_x] \left\{\frac{K_1[O_2(\ell)]}{1 + K_1[O_2(\ell)] + K_W[H_2O] + K_{Su}[Su]}\right\}$$

If the power rate form of the Freundlich isotherm[10] is used instead of the Langmuir form, the rate law becomes

$$\frac{d[SuO]}{dt} = k[C_x][O_2(\ell)]^n ,$$

which corresponds to the experimental results where n = 0.69. The activation energy (Ea) was determined to be 11.7 kcal/mole. The rate law as a function of temperature is

$$\frac{d[SuO]}{dt} = A[C_x][O_x(\ell)]^n \exp-(\frac{Ea}{RT})$$

where $A = 1.17 \times 10^5$ mole$^{0.3}$ $\ell^{0.7}$/g-sec, which is the average value determined for natural gas and acetylene soot.

We have ruled out the possibility that the oxidation of sulfurous acid is due to a reaction involving impurities such as iron in carbon particles. This was done by leaching a carbon sample with concentrated sulfuric acid for about a week before it was used for the study. This sample contained less than one-third of the original iron content; however, it still exhibited the same reaction rate as all samples without this treatment.

The possibility that the outgassing of SO_2 from the solution might contribute to the disappearance of sulfurous acid is ruled out because (1) there is a mass balance between the amount of sulfurous acid consumed and the amount of sulfuric acid produced, and (2) no significant consumption of sulfurous acid was observed over a 30-min interval for a solution without the addition of carbon particles.

We have examined the role of dissolved oxygen on the behavior of the reaction. It is conceivable that the initial rapid consumption of sulfurous acid could be due to the depletion in the amount of dissolved oxygen in the solution. The second, slower rate of consumption would then be limited by the rate of diffusion of the oxygen into the solution. This hypothesis was ruled out by noting that the behavior and the rate of the reaction were not affected by bubbling air into the solution or by increasing the stirring speed. The reaction rate speeds up, however, if one increases the concentration of dissolved oxygen (Fig. 3). We therefore conclude that the reaction rate is not limited by the mixing rate of gaseous oxygen molecules into the solution, but rather by the rate of formation of the activated oxygen complex.

We have also carried out a preliminary investigation on the possibility of chemical species in the atmosphere which might inhibit the soot-catalyzed process, since it is known that some organic substances retard the SO_2 aqueous oxidation

catalyzed by transition metal ions.[11] To explore these effects in a realistic atmosphere, liquid water was collected by condensing water vapor from the Berkeley atmosphere. This collection, used for the kinetic study, was found to have no effect on the oxidation rate of sulfurous acid. In a separate experiment, a gummy deposit taken from the wall of a highway tunnel was used for the study. The reaction rate of this sample is 50% faster than the same amount of Nuchar C-190. Therefore, no indication of inhibition from atmospheric contaminants has been observed so far.

The rate constants of several different types of carbon particles were studied and found to depend on the nature of the carbon particles. In principle, the reaction rate should be proportional to the concentration of active sites on the carbon particles, rather than to the concentration of carbon particles. The number of active sites per unit mass of carbon particles should vary from one type to the next[12] and is not necessarily proportional to the surface area. Using the electron paramagnetic resonance method, Sidelewski[12] has shown that free electrons on carbon particles can serve as active centers for the adsorption of oxygen molecules and for the oxidation of SO_2. The concentration of free electrons is related to the origin and thermal history of the carbon particles. The rate constant reported in this study represents the average value between the values of natural gas and of acetylene soot particles produced under rich flame conditions. Benner et al.[13] have recently found in a fog chamber study that the reaction rate of soot particles generated from a natural gas diffusion flame can be considerably faster than the reaction rate reported here for aqueous soot suspensions.

Our observation that the reaction behaves independently of the concentration of sulfite species and the pH of the solution is expected as long as the following conditions are satisfied:

$$k_2[\text{oxidizable sulfite species}] \gg k_{-2} \quad \text{and}$$

$$k_3[\text{oxidizable sulfite species}] \gg k_{-3} \ ,$$

where the oxidizable species can be $[SO_2 \cdot H_2O]$, $[HSO_3^-]$, or $[SO_3^=]$. However the possibility that two or three sulfite species are oxidized cannot be ruled out.

We have also investigated the kinetics at a much smaller sulfite concentration and at a much higher pH of the solution. Preliminary results indicate that the oxidation rate is considerably slower at pH > 7.6. This behavior could indicate that a reaction mechanism, different from the proposed one, is operating. However,

the proposed mechanism reproduces the results obtained under our experimental conditions. Further work is necessary to completely understand the actual reaction mechanism.

References

1. T. Novakov, S.-G. Chang, and A.B. Harker, "Sulfates as pollution particulates: Catalytic formation on carbon (soot) particles," Science 186, 259 (1974).

2. S.-G. Chang and T. Novakov, "Formation of pollution particulate nitrogen compounds by NO-soot and NH_3-soot gas-particle surface reactions," Atmos. Environ. 9, 495 (1975).

3. H. Rosen, A.D.A. Hansen, L. Gundel, and T. Novakov, "Identification of the graphitic carbon component of source and ambient particulates by Raman spectroscopy and an optical attenuation technique," in Proceedings, Conference on Carbonaceous Particles in the Atmosphere, Lawrence Berkeley Laboratory, Berkeley, California (in press).

4. A.D.A. Hansen, H. Rosen, R.L. Dod, and T. Novakov, "Optical attenuation as a tracer for the primary component of the carbonaceous aerosol," in Proceedings, Conference on Carbonaceous Particles in the Atmosphere, Lawrence Berkeley Laboratory, Berkeley, California (in press).

5. T. Novakov, S.-G. Chang, and R.L. Dod, "Application of ESCA to the analysis of atmospheric particulates," in Contemporary Topics in Analytical and Clinical Chemistry — Vol. I, D.M. Hercules, G.M. Hieftje, L.R. Snyder, and M.A. Evenson, eds. (New York, Plenum, 1977), p. 249.

6. R.J. Charlson, D.S. Covert, T.V. Larson, and A.P. Waggoner, "Chemical properties of tropospheric sulfur aerosols," Atmos. Environ. 12, 39 (1978).

7. S.-G. Chang, R. Brodzinsky, S.S. Markowitz, and T. Novakov, "Cataltyic oxidation of SO_2 on carbon in aqueous solutions," in Atmospheric Aerosol Research Annual Report 1976-77, Lawrence Berkeley Laboratory Report LBL-6819 (1977).

8. M. Hartman and R.W. Coughlin, "Oxidation of SO_2 in a trickle-bed reactor packed with carbon," Chem. Eng. Sci. 27, 867 (1972).

9. A. Clark, The Theory of Adsorption and Catalysis (New York, Academic, 1970).

10. L.C. Schroeter, Sulfur Dioxide: Application in Foods, Beverages, and Pharmaceuticals (Oxford, Pergamon Press, 1966), p. 56.

11. J. Siedlewski, "The mechanism of catalytic oxidation on activated carbon: The influence of free carbon radicals on the adsorption of SO_2," Int. Chem. Eng. 5, 297 (1965).

12. W.H. Benner, H. Rosen, and T. Novakov, "SO_2 oxidation by water droplets containing combustion nuclei," this report.

ATMOSPHERIC CHEMISTRY: MODELLING

A Carbon and Lead Emission Inventory for the Greater San Francisco Bay Area

A.D.A. Hansen, W.H. Benner, and T. Novakov

Introduction

The incomplete combustion of almost any fuel can result in the formation of trace particulates in the exhaust stream. Particulate carbon and lead are two of the most important anthropogenic contributions to the ambient aerosol and often reach large concentrations in urban situations under stagnant atmospheric conditions. As discussed elsewhere in this report,[1] there has been controversy over the relative importance of particulates directly emitted from sources versus those formed from gaseous precursors in atmospheric reactions. Calculations originally presented by Friedlander[2] called for a dominant contribution of secondary carbonaceous material in the ambient urban aerosol of the Los Angeles air basin. In essence, this method considered that the major primary source of particulate carbon and lead was automotive emissions characterized by a [C/Pb] mass ratio of the order of 1. To account for an observed [C/Pb] mass ratio of the order of 6, a mass balance calculation was performed that required carbonaceous particulates of secondary origin to be present in quantities considerably exceeding the primary contribution. In this paper we present emission factor estimates and a similar calculation to predict the inputs of particulate carbon and lead to the greater San Francisco Bay Area air basin. The results of this prediction are then compared with the results of the analysis of many ambient samples, and show that in principle it is possible to account for the observed ambient [C/Pb] ratio solely by proper consideration of source inputs.

Sources

The sources we consider here (with their contribution to the total energy consumption of the area[3]) are as follows: 1) domestic and commercial combustion of natural gas and refinery gas (61%); 2) vehicular use of gasoline (28%); 3) vehicular use of diesel fuel (4%); 4) aircraft use of jet fuel (2%); and 5) combustion of heavy fuel oil (5%). We further break down vehicular gasoline use into categories of high-speed (freeway) driving and start-stop driving.

Natural gas emission factor. Although it had long been believed that natural gas is a "clean" fuel, we have found considerable emission of particulate carbon from poorly regulated combustors. Stack sampling was done on three combustors representative of the various types used in this area in order to

estimate an overall emission factor. The particulates were collected on pre-fired absolute quartz fiber filters from 1) a 50,000-lb steam generator on the campus of University of California, Berkeley; 2) a 36,000-Btu/hr domestic-type hot water heater (30 gal); and 3) a 300,000-Btu/hr boiler at LBL used for heating a laboratory building. During sampling of the steam generator, enough heat was transferred from the stack gases to the filter holder to prevent water condensation on the filter. For the boiler and water heater, the filter holder was heated to ∿ 225°F with a length of electrical heating tape. The volumetric flowrate of stack gas from the steam generator was calculated from operating parameters supplied by the plant superintendent. The stack gas flowrate from the boiler and water heater were determined from pitot tube measurements. The filter samples were analyzed for carbon by a total combustion/CO_2 evaluation technique.[4] The results shown in Table 1 show wide variation in emission rates and indicate that the generation of particles is not a constant process. As the flame in a burner ignites, a short-term production of particles occurs, probably due to improperly mixed gases in the burner. The initial puff of particles may account for a sizable fraction of the entire amount of particulate carbon released during the burning cycle of a domestic unit. Even apart from this, the steady-state emission factor of the small units is much greater than that of the large steam generator. Commercial installations are usually well monitored, continuously burning, and maintained frequently in order to obtain the best economic return. In contrast, domestic units are neither as well designed nor carefully maintained and burn in cycles. From the data we propose emission factors within the following limits: commercial use of natural gas, 0.003-0.007 μg C/Btu; domestic use of natural gas, 0.2-2.5 μg C/Btu.

Vehicular gasoline emission factor. We use Refs. 5-7 and some of our own measurements to estimate the range of automotive emission factors for particulate carbon and lead. In all cases, the figures quoted are corrected for the 3:1 preponderance of leaded gasoline used vs. unleaded fuel.

Emission rates for highway driving in the ranges of 0.03-0.08 g C/mile and 0.01-0.05 g Pb/mile can be found in the literature. These rates are consistent with a [C/Pb] ratio of 2.2 ± 0.35 observed by us on a set of particulate samples taken in the exhaust vent of a local freeway tunnel; so we propose emission rates per gallon of "composite" gasoline of 0.6-1.6 g C/gallon and 0.2-1.0 g Pb/gallon.

Table 1. Particulate carbon released during combustion of natural gas.

Source	μg C/Btu	Comments
50,000# steam/hr generator, campus	0.005	Exhaust gas flowrate calculated from CH_4 feed rate, stoichiometry, and 2% excess O_2, @ 310°F (pitot tube not available at this time for Q measurements).
Domestic water heater, LBL Bldg. 44	2.81	Sample collection began ∿ 5 sec after ignition.
	1.85	Sample collection began 3.5 min after ignition.
Heating boiler, LBL Bldg. 73A	1.29	Sample collection began 1-2 min after ignition.
	1.00	Sample collection included initial puff of particles at ignition but stack was warmer than usual.
	0.27	Boiler had been running ∿ 30 sec before sampling started.
	0.15	Sample included initial puff of particles, but entire sample period = 4 min.
	0.46	Average of 4 determinations in which the first 30 sec of the firing cycle was sampled.
	0.20	Sample collection began 30 sec after ignition and extended for a total of 3.0 min.

Driving under urban conditions involves acceleration, deceleration, and the use of the choke on a cold engine. These have a strong influence on the emission of particulates, especially carbon. Emission rates of 0.1-0.4 g C/mile and 0.03-0.08 g Pb/mile have been reported. These are consistent with a [C/Pb] ratio of 7.8 ± 2.5 observed by us on a set of particulate samples taken in an underground parking garage. We assume a reduced fuel economy for this type of driving and propose emission rates per gallon of "composite" gasoline of 1-4 g C/gallon and 0.3-0.8 g Pb/gallon.

Diesel emission factor. The dominant use of diesel fuel is by heavy trucks, whose emissions are almost entirely carbonaceous. Emission rates of 0.5-4 g C/mile can be found in the literature, which correlate with the findings in Ref. 8 that diesel trucks emit approximately 25 times as much particulate carbon per mile as automobiles. We therefore propose emission rates in the range of 2.5-20 g C/gallon.

Jet fuel emission factor. Estimates of the emission rate of carbonaceous particles from jet engine exhaust range from 1 to 5 g C/kg fuel consumed[9,*]

*An emission factor may be obtained from Ref. 3 by dividing total particulate input estimates by fuel use data.

under full-power (takeoff) conditions. For the present calculation we shall use emission rates in the range of 3-15 g C/gallon jet fuel.

Heavy fuel oil emission factor. Power plants account for the major use of heavy fuel oil in the Bay Area. An emission factor for carbonaceous particulates in the range of 0.05-1 g C/gallon fuel oil is comparable with the emission factors for other liquid fuels' use and is consistent with the total particulate emission estimates of Ref. 3.

Emission Factor Table

The above emission factor estimates may be conveniently summarized:

		Grams produced per unit of fuel		
Fuel	Use	Lead	Carbon	Unit
Natural gas	Commercial	0	0.003-0.007	10^6 Btu
Natural gas	Domestic	0	0.2-2.5	10^6 Btu
Gasoline	Highway	0.2-1.0	0.6-1.6	gallon
Gasoline	City	0.3-0.8	1-4	gallon
Diesel		0	2.5-20	gallon
Jet fuel			3-15	gallon
Heavy oil			0.05-1	gallon

Emission Inventory

Fuel use data from Ref. 3 show the following approximate annual consumption in 1975: natural gas (commercial), 3.9×10^{14} Btu; natural gas (domestic), 1.8×10^{14} Btu; gasoline (total), 2.1×10^9 gallons; diesel fuel, 2.4×10^8 gallons; heavy fuel oil, 3.6×10^8 gallons; and jet fuel, 1.5×10^8 gallons. This last figure is an estimate of the fraction of the jet fuel sold in the area that is consumed within its air volume. We shall assume a gasoline consumption breakdown of 60:40, weighted toward "urban" driving conditions, and then multiply the emission factor estimates by the fuel use data to arrive at the following breakdown for yearly particulate inputs to the Bay Area air basin:

		Particulate input (10^9 g/year)	
Fuel	Use	Lead	Carbon
Natural gas	Commercial	0	0.001-0.003
Natural gas	Domestic	0	0.04-0.45
Gasoline	Highway	0.17-0.84	0.5-1.35
Gasoline	City	0.38-1.01	1.26-5.04
Diesel		0	0.6-4.8
Jet fuel		0	0.45-2.25
Heavy oil		0	0.02-0.36
	Total (10^9 g/yr)	0.55-1.85	2.87-14.25

Predictions of the Model

From the above estimates we may predict a range of properties that the ambient aerosol could possess if it were composed entirely of primary particulate material. Taking median values of the carbon and lead inputs, a [C/Pb] ratio of around 7.1 is predicted; by taking extrema, a wide range of values is covered. We also note that the automotive use of gasoline is estimated to contribute between 1760 and 6390 tonnes of particulate carbon per year, while other sources may account for between 1110 and 7860 tonnes per year; in other words, nonautomotive sources may well account for a large fraction of the total primary particulate carbon. The median value of the particulate carbon input estimate is 8560 tonnes/year. This quantity may be used in simple diffusion/dispersion models for the Bay Area air volume to predict mean particulate carbon loadings from primary emissions of the order of 10 μg C/m^3.

As a corollary, we note that if primary material were predominant in the ambient aerosol, we would expect to measure a good correlation coefficient between daily average carbon and lead loadings. This would occur if both were simply proportional to anthropogenic input rates (reflecting an average daily fuel use cycle) divided by a factor dependent on ventilation and air transport. A poor correlation coefficient could indicate that fuel use patterns varied widely from day to day, that there were selective scavenging mechanisms for carbon or lead aerosols, or that there were mechanisms capable of the substantial production of carbonaceous particulates whose contribution was not proportional to the lead input to the atmosphere.

Results from the Ambient Aerosol Sampling Program

Routine analysis of 24-hr ambient aerosol samples has been in effect for many months at two sites in the Bay Area air basin: LBL, Berkeley, and the Bay Area Air Quality Management District monitoring station, Fremont. The mean monthly average [C/Pb] ratios and carbon particulate loadings are:

Berkeley	Jun 77-Mar 78	[C/Pb] = 8.8 ± 1.3	180 samples
Fremont	Jul 77-Feb 78	[C/Pb] = 12.9 ± 2.2	126 samples
Berkeley	Jun 77-Jul 78	$\bar{C}$ = 6.9 ± 1.2 μg/m^3	286 samples
Fremont	Jul 77-Aug 78	$\bar{C}$ = 11.7 ± 3.1 μg/m^3	295 samples

The correlation coefficients for particulate carbon and lead loadings on the 24-hr samples were high at both sites: Berkeley, r = 0.84; Fremont, r = 0.83.

Conclusions

The emission factors we have presented are necessarily approximate, covering a wide range of values reported in the literature. However, we see that it is possible to construct a plausible model for the inputs of particulate carbon and lead which may account for the observed loadings of these constituents of the ambient aerosol by consideration of primary sources alone. This model does not set limits on the possible relative importance of primary and secondary contributions to the ambient aerosol, but it shows that one may account for phenomena observed in the Bay Area without the need for dominantly large quantities of secondary material. The wide ranges of reported emission factors, coupled with this demonstrated importance of primary particulate emissions, show that much more source sampling is necessary before better estimates of the probable composition of the ambient aerosol can be achieved.

References

1. A.D.A. Hansen, H. Rosen, R.L. Dod, W.H. Benner, and T. Novakov, "Optical characterization of ambient and source particulates," this report.
2. S.K. Friedlander, "Chemical element balances and identification of air pollution sources," Environ. Sci. Technol. 7, 235 (1973).
3. BAAPCD Base Year 1975 Emissions Inventory Summary Report, Bay Area Air Pollution Control District (now Bay Area Air Quality Monitoring District), 939 Ellis St., San Francisco, Calif. 94109, p. 7.
4. P.K. Mueller, R.W. Mosley, and L.B. Pierce, "Carbonate and non-carbonate carbon in atmospheric particulates," in Proceedings of the Second International Clean Air Congress (New York, Academic Press, 1971).
5. W.R. Pierson and W.W. Brachaczek, "Particulate matter associated with vehicles on the road," Paper 760039, SAE Congress, Detroit, Michigan, February 23, 1976.
6. K. Habibi, "Characterization of particulate matter in vehicle exhaust," Environ. Sci. Technol. 7, 223 (1973).
7. G. Provenzano, "Motor vehicle lead emissions in the United States," J. Air Poll. Contr. Assoc. 28, 1193 (1978).
8. C.D. Hollowell, P.J. Bekowies, R.D. Giauque, J.R. Wallace, and T. Novakov, "Chemical and physical characterization of vehicular emissions," in Report LBL-5214, Lawrence Berkeley Laboratory (1976), p. 54.
9. "Atmospheric pollution by aircraft engines," NATO-AGARD Conference Proceedings No. 125 (NTIS, Springfield Virginia, 1973), papers 22, 28, and 29.

Relative Importance of Various Sulfate Production Mechanisms in Aqueous Droplets

R. Toossi, T. Novakov, and S.-G. Chang

Atmospheric sulfate, a major constituent in ambient aerosol particles, is presumably formed by the oxidation of SO_2. The dominant mechanisms responsible for this transformation have not yet been established. One set of mechanisms thought to be important involves the dissolution of SO_2 in water droplets. When liquid water is present, as in clouds, fog, and plumes, the atmospheric SO_2 can dissolve in the droplets and be oxidized to sulfate. The purpose of this paper is to compare the relative importance of various SO_2 oxidation mechanisms in aqueous droplets.

The systems considered in our box-type calculation are: SO_2-$H_2O(\ell)$-air; NH_3-SO_2-$H_2O(\ell)$-air; O_3-SO_2-$H_2O(\ell)$-air; NH_3-O_3-SO_2-$H_2O(\ell)$-air; Fe^{+3}-SO_2-$H_2O(\ell)$-air; NH_3-Fe^{+3}-SO_2-$H_2O(\ell)$-air; Mn^{+2}-SO_2-$H_2O(\ell)$-air; and soot-SO_2-$H_2O(\ell)$-air. The kinetics of each of these processes other than the soot-catalyzed reactions have been studied by many investigators. The results of Beilke et al.,[1] Erickson et al.,[2] Freiberg,[3] and Matteson et al.[4] for oxygen, ozone, iron, and manganese systems respectively were used in this calculation. The aqueous oxidation rate of SO_2 on soot is from the work of Chang et al.[5] The following initial conditions were used in the calculation: liquid water, 0.05 g/m^3; SO_2, 0.01 ppm; O_3, 0.05 ppm; and CO_2, 0.000311 atm. For NH_3 a concentration of 5 ppb was used, which is higher than the highest equilibrium partial pressure of NH_3 over the United States as calculated by Lau and Charlson.[6] Concentrations of particulate Fe and Mn of 250 ng/m^3 and 20 ng/m^3 respectively were assumed. However, only 0.13% of the total iron and 0.25% of the manganese are water soluble, according to Gordon et al.[7] A soot particle concentration of 10 μg/m^3 was assumed. Tables 1 and 2 list the equilibrium equations and oxidation rate equations used for this comparative study.

The following assumptions were made in the calculations:

1. The size of liquid water drops suspended inside the box is so small that the absorption rate of gaseous species (SO_2 and NH_3) is governed by chemical reactions.

2. There is no mass transfer of any species across the box during the reaction; therefore, the SO_2 (and NH_3) in each box is depleted with time. The mass balance of the sulfur and ammonia (i.e., $\Delta[SO_2]g = \Delta[SO_2 \cdot H_2O] + \Delta[HSO_3^-] + \Delta[SO_3^=] + \Delta[HSO_4^-] + \Delta[SO_4^=]$, and $\Delta[NH_3]g = \Delta[NH_3 \cdot H_2O] + \Delta[NH_4^+]$ is always maintained.

Table 1. Chemical equilibria in SO_2-NH_3-CO_2-ℓH_2O system.[a]

1.	$H_2O \overset{K_w}{\rightleftarrows} H^+ + OH^-$	$K_w = 1.0008\times10^{-14}$
2.	$CO_2(g) + H_2O(\ell) \overset{H_c}{\rightleftarrows} CO_2\cdot H_2O$	$H_c = 3.4\times10^{-2}$
3.	$CO_2\cdot H_2O \overset{K_{1c}}{\rightleftarrows} HCO_3^- + H^+$	$K_{1c} = 4.45\times10^{-7}$
4.	$HCO_3^- \overset{K_{2c}}{\rightleftarrows} CO_3^= + H^+$	$K_{2c} = 4.68\times10^{-11}$
5.	$NH_3(g) + H_2O(\ell) \overset{H_a}{\rightleftarrows} NH_3\cdot H_2O$	$H_a = 57$
6.	$NH_3\cdot H_2O \overset{K_a}{\rightleftarrows} NH_4^+ + OH^-$	$K_a = 1.774\times10^{-5}$
7.	$SO_2(g) + H_2O(\ell) \overset{H_s}{\rightleftarrows} SO_2\cdot H_2O$	$H_s = 1.24$
8.	$SO_2\cdot H_2O \overset{K_{1s}}{\rightleftarrows} HSO_3^- + H^+$	$K_{1s} = 1.7\times10^{-2}$
9.	$HSO_3^- \overset{K_{2s}}{\rightleftarrows} SO_3^= + H^+$	$K_{2s} = 6.24\times10^{-8}$
10.	$HSO_4^- \overset{K_{3s}}{\rightleftarrows} H^+ + SO_4^=$	$K_{3s} = 1.2\times10^{-2}$

[a]Concentration in mole/ℓ and gas pressures in atmospheres.

3. The growth of liquid water droplets due to the vapor pressure lowering effect of the sulfuric acid formed in the droplets is neglected.

The amount of sulfate formed as a function of time was calculated according to the following procedure:

1. Initially, the droplets achieve chemical equilibrium with CO_2, SO_2, and NH_3 at the partial pressures adopted. The $[H^+]$, $[SO_2\cdot H_2O]$, $[HSO_3^-]$, $[SO_3^=]$, $[NH_3\cdot H_2O]$, and $[NH_4^+]$ are calculated when $[HSO_4^-]$ and $[SO_4^=]$ are equal to zero.

2. Assuming a time step Δt, the $[HSO_4^-]$ and $[SO_4^=]$ are calculated with the aid of the corresponding reaction rate law for each process.

3. Gaseous SO_2 and NH_3 are depleted. The remaining $[SO_2]$ and $[NH_3]$ are calculated using the mass balance equation.

Table 2. Rate of SO_2 oxidation by various mechanisms in aqueous droplets.

Mechanism	Reaction rate law
O_2	$\text{Rate} = \dfrac{H_S \left\{k_2 + k_{10}K_W/[H^+]\right\} K_{2S}k_3}{k_{-2}[H^+]^2 + k_{-10}[H^+] + K_{2S}k_3} P_{SO_2}$
O_3	$\text{Rate} = \left\{k_4[HSO_3^-] + k_5[SO_3^=]\right\} [O_3 \cdot H_2O]$
Fe^{+3}	$\text{Rate} = \dfrac{k_0 k_S{}^2 H_S{}^2 P_{SO_2}{}^2 [Fe^{+3}]}{[H^+]^3}$
Mn^{+2}	$\text{Rate} = 3.67\times10^{-3}[X] - 1.17 \left\{[HSO_4^-] + [SO_4^=]^2\right\} \left\{[Mn^{+2}] - [X]\right\} \times [H_2O(\ell)]^{-2}$
	$\text{where } X = \dfrac{K_1 H_S P_{SO_2} [Mn^{+2}]}{k_1 \left\{H_S P_{SO_2} + [H_2O(\ell)][Mn^{+2}]\times10^{-6}\right\} + 0.17}$
Soot	$\text{Rate} = k_6[C_x][O_2]^{0.7}$
	where $[H_2O(\ell)]$ in cc/m^3, concentration in mole/ℓ, gas pressure in atm, and time in sec, k_0 = 151.69 ℓ/mole-sec, $k_S = 1.84\times10^{-2}$ mole/ℓ, $k_1 = 8.12\times10^4$ ℓ/mole-sec, $k_2 = 3.4\times10^6\ sec^{-1}$, $k_{-2} = 2\times10^8$ ℓ/mole-sec, $k_{10} = 2.9\times10^5$ ℓ/mole-sec, $k_{-10} = 2.3\times10^{-7}\ sec^{-1}$, $k_3 = 1.7\times10^{-3}\ sec^{-1}$, $k_4 = 1.1\times10^5$ ℓ/mole-sec, $k_5 = 7.4\times10^8$ ℓ/mole-sec, $k_6 = 1.8\times10^{-4}\ \ell^{.7}\cdot mole^{.3}/gr\cdot sec$

4. Then the $[H^+]$, $[SO_2 \cdot H_2O]$, $[HSO_3^-]$, $[SO_3^=]$, $[NH_3 \cdot H_2O]$, and $[NH_4^+]$ are again calculated and the process is repeated until a 24-hr period is completed. The results of this calculation are given in Table 3 and Fig. 1. The conversion rate of SO_2 to sulfate by the soot process is 4.4%, very close to the rate observed in many field studies. Aqueous oxidation of SO_2 by the Mn^{+2}, O_2, Fe^{+3}, and O_3 processes does not appear to be important without the presence of a high concentration of NH_3. When there is a high concentration of NH_3 in the air, the O_3 and Fe^{+3} reactions can be important initially; but they slow down as the reaction proceeds because their reaction rates are inversely dependent on the acidity of the solution. From this comparison, we can conclude that the soot-catalyzed oxidation of SO_2 can be the dominant aqueous mechanism under realistic atmospheric conditions.

Table 3. Comparison of the relative significance of various SO_2 conversion processes in aqueous droplets.

Mechanisms	1 hr		6 hr		12 hr		24 hr	
	$SO_4^{=}$ μg/m^3	% conv.	$SO_4^{=}$ μg/m^3	% conv.	$SO_4^{=}$ μg/m^3	% conv.	$SO_4^{=}$ μg/m^3	% conv.
Mn^{+2}	2.55×10^{-5}	6.2×10^{-5}	1.6×10^{-4}	3.9×10^{-4}	3.1×10^{-4}	7.5×10^{-4}	6×10^{-4}	1.45×10^{-3}
O_2	1.8×10^{-3}	4.3×10^{-3}	9.6×10^{-3}	2.3×10^{-3}	1.8×10^{-2}	4.4×10^{-2}	3.4×10^{-2}	8.2×10^{-2}
Fe^{+3}	4.7×10^{-3}	1.1×10^{-2}	2.1×10^{-2}	5×10^{-2}	3.3×10^{-2}	8.0×10^{-2}	4.8×10^{-2}	0.12
O_3	0.13	0.33	0.27	0.66	0.35	0.85	0.47	1.13
O_2-NH_3	0.52	1.26	1.54	3.7	2.02	4.89	2.50	6.1
Fe^{+3}-NH_3	2.3	5.6	3.2	7.76	3.6	8.75	3.9	9.45
O_3-NH_3	4.51	10.94	5.14	12.5	5.28	12.8	5.28	12.8
C_x	1.8	4.4	10.8	26.4	21.6	52.4	41.25	100

Concentration: $H_2O(\ell)$: 0.05 g/m^3; SO_2: 0.01 ppm (10^{-8} atm); NH_3: 5 ppb (5×10^{-9} atm); O_3: 0.05 ppm (5×10^{-8} atm); Mn^{+2}: 20 ng x 0.25%/m^3; Fe^{+3}: 250 ng x 0.13%/m^3; C_x: 10 μg/m^3; temp.: 10°C.

0 0 0 0 3 5 0 1 4 5 0

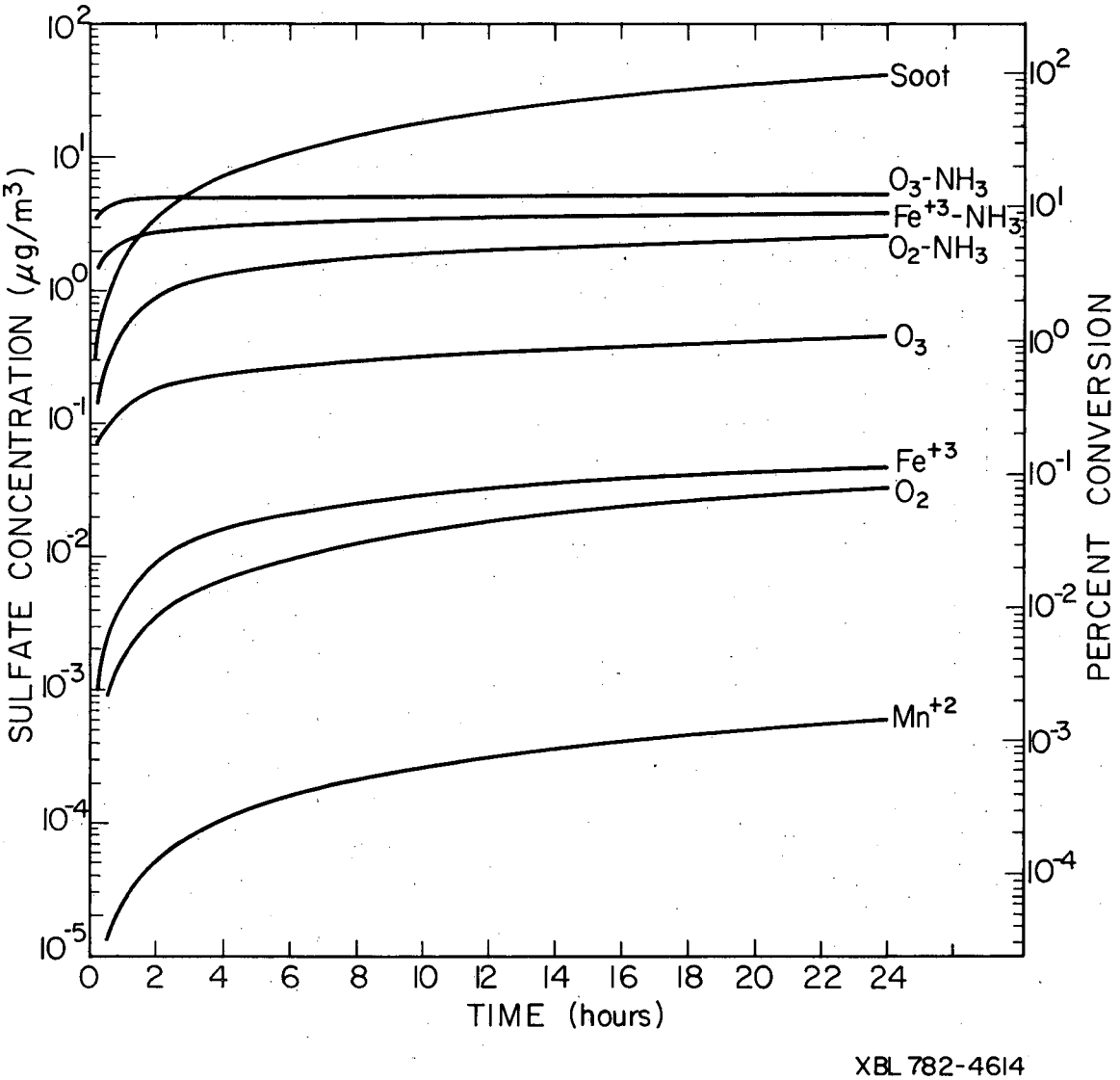

Figure 1. Comparison of the relative significance of various SO_2 conversion processes in aqueous droplets.

References

1. S. Beilke, D. Lamb, and J. Müller, "On the uncatalyzed oxidation of atmospheric SO_2 by oxygen in aqueous systems," Atmos. Environ. 9, 1083 (1975).

2. R.E. Erickson, L.M. Yates, R.L. Clark, and D. McEwen, "The reaction of sulfur dioxide with ozone in water and its possible atmospheric significance," Atmos. Environ. 11, 813 (1977).

3. J. Freiberg, "The mechanism of iron catalyzed oxidation of SO_2 in oxygenated solutions," Atmos. Environ. 9, 661 (1975).

4. M.J. Matteson, W. Stöber, and H. Luther, "Kinetics of the oxidation of sulfur dioxide by aerosols of manganese sulfate," Ind. & Eng. Chem. Fundam. 8, 677 (1969).

5. S.-G. Chang, R. Brodzinsky, R. Toossi, S.S. Markowitz, and T. Novakov, "Catalytic oxidation of SO_2 on carbon in aqueous suspensions," in Proceedings, Conference on Carbonaceous Particles in the Atmosphere, Lawrence Berkeley Laboratory, Berkeley, California (in press).

6. N.-C. Lau and R.J. Charlson, "On the discrepancy between background atmospheric ammonia gas measurements and the existence of acid sulfates as a dominant atmospheric aerosol," Atmos. Environ. 11, 475 (1977).

7. G.E. Gordon, D.D. Davis, G.W. Israel, H.E. Landsberg, and T.C. O'Haver, Atmospheric Impact of Major Sources and Consumers of Energy, Report NSF/RA/E-75/189 (1975) (available from NTIS as PB 262 574).

Sulfur Dioxide Oxidation in a Dispersing Plume

R. Toossi, S.-G. Chang, P. J. Pagni, and T. Novakov

Theoretical prediction of the spatial distribution of pollutant concentrations and the ultimate fate of SO_2 oxidation in plumes is important in environmental impact studies. SO_2 oxidation reactions in plumes are governed by both chemical and dispersion processes, which cannot be treated separately. Under unstable or slightly stable atmospheric conditions, plume reaction rates may be controlled by the rate of mixing and dilution by ambient air. A first or second order reaction rate has usually been considered in studies of SO_2 oxidation in plumes. However, in a recent paper,[1] it is suggested that the rate of plume expansion and quenching has a controlling influence on the order of the reaction. Many homogeneous[2] and heterogeneous[3-6] reactions are considered to be responsible for SO_2 oxidation in plumes. However, the role of soot particles emitted in large amounts by the combustion sources had been discounted until Novakov et al.[7] showed that under certain conditions, these particles can be responsible for the major conversion of sulfur dioxide to sulfate. Chang et al.[8] recently extended the research on the reactivity of these particles in aqueous solutions of pH between 1.45 and 7.4. The reaction was first order with respect to carbon concentration in the solution and was independent of pH and dissolved SO_2 concentration. A box-type calculation comparing the relative importance of "wet" soot-particle-catalyzed reactions with other catalytic reactions has been carried out. These calculations show that the soot-catalyzed oxidation of SO_2 can be the dominant mechanism under realistic atmospheric conditions.[9]

Liquid water may condense on the soot particles when plumes of hot exhaust gases cool rapidly through mixing with ambient air or as they pass through fog and cloud banks. A model for SO_2 oxidation in a dry environment plume was presented earlier.[10] The purpose of this study is to extend the model to predict the spatial distribution of sulfate concentration downwind from a plume resulting from aqueous oxidation of SO_2 catalyzed on soot particles.

Mathematical Formulation

The basic assumptions are:

1. Particulates are mainly fine soot particles which follow the streamlines of the gaseous pollutants and therefore can be treated as gases; i.e., $Ta \cdot Re_p << 1$,

where $Ta = \frac{\rho_p \cdot r_p}{\rho_g \cdot R}$ is the Taylor number and $Re_p = \frac{\bar{u} \cdot r_p}{\nu}$ is the Reynolds number based on particle radius r_p and gas kinematic vsicosity ν.

2. Flow velocity perpendicular to the plume trajectory is neglected.

3. Plumes are ejected from stacks which are sufficiently high and have enough source strength to ensure that the intensity of atmospheric turbulence is much less than that associated with the turbulent plume.

4. Velocity, density, and pollutant concentration profiles are similar in all sections normal to the plume. The validity of this assumption is verified experimentally by Ooms.[11]

5. Boussinesq's approximation is valid; i.e., density variation affecting inertia is neglected. This assumption is valid when the initial fractional density difference $\frac{\rho_\infty - \rho_i}{\rho_\infty}$ is smaller than 0.5.[12]

6. Molecular transport compared with turbulent transport is neglected.

The coordinate system is shown in Fig. 1. v is the cross wind velocity, assumed constant with z for simplicity; u, ρ, and c_j's are velocity, density, and species concentration respectively. The plume centerline makes an angle θ with the horizontal. s is the distance along the plume axis from the stack and b is the plume radius. s and θ are related to the Cartesian coordinate as

$$z = \int_0^s \sin\theta \, ds \tag{1}$$

and

$$x = \int_0^s \cos\theta \, ds \tag{2}$$

Governing equations consist of conservation of mass, momentum, energy, and chemical species as follows:

$$\text{Mass: } \frac{d}{ds} \int u dA = \varepsilon \tag{3}$$

where $\varepsilon = 2\pi b[\alpha|u - v\cos\theta| + \beta|v\sin\theta|]$ and α and β are entrainment coefficients determined experimentally.

Momentum along s direction:

$$\frac{d}{ds} \int u^2 \, dA = \frac{g \sin\theta}{\rho_1} \int (\rho_\infty - \rho) dA + \varepsilon \, v \cos\theta \, , \tag{4}$$

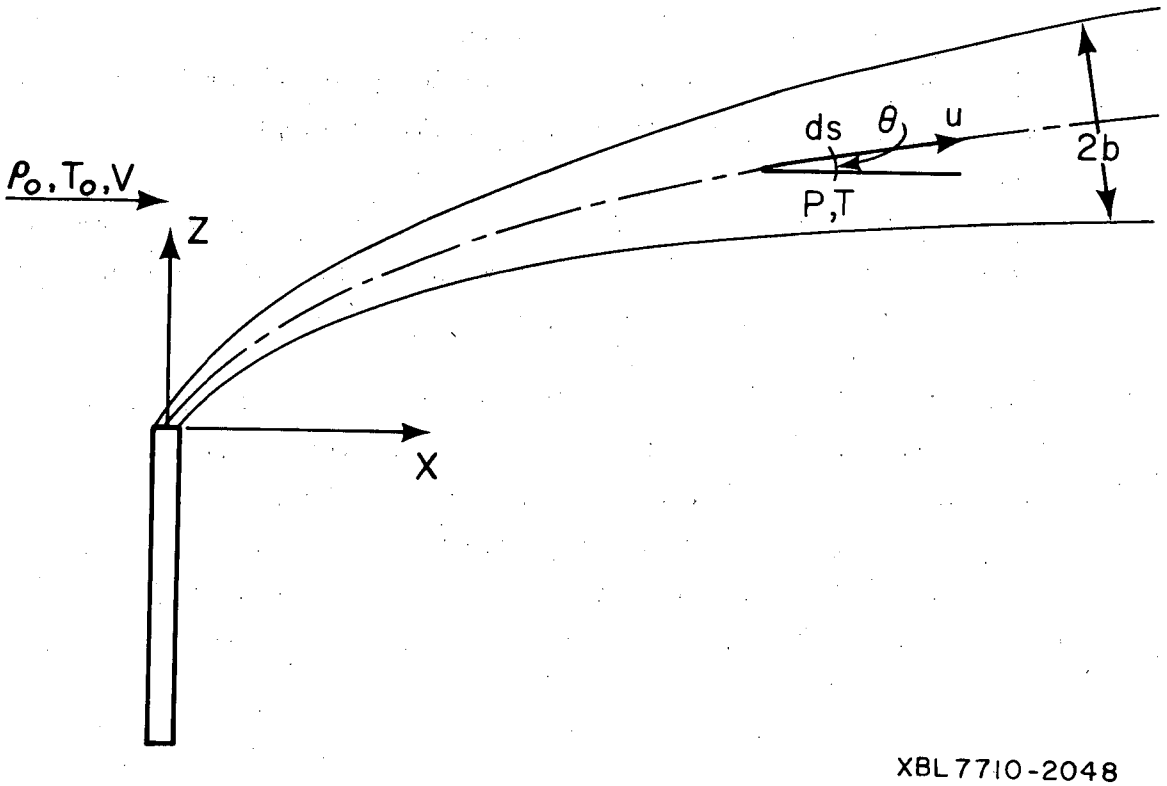

Figure 1. Coordinate system. P, T, and u are the potential density, absolute temperature, and velocity; b is half the plume diameter, and V is wind velocity.

where g is acceleration of gravity.

Momentum in transverse direction:

$$\frac{d\theta}{ds}\int u^2\, dA = \frac{g\cos\theta}{\rho_1}\int(\rho_\infty-\rho)dA - \varepsilon\, v\sin\theta \tag{5}$$

Energy:

$$\frac{d}{ds}\int \rho\, u\, C_p(T-T_\infty)dA = \rho_\infty\, \varepsilon\, C_p(T-T_\infty)\ , \tag{6}$$

where C_p is the specific heat.

Chemical species:

$$\frac{d}{ds}\int C_j\, u\, dA = \varepsilon\, C_{j,\infty} + \int W_j''\, dA\ , \tag{7}$$

where $j = 1, \ldots, N$.

C_j is the concentration of species j inside the plume, W_j'' is the rate of production of species j, and N is the number of species examined. The subscripts ∞ and 1 denote the value in the background ambient condition outside the plume trajectory and at the plume stack height.

Equations (1) through (7) can be solved numerically for (N + 4) unknowns ρ, u, b, θ, C_1, C_2,. . ., C_N. Initial conditions are values of the above parameters at the stack. The rate law can be written as

$$\frac{d[\text{sulfate}]}{dt} = W''_{sulf} = A[C_x][O_2]^n \exp\left(\frac{-5888}{T}\right) \tag{8}$$

where $A = 9.61 \times 10^4\ \ell^n/g\cdot sec\cdot mole^{n-1}$; $[C_x]$ is soot concentration in gr/ℓ; and $[O_2]$ is dissolved oxygen concentration in mole/ℓ and n = 0.7. Assuming all sulfate produced is in the form of sulfuric acid, Equ. (8) can be written as

$$\frac{d[\text{sulf}]}{dt} = W''_{sulf} = A'[C_x][O_2]^n \exp\left(\frac{-5888}{T}\right) \tag{8'}$$

with $A' = 9.42 \times 10^6$ when sulfate and soot concentrations are expressed in units of g/m^3. The rate of SO_2 depletion is

$$W''_{SO_2} = \frac{64}{98} W''_{sulf}\ . \tag{9}$$

Also note that carbon acts only as a catalyst and therefore no carbon is destroyed or produced. We then have

$$W''_{soot} = 0\ . \tag{10}$$

The set of differential equations with appropriate initial conditions is solved, using Gear-Hindmarsh integration routine, to evaluate plume trajectory and concentration of inert and reactive pollutants in the plume. At each point the conversion rate is evaluated from the following equation:

$$\text{percent conversion} = \frac{C_{SO_2} - C_{SO_2}^{(t=0)}}{C_{SO_2}} = 100\left(1 - \frac{\pi b^2 u C_{SO_2}}{\Gamma_{SO_2}}\right) \quad (11)$$

As an example of the use of this model, the rate of sulfate formation from the Keystone #1 plant described in the LAPPES[13] study is considered. The plant geometry and meteorological data on three different days, along with other assumptions made in the calculations, are listed in Table 1.

Table 1. Meteorological data and plant conditions for three worked examples (Ref. 13).[a]

		Example 1 (May 3)	Example 2 (Oct. 9)	Example 3 (Oct. 10)
Velocity of effluent at the stack	u_i (m/sec)	21	10	20
Stack height	H (m)	244	244	244
Stack radius	b_i (m)	4.1	4.1	4.1
Stack temperature	T_i (°C)	160	115	135
SO_2 flux at the stack	Γ_{SO_2} (gr/sec)	3500	1500	2900
Wind velocity	v (m/sec)	10	3	4
Potential temperature gradient	$\frac{d\theta}{dz}$ (°C/m)	2.5×10^{-3}	3.5×10^{-3}	10^{-3}
Ambient temperature	T_∞ (°C)	20	20	20
Ambient temperature at stack height	T_1 (°C)	17.6	17.6	17.6

[a]Other parameters assumed in calculations:

Soot concentration at the stack $C_{i,1} = 0.36$ gr/m^3

Water vapor concentration at the stack $C_{i,3} = 10.0$ gr/m^3

Sulfate concentration at the stack $C_{i,sulf} = 0.0$ gr/m^3

Background concentrations $C_{\infty,sul} = C_{\infty,1} = C_{\infty,2} = 0.0$ gr/m^3

Results

The data in Table 1 show that the plume is moderately stable for all three days of interest. It is assumed that the effect of inversions is neglected since stack height is greater than the ground-level inversion depth.[13] The plume

trajectory is calculated for these plumes and plotted for the plumes of October 9 in Fig. 2. It can be seen that most dispersion occurs in the first 30 minutes only a kilometer away from the source. Thereafter the plume is stable and can travel several kilometers before touching the ground.

The periodic nature of the plume trajectory can be explained on physical grounds. When a piece of air mass expands adiabatically to a new position, it cools. However, if the temperature decrease is less than the atmospheric lapse rate, the air mass is colder than the ambient air and is driven back to its original position. Under these conditions, the restoring force is balanced by the acceleration, so that

$$\rho \frac{g}{T} \frac{d\theta}{dz} \Delta z = \rho \frac{d^2 \Delta z}{dt^2}$$

$\frac{1}{T} \frac{d\theta}{dz}$ represents the change in density per meter of rise and $\theta = T + 0.0098\ z$ is the potential temperature. The solution of this equation leads to the general form for a harmonic oscillation with frequency $\omega = \frac{g}{T} \frac{d\theta}{dz}$.[10] Numerical calculations show that temperature and velocity in the plume approach their ambient values as the plume rises to the equilibrium rise. The entrainment rate decreases, and the plume expands very slowly. Transport becomes negligible, and chemical reactions can be considered as they occur in a static batch reactor.

A graph of the concentration of sulfate and the percent of total SO_2 conversion is plotted on the single graph against the distance downstream from the stack and the time of travel in Fig. 3. As the plume travels downstream from the stack, total sulfate conversion increases. However, in the first kilometer of transport, the plume is entrained significantly. When the plume reaches its maximum height, the entrainment rate is insignificant and the chemical reaction is rate controlling. The result is a minima in the sulfate concentration curve at the point where the plume is bent appreciably. The conversion rate is 1.6% for the first hour and increases in a similar fashion to 40% in 24 hours at 250 km from the stack. The relative humidity has been taken as 100%, and therefore there is always some liquid water present for the wet mechanism to take place.

The effect of relative humidity on the rate of oxidation can be investigated by considering its effect on the lifetime of water droplets present in the plume gases. For this calculation we have assumed a surfactant layer on the droplets, which reduces the evaporation coefficient α to 10^{-6}. It has been shown[9] that

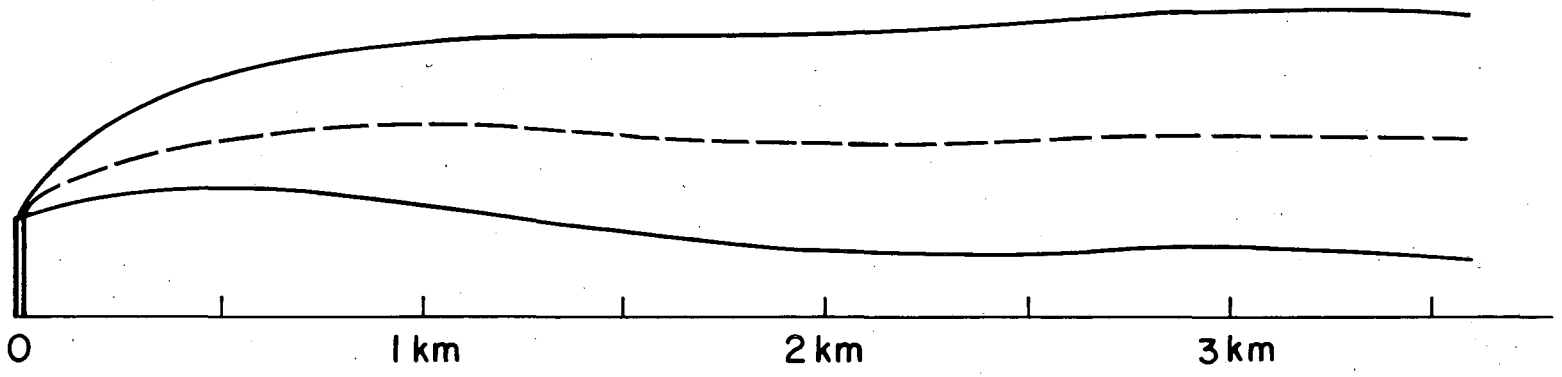

XBL7710-2155

Figure 2. Plume trajectory. The dotted line is the centerline. Note the periodic nature of the plume due to the stratification. The plume eventually stabilizes at its maximum rise.

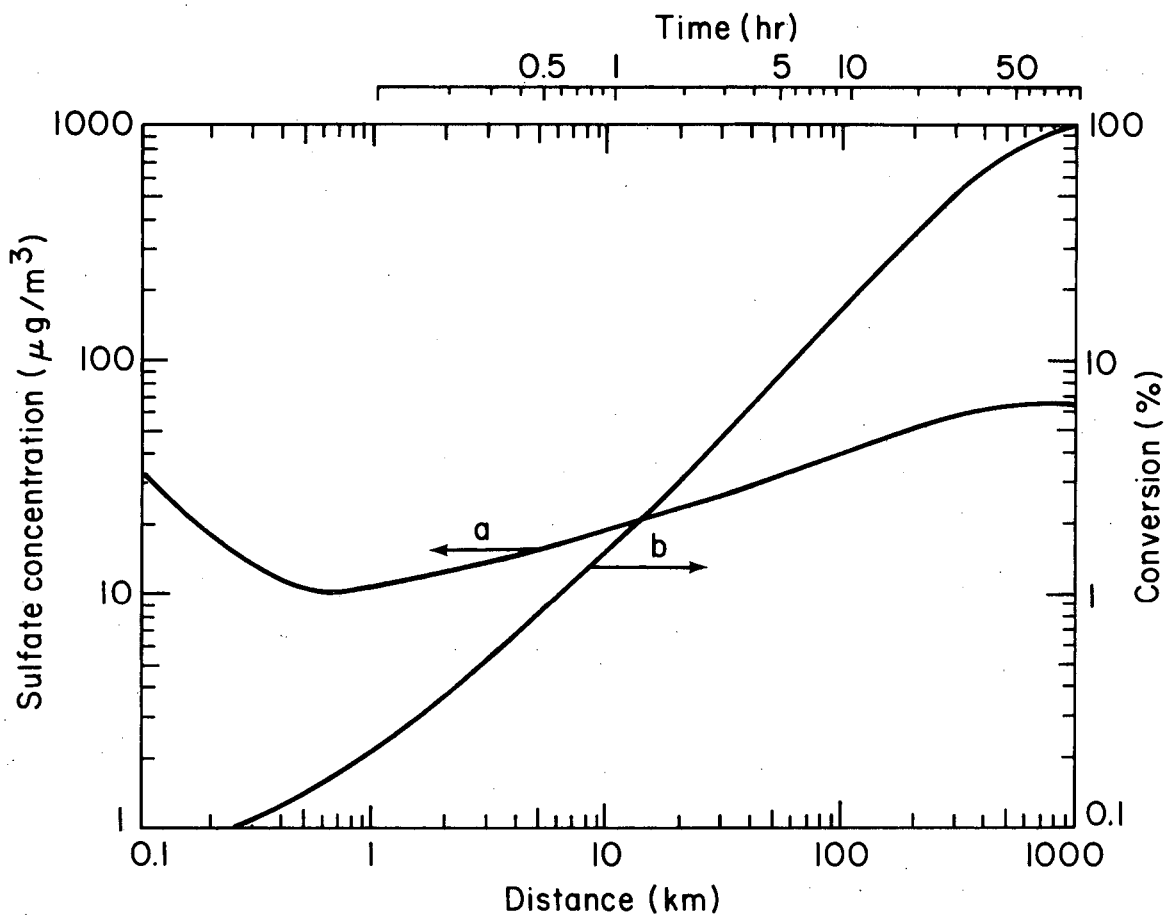

XBL 7812-13506

Figure 3. a) Sulfate concentration and b) fraction converted in the plume as a function of distance downstream of the stack. Parameters used in the calculations are given in Table 1.

droplets of solution cannot theoretically evaporate completely if there is a formation of nonvolatile species inside the droplet. As the droplet evaporates, the concentration of nonvolatile species increases, which gradually reduces the vapor pressure of water at the droplet surface below that of ambience. Under these conditions, a droplet becomes so concentrated that the validity of the Henry, Raoult Law and the Debye-Hückel theory[14] becomes inadequate.

The lifetime of the droplets has been taken as the time in which the droplets reach this concentration, and therefore calculations have been stopped. At this point, we do not know how long the oxidation reaction continues. Research is under way to solve this problem.

The rate of oxidation is calculated for three examples and is tabulated in Table 2. These calculations show that although the reaction rate is independent of the liquid water concentration, total conversion inside the plume depends strongly on ambient humidity. As long as humidity is high enough to ensure the presence of enough liquid water around the soot nuclei, the wet mechanism prevails.

Conclusions

Based on the calculations presented in this report, it is concluded that under certain meteorological conditions, catalytic oxidation of SO_2 on soot particles, emitted as the natural products of incomplete combustion, can be very important for the production of sulfate in plumes. The discrepancies on the data reported in the literature on the SO_2 conversion rate might be related in part to variations in particulate emissions and ambient humidity.

References

1. S.E. Schwartz and L. Newman, "Processes limiting oxidation of sulfur dioxide in stack plumes," J. Am. Chem. Soc. 12, 17 (1978).
2. J.G. Calvert and F. Su, "Mechanism of the heterogeneous oxidation of sulfur dioxide in the troposphere," Atmos. Environ. 12, 197 (1978).
3. L. Newman, J. Forrest, and B. Manowitz, "The application of an isotopic ratio technique to a study of the atmospheric oxidation of sulfur dioxide in the plume from an oil-fired power plant," Atmos. Environ. 9, 959 (1975).
4. M.J. Matteson, W. Stöber, and H. Luther, "Kinetics of the oxidation of sulfur dioxide by aerosols of manganese sulfate," I. & E.C. Fund. 8, 667 (1969).
5. J. Freiberg, "Effects of relative humidity and temperature on iron-catalyzed oxidation of SO_2 in atmospheric aerosol," Environ. Sci. Technol. 8, 731 (1969).
6. M.R. Burke, R.K. Baker, and T.L. Moyers, "The interaction of SO_2 with airborne particulate matter," Chromatog. Sci. J. 11, 575 (1973).
7. T. Novakov, S.-G. Chang, and A.B. Harker, "Sulfates as pollution particulates: Catalytic formation on carbon (soot) particles," Science 186, 259 (1974).

Table 2. Percent of SO_2 conversion under different meteorological conditions, $\alpha = 10^{-6}$, T = 20°C.

Example 1

R.H. \ Time (hr)	1	2	4	6	12	24
100	1.6	3.1	6.1	9.0	17.8	35.6
95	1.6	3.1	6.1	9.0	17.8	
90	1.6	3.1	6.1			
80	1.6	3.1				
70	1.6	3.1				
60	1.6					
50	1.6					

Example 2

R.H. \ Time (hr)	1	2	4	6	12	24
100	1.6	3.3	6.6	10.0	19.7	39.5
95	1.6	3.3	6.6	10.0	19.7	
90	1.6	3.3	6.6			
80	1.6	3.3				
70	1.6	3.3				
60	1.6					
50	1.6					

Example 3

R.H. \ Time (hr)	1	2	4	6	12	24
100	1.8	3.5	6.9	10.4	20.8	40.8
95	1.8	3.5	6.9	10.4	20.8	
90	1.8	3.5	6.9			
80	1.8	3.5				
70	1.8	3.5				
60	1.8					
50	1.8					

8. S.-G. Chang, R. Brodzinsky, R. Toossi, S.S. Markowitz, and T. Novakov, "Catalytic oxidation of SO_2 on carbon in aqueous suspensions," in Proceedings, Conference on Carbonaceous Particles in the Atmosphere, Lawrence Berkeley Laboratory, Berkeley, California (in press).

9. R. Toossi, S.-G. Chang, and T. Novakov, "Lifetime of liquid water drops in ambient air: Consideration of the effects of surfactants and chemical reactions," this report.

10. D.P. Hoult and J.C. Weil, "Turbulent plumes in a laminar cross flow," Atmos. Environ. 6, 513 (1972).

11. G. Ooms, "A new method for the calculation of the plume path of gases emitted by a stack," Atmos. Environ. 6, 899 (1972).

12. P.F. Crapper and W.D. Baines, "Non-Boussinesq forced plumes," Atmos. Environ. 11, 415 (1977).

13. F.A. Schiermeier and N. Laurence, Large Power Plant Effluent Study (Raleigh, N.C., U.S. Dept. of Health, Education, and Welfare, 1970), v. 2.

14. G.N. Lewis and M. Randall, Thermodynamics (New York, McGraw-Hill, 1961), Ch. 23.

Lifetime of Liquid Water Drops in Ambient Air: Consideration of the Effects of Surfactants and Chemical Reactions

R. Toossi, S.-G. Chang, and T. Novakov

Heterogeneous reactions involving liquid water are of great interest to environmentalists and air pollution scientists. The importance of the aqueous reactions in the atmosphere depends on three factors: (1) rate of chemical reaction, (2) availability and nature of the condensation nuclei, and (3) lifetime of the liquid drops in the atmosphere.

The rate of growth or depletion of the water droplets can be calculated by simultaneous solution of the diffusion and energy equations around the droplet:

$$\nabla^2 n(R) = 0 \tag{1}$$

$$\nabla^2 T(R) = 0 \tag{2}$$

where n is the concentration of the vapor molecule and T is the temperature at distance R from the droplet center. Boundary conditions are given by the values of n and T at large distances from the drop and by assuming that the equilibrium between vapor and temperature holds at the droplet surface. Using this approach and assuming a hyperbolic vapor density distribution,

$$\rho = (\rho_r - \rho_\infty)\left(\frac{r}{R}\right) + \rho_\infty \ . \tag{3}$$

Mason[1] derived the rate of growth or evaporation of a droplet of radius r for quasi-steady-state condition and a small Knudson number as follows:

$$r\frac{dr}{dt} = \frac{P_\infty - P_s}{\dfrac{L^2\rho_\ell P_s}{KR_vT^2} + \dfrac{R_vT\rho_\ell}{D}} \tag{4}$$

P_∞ and P_s are ambient vapor pressure and saturated vapor pressure over the droplet surface, D is the vapor diffusion coefficient, K is the thermal conductivity of the gas, L is the latent heat of condensation, and ρ_ℓ is the density of the liquid droplet. Equilibrium vapor pressure over a droplet's surface depends on its curvature, and the concentration of solute in the solution droplet and is given by[2]

$$P_s = P_s(\infty)\ \exp\left(\frac{2\sigma}{rR_v\rho_\ell T}\right)\cdot\left(\frac{n_o}{n+n_o}\right) \tag{5}$$

where $P_s(\infty)$ is the saturation vapor pressure over the bulk of the water, with surface tension σ at temperature T. n_o and n are molar concentrations of water and solute. When a droplet is large enough for the Kelvin effect to be negligible, P_s will be independent of the radius; and Equ. (4) predicts a linear change in the surface area of the drop as a function of time. When the mean free path of escaping molecules is large compared with the droplet diameter (large Knudson number), the continuum theory as applied above fails, and the classical kinetic theory of gases can be applied to determine the evaporation rate.[3] However, this condition applies only for submicron droplets or at reduced pressure, which is of little significance in atmospheric studies. Equation (4) approximates the rate of change of droplet surface area to a good accuracy of pure water droplets where diffusion in the gas phase is the rate controlling mechanism. For the atmospheric droplets, where a layer of surfactants is often present, resistance in the interphase is dominant; and Equ. (4) underestimates the lifetime of drops up to many orders of magnitude. For example, according to Equ. (4), it takes only a fraction of a second for a 1.0-μm particle to vanish completely in an atmosphere saturated with water vapor. However, experiments of Gurdis et al.[4] show that it takes 40 minutes for a 4.0-μm drop to reduce to 0.74 μm in a mixture of 70% hydrogen and 30% air. Similar results have also been found in our laboratory.[5]

The evaporation rate of droplets containing insoluble monolayers for nonvolatile droplets (L = 0) has been calculated elsewhere.[6,7] According to these theories, droplet evaporation is assumed to proceed by a two-stage process. The first evaporation occurs in a virtually vacuous spherical shell, of thickness Δ comparable to the mean free path of the diffusing molecule. The evaporation takes place in a Knudson flow. The second step is diffusion of the vapor shell at $r + \Delta$. Using the Maxwell equation of diffusion and making the mass balance between the molecules arriving at the shell surface at distance $r + \Delta$ and leaving by diffusion, the rate of evaporation can be written as

$$r\,\frac{dr}{dt} = \frac{P_\infty - P_s}{\rho_\ell R_v T\left(\frac{1}{r\nu\alpha} + \frac{r}{r+\Delta}\right)} \qquad (6)$$

where $\nu = \frac{\bar{v}}{4}$ and $\bar{v}$ is the velocity of the evaporating molecule calculated from the kinetic theory of gases, $\Delta = \frac{KT}{AP_\infty}$ is the distance between collisions. The collision cross section is $A = \pi(a_1 + a_2)^2$ where a_1 and a_2 are the radii of the diffusing and ambient gaseous molecules. The evaporation coefficient α is a function of the film thickness δ[8] and the degree of coverage and the nature of the monolayer.

Deryaguin et al.[9] determined a critical film thickness, beyond which a surface active material strongly suppresses any exchange of water vapor, either through condensation or evaporation.

Formulation of the Problem

The general form of a governing equation describing evaporation and the growth of droplets can be derived by combining Equs. (4) through (6). Assuming that resistance through the liquid drop is negligible, and taking $\rho_{eq}(\infty)$ as the equilibrium vapor density at large distances from the droplet, the evaporation rate for the drop shown in Fig. 1 can be written as

$$r\,\frac{dr}{dt} = \frac{\rho_{eq}(\infty)}{\rho_\ell} \cdot \frac{S - \frac{n_o}{n+n_o}\exp[2\sigma\rho_{eq}(\infty)/r\rho_\ell]}{R_i + R_g + R_k} \tag{7}$$

where $S = \frac{P_\infty}{P_s}$ is the saturation ratio,

$R_i = \frac{1}{r\nu\alpha}$ is the resistance in the interface,

$R_g = \frac{r}{D(r+\Delta+\delta)}$ is the resistance to mass diffusion,

$R_k = \frac{bL}{K}$ is the resistance to heat diffusion,

and $b = \frac{L\cdot\rho_{eq}(\infty)}{R_v T^2}$ is the slope of the vapor density equilibrium curve $(\frac{\Delta V}{\Delta T})$.

Chemical Equilibrium in the Droplet System

It is assumed that the gaseous SO_2, CO_2, and NH_3 are in equilibrium with sulfite (IV), carbonate, and ammonium species in the aqueous droplet, as demonstrated by Beilke[10] and Miller.[11] Table 1 lists the chemical equilibrium processes in the droplet-ambient system.

Results and Conclusions

The rate of change of droplet size is found by solving Equ. (6) under different conditions. The molar concentration of solute n is taken as the summation of the total concentration of ions in the solution. Therefore it can be seen that this equation is coupled with the rate equation and other equilibrium equations used to explain the chemistry occurring in the solution droplet. It is assumed that

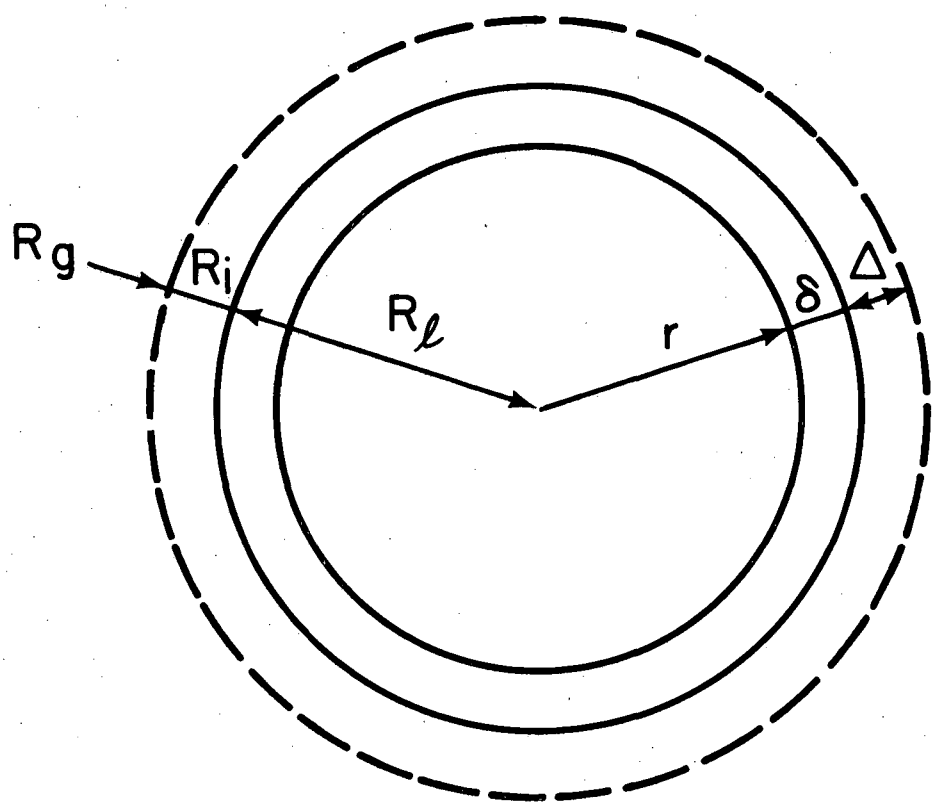

XBL 7812-13501

Figure 1. Model of a solution droplet of radius r covered by a thin layer of surfactant of thickness δ. Δ is the molecular flow layer thickness. R_ℓ, R_i, and R_g are resistances in the bulk of the liquid, at the interface, and in the gas phase respectively.

Table 1. Chemical equilibria in a droplet system.

Reaction	Equil. constant expression[a]	Value of equil. constant at 25°C
$H_2O \rightleftarrows H^+ + OH^-$	$K_w = [H^+][OH^-]\gamma+\gamma-$	1.008×10^{-14}
$SO_{2(g)} + H_2O \rightleftarrows SO_2\cdot H_2O$	$H_s = [SO_2\cdot H_2O]/P_{SO_2}$	1.24
$SO_2\cdot H_2O \rightleftarrows H^+ + HSO_3^-$	$k_{1s} = [H^+][HSO_3^-]\gamma+\gamma-/[SO_2\cdot H_2O]$	0.0127
$HSO_3^- \rightleftarrows H^+ + SO_3^{2-}$	$k_{2s} = [H^+][SO_3^{2-}]\gamma+\gamma_2-/[HSO_3^-]\gamma-$	6.24×10^{-8}
$NH_{3(g)} + H_2O \rightleftarrows NH_3\cdot H_2O$	$H_a = [NH_3\cdot H_2O]/P_{NH_3}$	57
$NH_3\cdot H_2O \rightleftarrows NH_4^+ + OH^-$	$K_a = [NH_4^+][OH^-]\gamma+\gamma-/[NH_3\cdot H_2O]$	1.774×10^{-5}
$CO_{2(g)} + H_2O \rightleftarrows CO_2\cdot H_2O$	$H_c = [CO_2\cdot H_2O/P_{CO_2}$	0.034
$CO_2\cdot H_2O \rightleftarrows H^+ + HCO_3^-$	$K_{1c} = [H^+][HCO_3^-]\gamma+\gamma-/[CO_2\cdot H_2O]$	4.45×10^{-7}
$HCO_3^- \rightleftarrows H^+ + CO_3^{2-}$	$K_{2c} = [H^+][CO_3^{2-}]\gamma+\gamma_2-/[HCO_3^-]\gamma-$	4.68×10^{-11}

[a]The activities follow the Davies relation $\log \gamma_z = (-Az^2 \sqrt{I})/(1 + \sqrt{I}) + 0.2\ IAz^2$, where I is the ionic strength, $I = 1/2 \sum_i |c_i| z_i^2$, and A = 0.5085 for water at 25°C.

the film thickness δ is much smaller than the droplet radius. Substituting for the values of the Boltzman constant and taking a_1 and a_2 as the radius of water vapor and air molecules, we have

$$\Delta = 4.86 \times 10^{-8}\ T/P\ \text{cm}$$

$$\nu = 857\ \sqrt{T}\ \text{cm/sec}$$

The thermal conductivity and diffusion coefficient are approximated by the empirical relations

$$K(T) = 5.803 \times 10^{-5}\ \left(\frac{393}{T+120}\right)\left(\frac{T}{273}\right)^{3/2}\ \frac{\text{cal}}{\text{cm}\cdot\text{sec}\ {}^\circ\text{K}}$$

$$D(T) = 0.226\ \left(\frac{393}{T+120}\right)\left(\frac{T}{273}\right)^{5/2}\cdot\frac{1}{P}\ \text{cm}^2/\text{sec}$$

The latent heat of evaporation is also a function of temperature and can be approximated by the equation

$$L = -0.57\ T = 753.1\ (L \text{ in cal/g and } T \text{ in } {}^\circ\text{K})$$

between temperature range of interest, $253 < T < 313$. The value of $\sigma = 75$ dynes/cm and $\rho_\ell = 1\ \text{gm/cm}^3$ is assumed for water. The values of α strongly depend on the nature of the surfactants in the solution and can vary several orders of magnitude. For plain water, $\alpha = 0.034$. Reduction in the value of α to 6×10^{-6} resulted from coating the drop with a monomolecular layer of long-chain acids.[12] The importance of R_i relative to R_g in determining the rate of evaporation of droplets is reflected by the effect of impurities on the rate of evaporation. Table 2 gives the values of R_i and R_g in the limiting conditions for pure water droplets ($\alpha = 0.034$) and droplets containing a monolayer of insoluble surfactants ($\alpha = 10^{-6}$).

Table 2. Comparison of the magnitude of R_i, R_g, and R_k at different droplet size and α.[a]

a(μm)	R_i(sec·cm^{-2}) α=0.034	R_i(sec·cm^{-2}) $\alpha=10^{-6}$	R_g(sec·cm^{-2})	R_k(sec·cm^{-2})
0.1	200	6.02×10^6	1.60	10.08
1	20	6.02×10^5	3.41	10.08
10	2	6.02×10^4	3.84	10.08
50	0.4	1.2×10^4	3.88	10.08

[a] $T = 20°C$, $\Delta = 1.425 \times 10^{-5}$ cm, $P = 1.0$ atm, $b = 1.06 \times 10^{-6}\ {}^\circ\text{K}^{-1}$

Thus a monolayer of a long-chain alcohol or acid should be able to reduce the rate of evaporation by more than four orders of magnitude. The lifetime of a 10-μm drop in air of 80% relative humidity increased from 2.5 sec to 1300 sec[13] when α decreased from 0.04 to 1.5×10^{-5}. These results are based on the assumption that the solution effect is negligible. In practice the lifetime of these droplets can be longer because of the reduction in surface vapor pressure due to an increase in the solute concentration as the drop evaporates. This point will be discussed in more detail in the next section. Table 2 shows that for droplets of pure water < 10 μ or at reduced pressure, R_g is small compared with R_i and R_k; therefore the rate is controlled by the rate of diffusion in the vacuum and by conduction. When a monolayer is present, however, a very small percentage of the water molecules striking the surface enters it, and a very high free energy of activation is needed to produce or find a hole in the liquid surface in which to be accommodated.

Figure 2 shows graphs of droplet lifetime as a function of ambient relative humidity and evaporation coefficients. These graphs show a strong moisture effect, especially at relative humidities greater than 90%. The effect of temperature on the lifetime can be seen in Fig. 3. The evaporation rate is increased exponentially with an increase in temperature. When a slight amount of supersaturation is present, droplets start to grow. The rate of growth is a strong function of the supersaturation ratio and the nature of the surfactants. Fig. 4 shows the size that a 5-μm droplet reaches after it is exposed to 0.05% of supersaturation for 24 hr. When α is reduced, most of the resistance is in the interface; and since there is little chance of diffusing water vapor through this barrier, the droplet grows very slowly. When no surfactant is present, evaporation is diffusion controlled, the evaporation rate is independent of the evaporation coefficient α, and growth occurs very rapidly. The result is an S-shaped curve (Fig. 4).

When irreversible reactions lead to nonvolatile products in the droplet, their concentrations increase as the droplet evaporates and the solution effect eventually becomes important. This happens to many heterogeneous reactions occurring in the atmospheric droplets. As an example, catalytic oxidation of SO_2 on soot particles is considered here. The rate of reaction for this mechanism has been determined as[14]

$$\frac{d\left\{[HSO_4^-] + [SO_4^=]\right\}}{dt} = A[O_2]^{0.7}[C_x]\exp\left(\frac{-5888}{T}\right) \qquad (8)$$

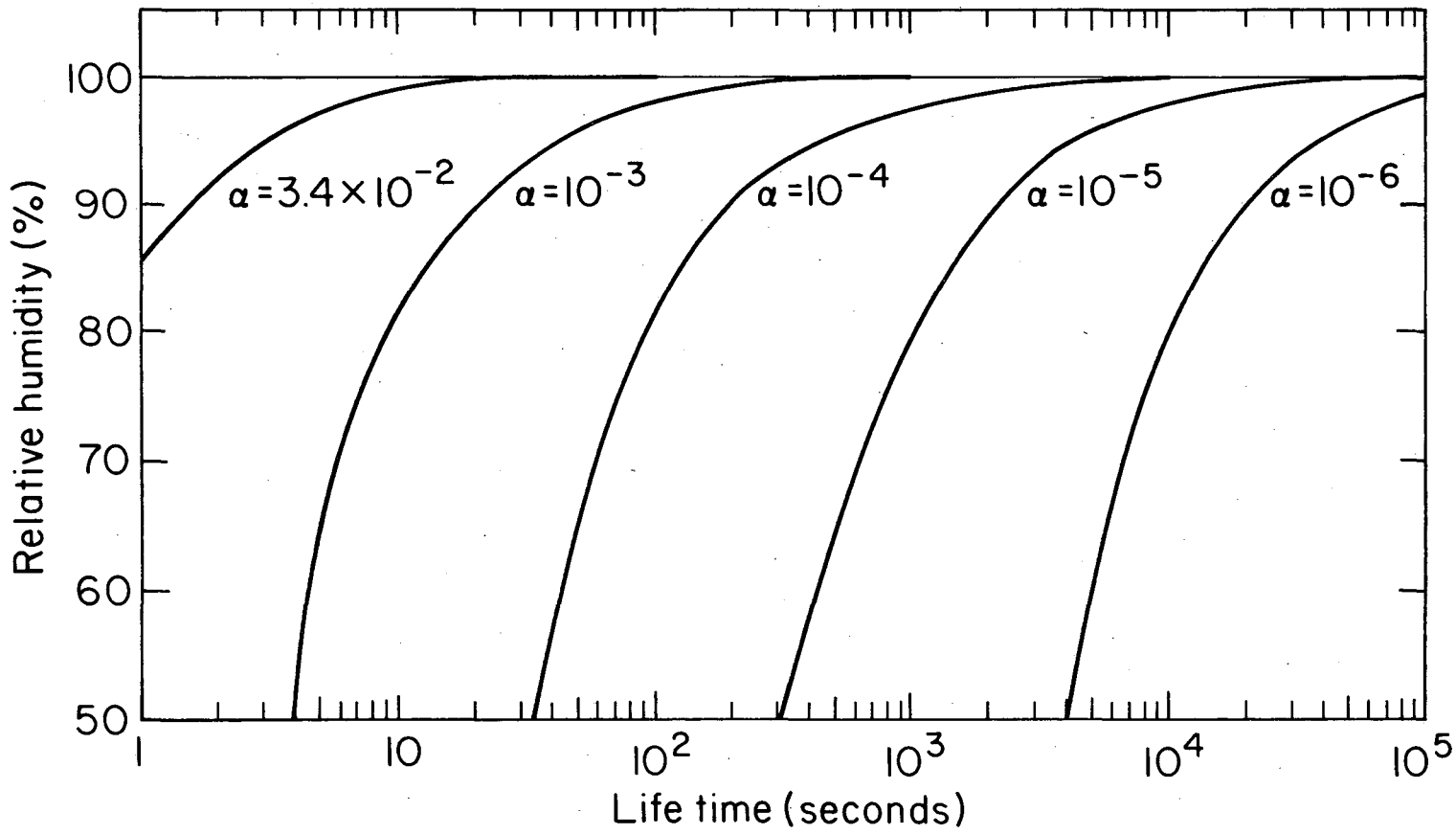

XBL 7812-13502

Figure 2. Lifetime of droplets at different relative humidities. Different curves represent effects of surfactants on the lifetime. For a pure water droplet, $\alpha = 0.034$; and the lifetime is several orders of magnitude smaller than that of droplets covered by a thin film of surfactants. Other parameters used in the calculation are $T = 20°C$, $R_o = 5\ \mu m$, $P_{SO_2} = 10^{-8}$, $P_{CO_2} = 3 \times 10^{-4}$, and $P_{NH_3} = 5 \times 10^{-8}$ atm.

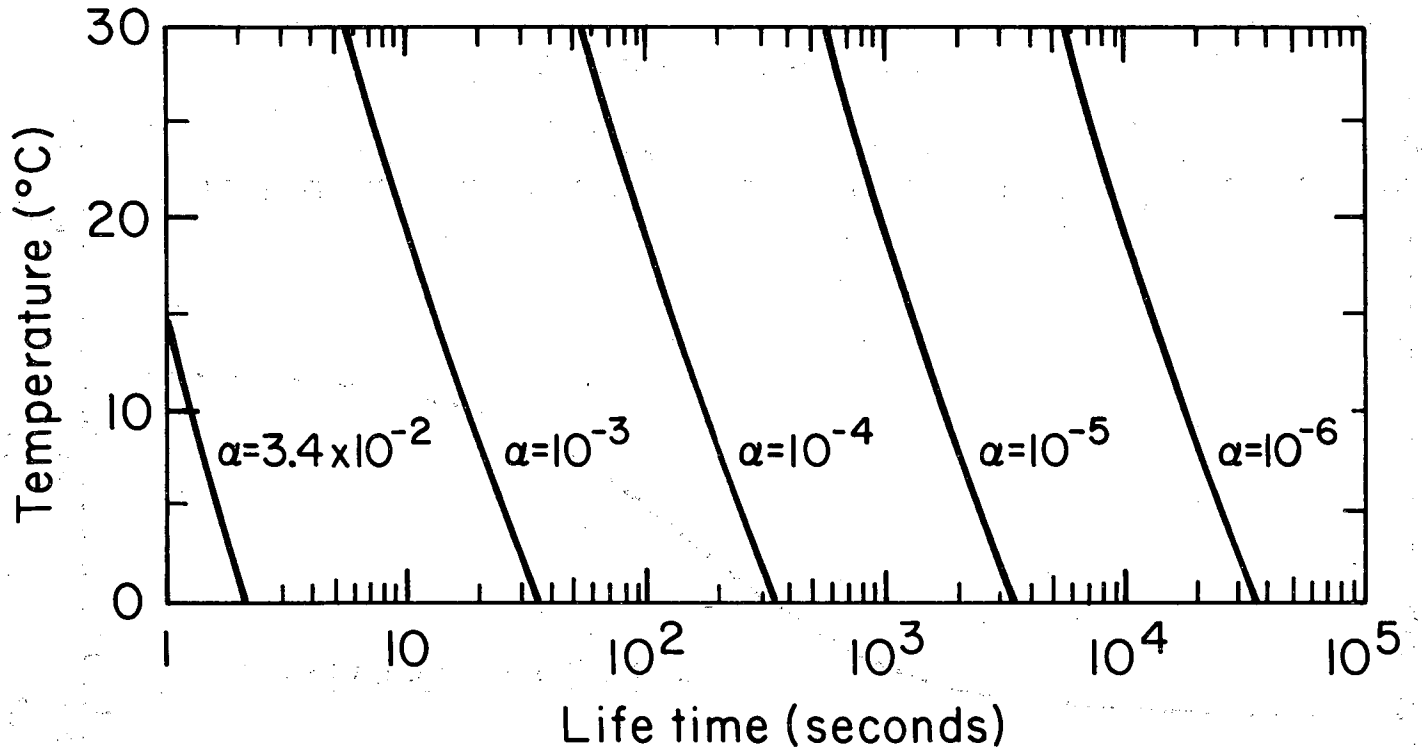

XBL 7812-13503

Figure 3. The effect of temperature on the lifetime of droplets. The lifetime is increased exponentially with a decrease in ambient temperature but varies linearly with inverse accommodation coefficient. RH = 80%, R_o = 5 μm, $P_{SO_2} = 10^{-8}$, $P_{CO_2} = 3 \times 10^{-4}$, and $P_{NH_3} = 5 \times 10^{-8}$ atm.

0 0 0 0 5 3 0 1 4 6 1

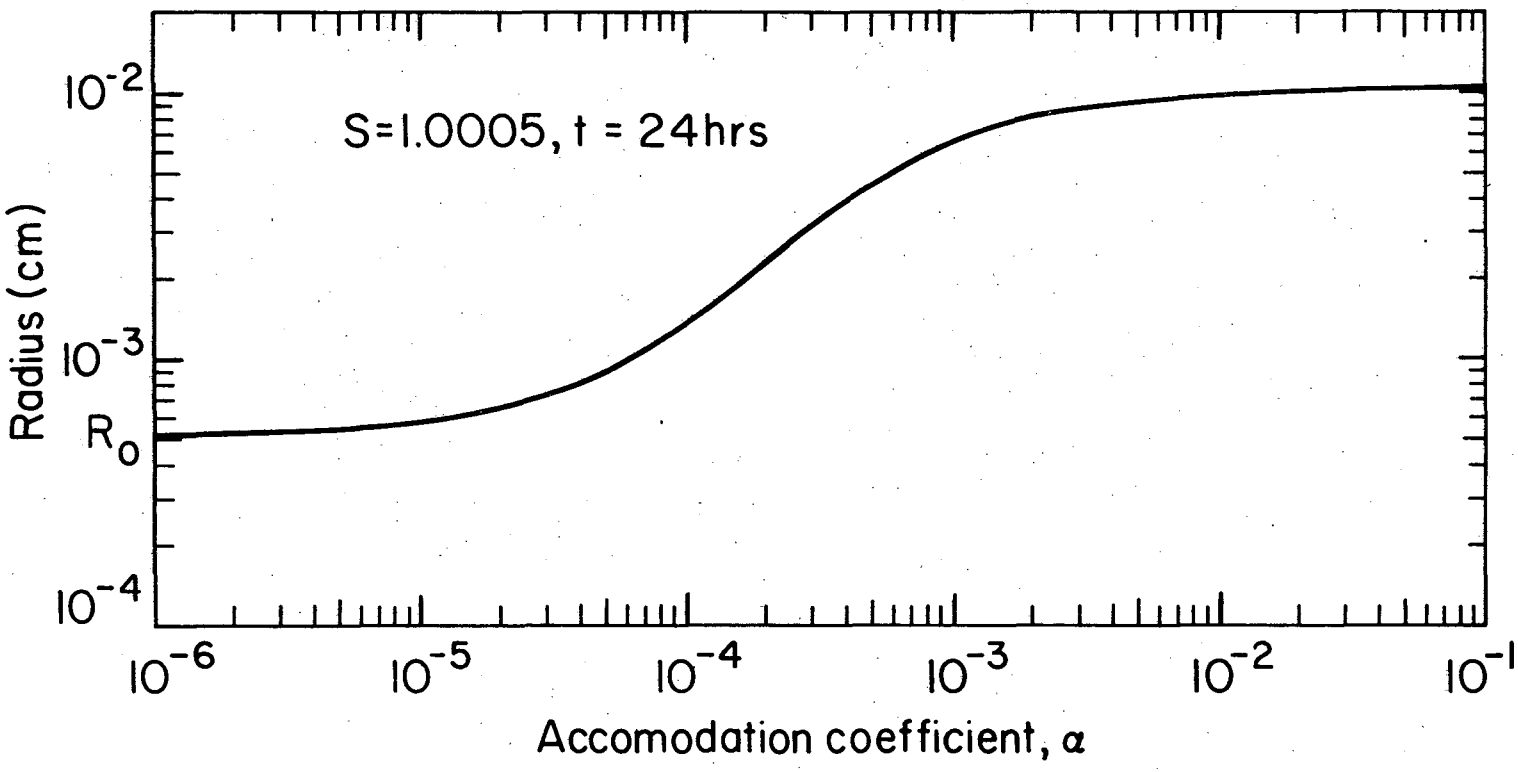

XBL 7812-13504

Figure 4. Growth of the droplets with supersaturation. Final radius of the droplets after 24-hr exposure in clouds with 0.05% supersaturation. R_o = 5.0 μm, T = 20°C, $P_{SO_2} = 10^{-8}$, $P_{CO_2} = 3 \times 10^{-4}$, and $P_{NH_3} = 5 \times 10^{-8}$ atm.

where $A = 9.61 \times 10^4$ mole·^{3}/g·sec, $[C_x]$ is the soot concentration, and $[O_2]$ is the dissolved oxygen concentration. This equation, the equilibrium relations listed in Table 1, the second dissociation step of the sulfuric acid,

$$HSO_4^- \rightleftarrows H^+ + SO_4^= \qquad K = 1.2 \times 10^{-2} , \tag{9}$$

and the charge balance

$$[H^+] = [HSO_4^-] + 2[SO_4^=] + [HSO_3^-] + 2[SO_3^=] + [OH^-] \tag{10}$$

have been solved at every point to calculate concentrations of products and the rate of evaporation of the droplet as a function of time (Fig. 5). The dotted line represents the condition when the rate is assumed to be equal to zero. It is seen that as the droplet evaporates, solute concentration increases and eventually the vapor pressure reaches below the ambient level and the droplet starts to grow again (solid line). Unfortunately, a short time later, the concentration of sulfate in the droplet is so high that the validity of Henry's Law and the Debye-Hückel[15] equations used in evaluating the activity coefficients fail and the calculations were stopped. Further work is under way to investigate behavior of the droplets under highly concentrated conditions.

References

1. B.J. Mason, The Physics of Clouds, Oxford, Clarendon, 1971.
2. R.R. Rogers, A Short Course in Cloud Physics, London, Pergamon, 1976.
3. R. Chang and E.J. Davis, "Knudson aerosol evaporation," J. Colloid Interface Sci. 54:3, 352 (1976).
4. N. Gurdis and L. Kulikova, "Die Verdampfung kleiner Wassertropfen," Z. Physik 25, 121 (1924).
5. W.H. Benner, H. Rosen, and T. Novakov, "SO_2 oxidation by water droplets containing combustion nuclei," this report.
6. R.S. Bradley, "The rate of evaporation of micro-drops in the presence of insoluble monolayers," J. Coll. Sci. 10, 571 (1955).
7. N.A. Fuchs, Evaporation and Droplet Growth in Gaseous Media (English translation), New York, Pergamon (1959).
8. J. Podzimex and A.N. Saad, "Retardation of condensation nuclei growth by surfactants," J. Geophys. Res. 80:24, 3386 (1975).
9. B.V. Derjaguin, S. Kurghin, L.A. Rosenzweig, and V.A. Fedoseyev, "Study of passivation of condensation growth of drops of water and salt solutions," J. Coll. Interface Sci. 37:2, 484 (1971).
10. S. Beilke and G. Gravenhorst, "Heterogeneous SO_2-oxidation in the droplet phase," paper presented at the International Symposium on Sulfur in the Atmosphere, Dubrovnik, Yugoslavia (1977).

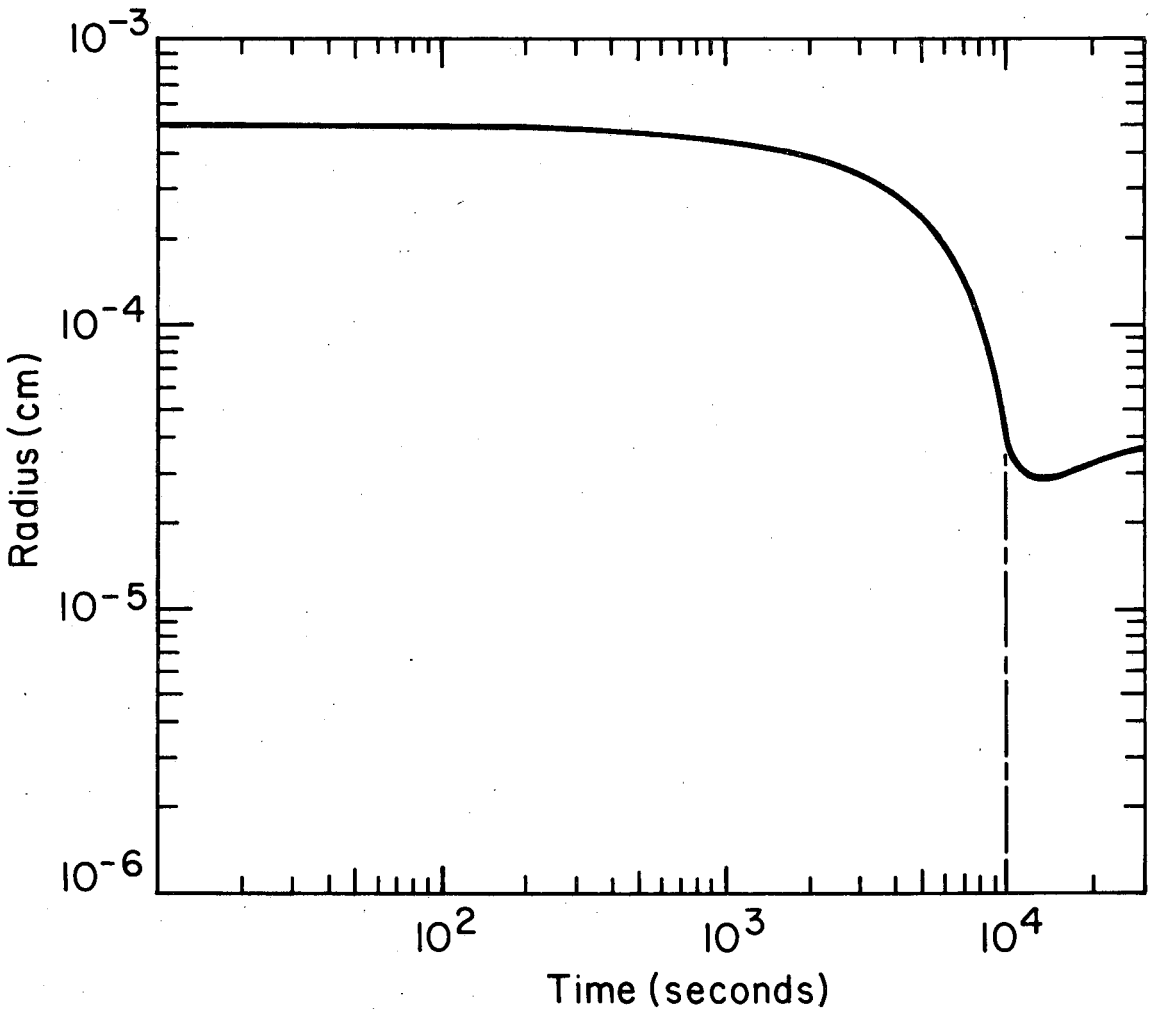

XBL 7812-13505

Figure 5. Change in the droplet size as a function of evaporation time when droplets contain soot particles and catalytic oxidation of SO_2 takes place in the liquid droplet. The dotted line represents the condition when equilibrium is present between the liquid and gaseous atmosphere. RH = 80%, T = 20°C, $\alpha = 10^{-6}$, $R_o = 5.0$ μm, $P_{SO_2} = 10^{-8}$, $P_{CO_2} = 3 \times 10^{-4}$, and $P_{NH_3} = 5 \times 10^{-8}$ atm.

11. J.M. Miller and R.G. DePena, "Contribution of scavenged sulfur dioxide to the sulfate content of fresh water," J. Geophy. Res. 77, 5905 (1972).

12. R.J. Archer and V.K. LaMer, "The rate of evaporation of water through fatty acid monolayers," J. Phys. Chem. 59, 200 (1955).

13. H.S. Eisner, F.R. Brookes, and B.W. Quince, "Stabilization of water mist," Nature 192, 1724 (1958).

14. S.-G. Chang, R. Brodzinsky, R. Toossi, S.S. Markowitz, and T. Novakov, "Catalytic oxidation of SO_2 on carbon in aqueous suspensions," in Proceedings, Conference on Carbonaceous Particles in the Atmosphere," Lawrence Berkeley Laboratory, Berkeley, California (in press).

15. W. Stumm and J.J. Morgan, Aquatic Chemistry, New York, Wiley-Interscience, 1970.

This report was done with support from the Department of Energy. Any conclusions or opinions expressed in this report represent solely those of the author(s) and not necessarily those of The Regents of the University of California, the Lawrence Berkeley Laboratory or the Department of Energy.

Reference to a company or product name does not imply approval or recommendation of the product by the University of California or the U.S. Department of Energy to the exclusion of others that may be suitable.

TECHNICAL INFORMATION DIVISION
LAWRENCE BERKELEY LABORATORY
UNIVERSITY OF CALIFORNIA
BERKELEY, CALIFORNIA 94720